N° d'ordre : **41086**

UNIVERSITE LILLE 1 – SCIENCES ET TECHNOLOGIES

ECOLE DOCTORALE SCIENCES DE LA MATIERE,

DU RAYONNEMENT ET DE L'ENVIRONNEMENT

THESE

présentée par

Kaew-arpha THAVORNPRASERT

pour l'obtention du

TITRE DE DOCTEUR EN MOLECULES ET MATIERE CONDENSEE

intitulée

PRODUCTION OF ACETALS FROM BIO-RESOURCED ALCOHOLS OVER BIFUNCTIONAL CATALYSTS

Soutenance prévue **le 14 Mars 2013** devant la commission d'examen composée de:

Président du Jury:	**Franck DUMEIGNIL**, Professeur, Université Lille 1
Rapporteurs:	**Jean-Marc MILLET**, Directeur de Recherche CNRS, IRCELYON
	Michèle BESSON, Directrice de Recherche CNRS, IRCELYON
Examinateurs:	**Jean-Luc DUBOIS**, Directeur Scientifique, ARKEMA
	Karine DE OLIVEIRA VIGIER, Maître de Conférences, Université de Poitiers
Directeur de thèse:	**Louise JALOWIECKI-DUHAMEL**, Chargée de Recherche CNRS, Université Lille 1
Co-directeur:	**Mickaël CAPRON**, Maître de Conférences, Université Lille 1

Acknowledgement

This work was carried out from March 2010 until March 2013 in the Unité de Catalyse et Chimie du Solide, UMR 8181, at the Université des Sciences et Technologies de Lille. The research leading to all the results included in this thesis has received funding from the European Union Seventh Framework Program (FP7/2007-2013) under grant agreement n° 241718 EuroBioRef.

I would like to express my sincere thanks to everyone who has contributed to my PhD thesis. Above all, special thanks to Dr. Louise Jalowiecki-Duhamel, my thesis director, and Assoc. Prof. Dr. Mickaël Capron, my thesis co-director, for their valuable advice, helpful discussions, their constant support and encouragement, not only when I meet difficulties, but in every situation.

I would like to thank Prof. Franck Dumeignil for kindly providing me this interesting and challenging research topic, for his motivation and support, for his fruitful discussions on the thesis work, also for accepting the role of presidency of the committee of examination.

I am very grateful to Dr. Jean-Marc Millet and Dr. Michèle Besson for accepting their role as a referee and for kindly reviewing this thesis; to Dr. Jean-Luc Dubois and Dr. Karine de Oliveira Vigier for kindly accepting their role as a thesis examiner.

I wish to thank Mr. Olivier Gardoll, Ms. Nora Djelal, Ms. Laurence Burylo, Mr. Romain Descamps, Prof. Gabriel Billon, Ms. Nadia Toüati, Dr. Hervé Vezin, Mr. Arnaud Beaurain, Ms. Martine Trentesaux, Prof. Sylvain Cristol, Prof. Jean-François Paul, Asst. Prof. Dr. Anne-Sophie Mamade, Dr. Jérémy Faye, Dr. Pierre Miquel, and Dr. Benjamin Katryniok for their assistance, ideas, and fruitful discussions.

Moreover, I would like to thank my PhD colleagues, Mr. Guillaume Tesquet, Mr. Jeorge Miguel Beiramar, Dr. Alexia Cordova, Dr. Lishil Silvester, Dr. Carsten Liebig, and many others for their help and many enjoyable discussions. I would like also to thank all UCCS members for their part of creating the very pleasant environmental working conditions.

Many thanks to my office mates, Dr. Asma Tougerti, Dr. Elise Berrier, Dr. Cyril Pyrez, Mr. Lei Zhang and Mr. Wenhao Fang, for their help and a joyful environment in our ‘biscuits lover’ office. Special thanks to Asma for her being so supportive and a friend indeed. Also, thanks to my friends back at home and here in Lille for their support and plenty of cheerful moments.

Last but not least, I would like to thank my parents and my family with all my heart for their unconditional love and trust, for their support and encouragement during my study.

Abstract

The severe environmental issues caused by the fossil-based sources consumption have driven numerous studies to find alternative sustainable resources. Biomass is a renewable feedstock for a large spectrum of valuable chemicals, especially for fuels applications. Acetals, dimethoxymethane (DMM) and diethoxythane (DEE), can be produced from biomass-derived methanol and ethanol, respectively. Herein, a concept of synthesizing acetals *via* a one-step alcohol conversion is applied instead of the currently used two-steps reactions of alcohol partial oxidation/acetalization. The DMM synthesis is studied on FeMo mixed oxide having needed redox/acidic functions. 50 % of DMM yield is achieved at 255 °C on the catalyst with a Mo/Fe ratio of 3.2. DMM selectivity is boosted when using a methanol-rich (40 mol.%) feed and a high selectivity is kept up to 60 % of methanol conversion. A synergistic effect between Mo and Fe species on the conversion is clearly shown. An active site incorporating Mo and Fe cations is proposed, involving lattice O^{2-} and anionic vacancies generated by surface dehydroxylation. LEIS analysis confirms the presence of Mo and Fe species in the outermost atomic layer. XPS and *in situ* EPR studies show that Fe centers provide the redox property. The acidity is brought by anionic vacancies acting as Lewis acids. XPS results confirm the role of gas-phase O_2 to reoxidize the surface and regenerate the active sites. FeMo-based catalysts were applied in the DEE synthesis due to possible analogous pathways of methanol/ethanol reactions. The catalyst is not selective to acetal DEE, probably due to the steric hindrance or to the inadequate acidic strength of the FeMo system.

Résumé

La biomasse est une matière première renouvelable pour un large éventail de produits chimiques à haute valeur ajoutée, comme les carburants. Les acétals, tels que le diméthoxyméthane (DMM) et le diethoxyéthane (DEE), peuvent être ainsi produits à partir respectivement du méthanol et de l'éthanol. Cette étude concerne la synthèse des acétals via une conversion directe de l'alcool. La synthèse en DMM est étudiée sur un catalyseur oxyde mixte FeMo faisant intervenir les fonctions d'oxydo-réduction et acide. 50% de rendement en DMM est obtenu à 255 °C sur le catalyseur comportant un rapport Mo/Fe de 3,2. La sélectivité en DMM est améliorée lors de l'utilisation d'une phase riche en méthanol (40 mol.%) et une sélectivité élevée est maintenue jusqu'à 60% de conversion du méthanol. Un effet de synergie entre les espèces Mo et Fe est clairement observé sur la conversion. Un site actif constitué de cations Fe et Mo est proposé, impliquant l'espèce O^{2-} du solide et des lacunes anioniques générées par la déshydroxylation de la surface. L'analyse LEIS confirme la présence d'espèces Fe et Mo dans la couche atomique la plus externe. L'XPS et les études par EPR in situ montrent que les cations Fe fournissent la propriété d'oxydo-réduction. L'acidité est apportée par des lacunes anioniques agissant comme acide de Lewis. Les résultats XPS confirment le rôle de la phase gazeuse O_2 pour la réoxydation de la surface et la régénération des sites actifs. Les catalyseurs FeMo ont également été étudiés pour la synthèse en DEE. Le catalyseur n'est pas sélectif pour la formation en acétal DEE, probablement en raison de l'encombrement stérique ou de la force acide inadéquate du système FeMo.

Table of contents

Introduction and aim of work

The price of commercial fuels has drastically increased during the last decades following a never-ending increase in the crude oil prices (Figure I) [1]. The rising price trend will presumably continue due to a fast-growing demand (Figure II) [2], especially in the energetic needs, and the progressive and irremediable exhaustion of fossil resources. This situation strongly motivates numerous research efforts focusing on renewable energy sources. In the concept of renewability, biomass feedstock is a good candidate owing to its natural abundance and the energy from biomass is considered carbon neutral. In France, the renewable energy is accounted for 15.3 % of the total energy consumption and biomass is the leading source of renewable energy in the country with 52 % of renewable consumption – second in Europe after Germany [3].

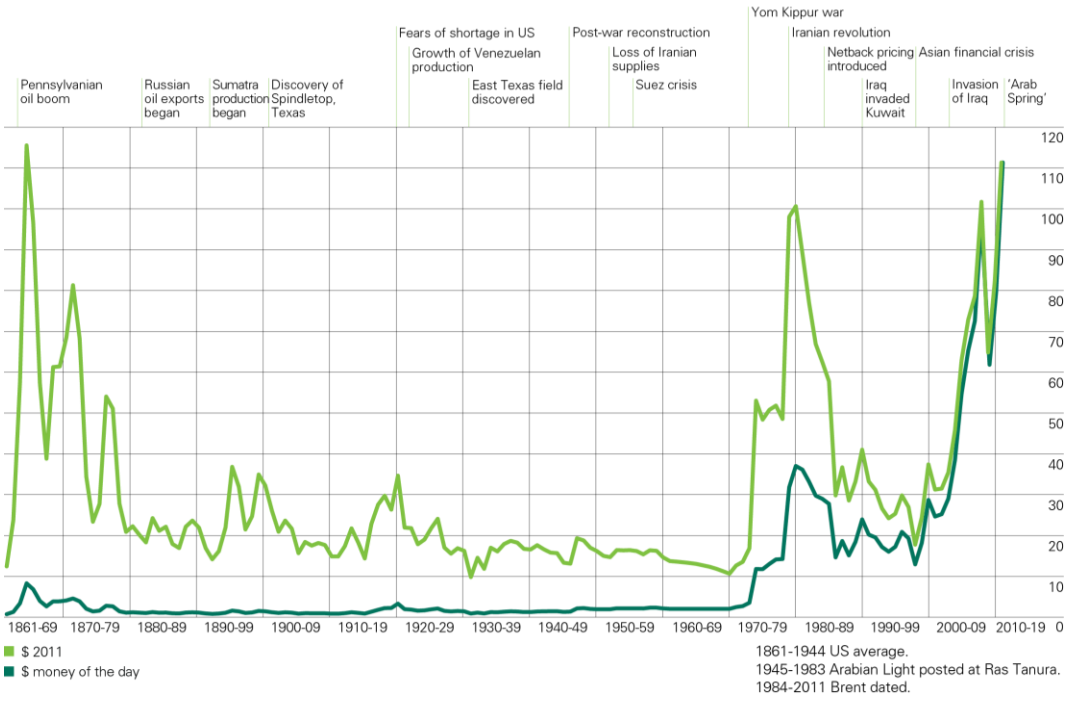

Figure I: Variation of crude oil prices (US dollars per barrel) during the year 1861-2011 in correlation with world events [1].

Acetals, such as *1,1*-dimethoxymethane (DMM) and *1,1*-diethoxyethane (DEE), are highly valuable chemicals which can be produced from biomass-derived alcohols. Biomethanol can be obtained *via* the conversion of syngas produced by the gasification of biomass while bioethanol can be easily obtained from biomass mainly by sugar fermentation. The synthesis of DMM and DEE is the main goal of this thesis. Both acetals are widely used, for instance, as starting materials in fragrance and pharmaceutical industries, and more importantly as additives to gasoline or diesel blends.

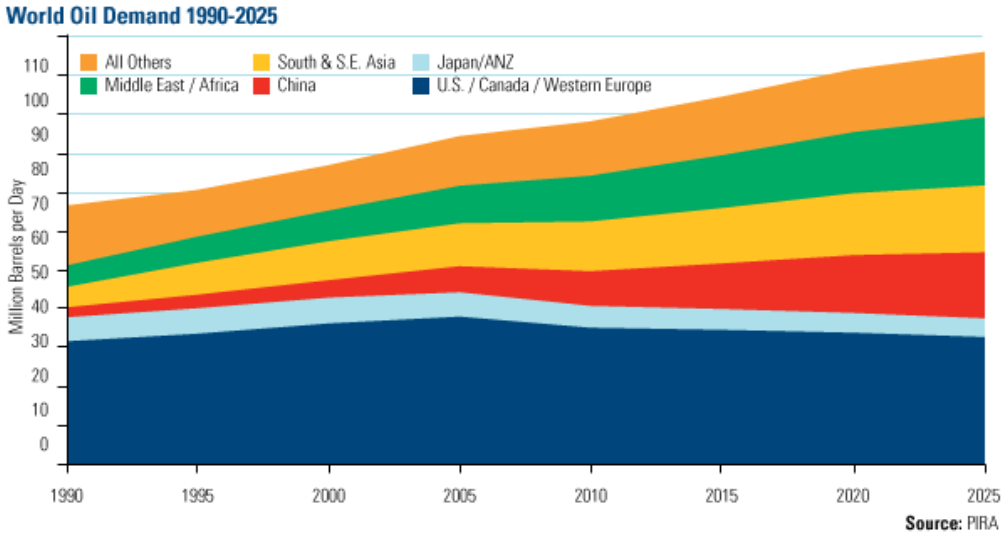

Figure II: World oil demand in millions barrel per day recorded from the year 1990 to 2025 [2].

At the industrial scale, the current acetals production is carried out in a sequential manner *via* two consecutive steps involving

- partial oxidation of the alcohols to aldehydes over oxidation catalysts, and
- acetalization reaction between the obtained aldehydes and alcohol molecules over acid catalysts.

From an economic point of view, producing acetals in a single-step process would be much more preferable by means of reducing the production cost as well as the energy consumption. Researches aimed at realizing the direct DMM synthesis from methanol in a single step have been undertaken for ten years in our laboratory. As mentioned before, the 'one-pot' synthesis of DMM requires bifunctional catalyst with redox and acidic characters. We started with a model catalyst 'Mo/Al_2O_3' placed under a classical reaction condition (7 mol.% of methanol in air). Thanks to the results obtained in this study, we confirmed that molybdenum loading plays an important role in the activity of reaction and this is certainly due to the nature of active phases created at different Mo loadings.

- Low Mo loading leads to isolated molybdenum entities (MoO_4) dispersed on the support surface. This species is not active in methanol oxidation reaction.
- High Mo loading leads to polymolybdate structures which are able to transform methanol with as high as 95 % conversion at 250 °C. Unfortunately, the selectivity to DMM is quite low. The main products are dimethylether and formaldehyde. This is

mainly due to the fact that redox and acid functions necessary to produce DMM are not concomitant and/or have not the adequate strength.

Afterwards, we focused on rhenium based catalysts known to exhibit good DMM selectivity [4]. Rhenium atoms were deposited on the surface of different supports using different synthesis methods (incipient wetness, sublimation, and deposition). Similar to molybdenum, isolated ReO_4 are formed at low Re loading and polyoxorhenate species are formed at high Re loading. However, the catalysts in this family both with low and high contents of Re are active in the oxidation reaction of methanol. The main difference is found in the selectivity, the isolated ReO_4 entities produce mainly molecules coming from oxidation reactions (*i.e.*, formaldehyde and CO_x) while the polyoxorhenate forms mainly DMM. Although this family of catalysts exhibits good DMM selectivity, it is well-known that the catalyst deactivation continuously occurs during the reaction course due to rhenium sublimation. For industrial use, we had to develop more robust catalysts.

With the framework supported by the financial help of the ARKEMA society, we carried out a screening of industrial catalysts having inherent properties (*i.e.*, redox and acid) needed for the direct synthesis of DMM from methanol. Among those screened catalysts, two of them present good activity. The first type is an amorphous material with a stoichiometry close to $Mo_{12}V_3W_{1.2}Cu_{1.2}Sb_{0.5}O_x$. After optimizing the reaction conditions, we were able to increase the DMM productivity drastically and obtained a considerably high value ($128*10^{-5}$ $mol_{DMM}.min^{-1}.g_{cat}^{-1}$) compared to what was published at that moment.

The second type was a FeMo based catalyst that is generally used to form formaldehyde from methanol. In the tested conditions (*i.e.*, 7 mol.% of methanol in the feed), this catalyst presents small amount of DMM selectivity. By increasing the feed composition to 40 mol.% of methanol a drastic variation of the selectivity is obtained while keeping a high conversion. A huge increase in DMM productivity is obtained as depicted in Figure III. This phenomenon is observed only with the FeMo-based catalysts whereas for the other types of compounds the selectivity to DMM drops with the increase of methanol quantity in the feed.

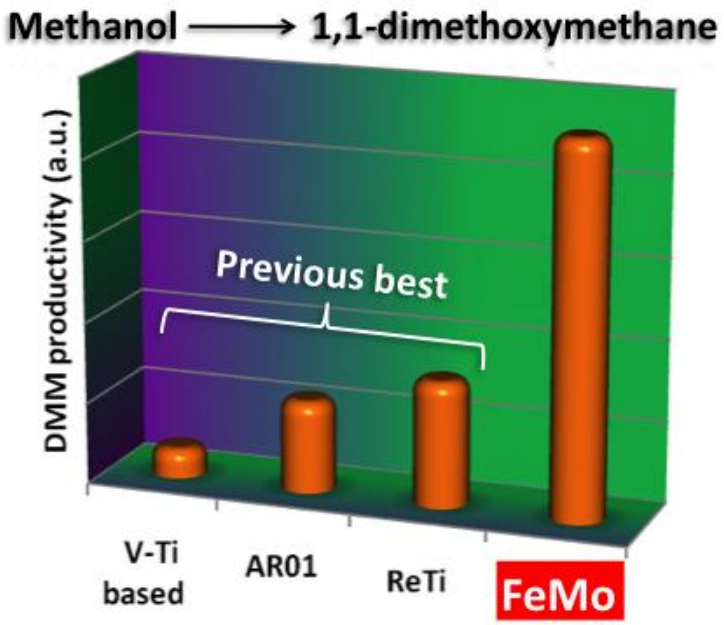

Figure III: Comparison of DMM productivity obtained on various screening catalysts.

As a part of the EuroBioRef project (European Multilevel Integrated Biorefinery Design of Sustainable Biomass Processing) – a European project supported within the EU's Seventh Framework Program, the aim of this thesis is to develop the catalytic formulation capable of catalyzing the direct transformation of alcohols (methanol and ethanol) to their corresponding acetals (DMM and DEE) in a single-step process. According to our previous work, the iron molybdate catalytic formulation is the primary candidate in the direct DMM synthesis from methanol. The selected formulation is then optimized to a maximum DMM production. Thereafter, inherent redox and acid properties of the FeMo catalyst are investigated in detail, aiming to correlate these properties to its excellent catalytic behavior and to gain more knowledge of the working active sites. Better understanding of this system could indeed give precious hints for further developments towards industrialisation. Afterwards, because the oxidation/acetalization reactions pathway of methanol seems to be nearly identical to that of ethanol, the knowledge we will acquire in the study of methanol reaction to DMM (*i.e.*, the optimized catalyst formulation and experimental conditions) might be then transposed to the DEE synthesis application.

The thesis is divided into four chapters. The first chapter presents a literature review focusing on the production of acetals DMM and DEE via a two-step process starting from alcohols on redox catalyst (in the partial oxidation reaction) or acidic catalyst (in the acetalizaton reaction), and through a single-step direct alcohol conversion over bifunctional catalysts including heterogeneous FeMo mixed oxide system. The second chapter is concerning the procedures for

the preparation of different FeMo mixed oxide solids and the experimental techniques for their characterizations. The description of catalytic tests in the selective partial oxidation reaction of methanol and ethanol and for the acetalization reaction of ethanol with acetaldehyde, as well as the operating conditions are reported. The procedure to analyse the reaction products is also described in this chapter. The transformation of methanol to DMM constitutes the main part of chapter 3 where the performances of FeMo mixed oxide catalysts are presented and discussed in correlation with their physico-chemical properties. Chapter 4 includes the results obtained with the reaction of ethanol on FeMo-based catalysts. The acetalization reaction of ethanol and acetaldehyde on acidic catalysts is also realized in this chapter. The obtained results are then corroborated with thermodynamic considerations. To summarize, the general discussion of all the results and conclusions, as well as the research perspectives, are given in the last part of the thesis.

References

[1] http://www.bp.com/liveassets/bp_internet/globalbp/globalbp_uk_english/reports_and_publications/statistical_energy_review_2011/STAGING/local_assets/pdf/statistical_review_of_world_energy_full_report_2012.pdf, verified on January 10, 2013.

[2] http://www.advisorperspectives.com/commentaries/global_111211.php, verified on January 10, 2013.

[3] http://ressources.campusfrance.org/catalogues_recherche/recherche/en/rech_energies_en.pdf, verified on January 10, 2013.

[4] Y. Yuan, Y. Iwasawa, J. Phys. Chem. B 106 (2002) 4441.

Chapter 1

Literature review

A global concern of dramatic environmental impacts, mainly originated from the extensive consumption of fossil-based resources served for energetic needs, has imposed numerous researches for disclosing and developing more efficient and cleaner fuels that could result in a severe reduction of pollutant emissions. In this respect, alcohols as well as their derivatives are currently being of interest as alternative energy sources. The production and uses of primary alcohols like methanol and ethanol are described in the following sections.

1.1. Methanol and ethanol production

1.1.1 Methanol

Methanol was primarily produced in history as a by-product of slow destructive pyrolysis of timber, from which it was named 'wood alcohol' and was used in the embalming process by the ancient Egyptians. Much of today's methanol comes from methane in natural gas. In a commercial plant, methane is first converted to synthesis gas (or syngas) consisting of H_2, CO and CO_2 either by steam reforming (Eq. 1) or partial oxidation with molecular oxygen (Eq. 2). The steam reforming of methane is carried out commercially on a nickel catalyst at high temperature 850 °C and at moderate pressure of 40 atm. The partial oxidation of methane is performed at atmospheric pressure and it can be conducted with or without a catalyst. However, the use of a catalyst is preferable to proceed the reaction at a lower temperature. The partial oxidation of methane is exothermic and the heat released from the reaction can be supplied to the endothermic steam-methane reforming. A concept of combining two reactions in a single reactor to maximize heating efficiency is commonly known as autothermal reforming.

$$CH_4 + H_2O \rightarrow CO + 3H_2 \qquad (\Delta H^0 = +206\ kJ.mol^{-1}) \qquad (1)$$

$$CH_4 + 1/2O_2 \rightarrow CO + 2H_2 \qquad (\Delta H^0 = -36\ kJ.mol^{-1}) \qquad (2)$$

Methanol is produced afterwards *via* the catalytic conversion of syngas through water gas shift (WGS) and hydrogenation of CO_2 reactions, Eqs. 3 and 4, respectively. The synthesis of methanol is usually conducted at temperatures between 220 and 300 °C and pressures between 50 and 100 bar over a $Cu/ZnO/Al_2O_3$ catalyst [1,2].

$$CO + H_2O \leftrightarrow CO_2 + H_2 \qquad (\Delta H^0 = -41.1\ kJ.mol^{-1}) \qquad (3)$$

$$CO_2 + 3H_2 \leftrightarrow CH_3OH + H_2O \qquad (\Delta H^0 = -49.4\ kJ.mol^{-1}) \qquad (4)$$

$$CO + 2H_2 \leftrightarrow CH_3OH \qquad (\Delta H^0 = -92\ kJ.mol^{-1}) \qquad (5)$$

The overall reaction for producing methanol from syngas is shown in Eq. 5. It is notable that the production of syngas from methane produces a considerable surplus of hydrogen in comparison to the amount required in the overall methanol synthesis reaction. With an external source of CO_2 feeding into the methanol synthesis reactor, the excess hydrogen can be converted to additional methanol following the hydrogenation reaction shown in Eq. 4. The WGS reaction (Eq. 3) is also used to adjust the ratio between H_2 and CO in the syngas to provide appropriate stoichiometry for the synthesis of methanol.

As the most basic alcohol, methanol has the distinct advantage whereby it can be made from any resource that can be converted first into syngas. Biomass feedstocks including energy crops such as switch grass and miscanthus, agricultural sources such as corn husks, wood pellets, lumbering and timbering wastes, municipal wastes, and bio-solids like treated sewage sludge can be gasified to syngas which is then catalytically transformed to methanol. Three major types of reaction occur during the process of biomass gasification – pyrolysis, partial oxidation, and reforming. Biomass constitutes mainly cellulose $(C_6H_{10}O_5)_n$ thereby, using a cellulose-derived molecule as a feedstock, these reactions are summarized in Table 1-1 [3,4]. The feedstock is first dried to evaporate moisture. It is then thermally decomposed into gases, tars, oils, and a solid char residue without steam or oxygen in the pyrolysis step. In the partial oxidation processes, the gas, liquid, and solid products after pyrolyzation then react with air to give permanent gases (CO, CO_2, and H_2) and lesser amounts of hydrocarbon gases. The solid char is oxidized to CO and CO_2 in the char gasification, and H_2 is then generated through the steam reforming. The water gas shift and methanation reactions are also important reactions occurred during the gasification.

The syngas derived from biomass contains small amount of H_2S, at concentrations range from about 20-50 part per million by volume (ppmv) for hardwood to 500-600 ppmv for corn stover, on a dry a basis [5]. The presence of H_2S in the syngas is corrosive and deactivates the downstream catalysts, as well as decreases the efficiency of gas-to-liquid catalytic conversion process [5,6].

Table 1-1: Fundamental reactions of selected cellulose gasification reactions adapted from [4].

Classification	Stoichiometry	Enthalpy (kJ.mol^{-1})[a]
Pyrolysis	$C_6H_{10}O_5 \rightarrow 5CO + 5H_2 + C$	180
	$C_6H_{10}O_5 \rightarrow 5CO + CH_4 + 3H_2$	300
	$C_6H_{10}O_5 \rightarrow 3CO + CO_2 + 2CH_4 + H_2$	-142
Partial Oxidation	$C_6H_{10}O_5 + ½O_2 \rightarrow 6CO + 5H_2$	71
	$C_6H_{10}O_5 + O_2 \rightarrow 5CO + CO_2 + 5H_2$	-213
	$C_6H_{10}O_5 + 2O_2 \rightarrow 3CO + 3CO_2 + 5H_2$	-778
Steam Gasification	$C_6H_{10}O_5 + H_2O \rightarrow 6CO + 6H_2$	310
	$C_6H_{10}O_5 + 3H_2O \rightarrow 4CO + 2CO_2 + 8H_2$	230
	$C_6H_{10}O_5 + 7H_2O \rightarrow 6CO_2 + 12H_2$	64
Water Gas Shift	$CO + H_2O \rightarrow CO_2 + H_2$	-41
Methanation	$CO + 3H_2 \rightarrow CH_4 + H_2O$	-206

[a]reference temperature of 27 °C

1.1.2 Ethanol

Synthetic ethanol is manufactured through direct hydration of ethylene produced in the petrochemical industry by steam cracking. The process involves reacting ethylene with steam (Eq. 6) over phosphoric acid coated on silicon dioxide support (H_3PO_4/SiO_2) at 300 °C and 60-70 atm. In practice, an excess of steam is used to convert approximately 5% of ethylene into ethanol at each pass through the reactor. Nonetheless it is possible to achieve an overall 95 % conversion by continuously removing ethanol from the equilibrium mixture and ethylene recycling.

$$CH_2{=}CH_2 + H_2O \leftrightarrow CH_3CH_2OH \qquad (\Delta H^0 = -45\ \text{kJ.mol}^{-1}) \qquad (6)$$

In the renewable context, ethanol can be produced by fermentation of sugars usually with the yeast *Saccharomyces cerevisiae* (Eq. 7). High theoretical yields of ethanol are obtained from this reaction and only small amounts of byproducts including glycerol, acetic acid, lactic acid, succinic acid, and fusel alcohols are formed, with a small amount of sugar required as a starting material.

$$C_6H_{12}O_6 \rightarrow 2C_2H_5OH + 2CO_2 \qquad (7)$$

Different types of feedstocks can be used for producing ethanol as depicted in Figure 1-1, *i.e.*, sugarcane, corn grain or grain starches, and lignocellulosic biomass. Ethanol is produced from corn grains and other starches by either wet or dry milling [3,4,7]. Sugarcane is first converted into sugarcane juice and water-insoluble lignocelluloses, *i.e.*, sugarcane bagasse. The fermentation of sugarcane juice proceeds without any extensive pretreatment and the sugarcane bagasse is burned to provide heat for the process. Production of ethanol from lignocellulosic biomass is currently promising due to the lowest feedstock cost, for instance, the cost of corn stover is approximately two to three times lower than those of sugarcane and corn seeds [4]. The process for conversion of lignocelluloses to ethanol, modeled by the National Renewable Energy Laboratory (NREL − the United States) is based on dilute acid prehydrolysis and enzymatic hydrolysis [8]. It is notable that the sugars derived from sugarcane and corn grains are fermented to ethanol with the yeast *S. cerevisiae* whereas the mixture of glucose and xylose derived from lignocelluloses is fermented to ethanol with the recombinant *Zymomonas mobilis* bacterium. In all cases of feedstock use, ethanol-water solution from fermentation is distilled to azeotropic point around 95 % ethanol in water. Ethanol is purified afterwards using molecular sieves [4].

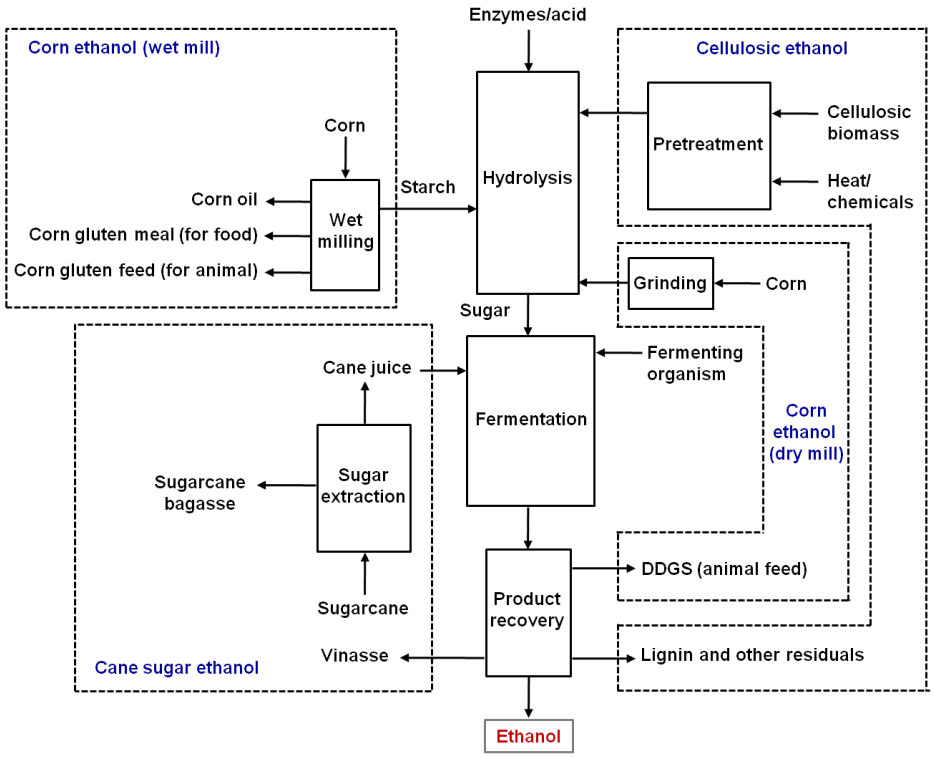

Figure 1-1: Block flow diagram for ethanol production from corn, sugarcane and cellulosic biomass adapted from [4].

In comparison, the production of ethanol *via* ethylene hydration is much simpler and more efficient than fermentation, also producing high purity of ethanol. However, the major disadvantages of ethylene process are that the reaction takes place at high temperatures and pressures thereby a lot of energy input is needed. The process also uses finite resources based on crude oil that is not considerable to be environmental friendly [9]. The renewable approach to obtain ethanol from biomass is thus more preferable owing to significant reduction of CO_2 emission from 90 % to 75 %, compared to petroleum-derived ethanol production [10].

1.2 Uses of methanol and ethanol

Methanol is used as a starting material in the synthesis of chemicals including dimethyl ether, methyl *tert*-butyl ether (MTBE), acetic acid, formaldehyde, and olefins. Formaldehyde, MTBE, and acetic acid are of major downstream products from methanol, which contribute 35 %, 25 % and 9 % of methanol use, respectively [11]. MTBE is exclusively used as an oxygenated fuel additive for gasoline engines. The largest use of acetic acid is in the production of vinyl acetate monomer which can then be polymerized to polyvinyl acetate used in paints and adhesives.

Methanol is served as a feed for direct methanol fuel cells (DMFC) equipped in methanol fuel cartridges used, for instance, to power laptop computers and electronic devices on the aircraft board [12,13]. Onboard reforming of methanol, of which methanol is converted to hydrogen by steam reforming (Eq. 8) or partial oxidation (Eq. 9) reactions, is also the promising method of supplying hydrogen to proton-exchange membrane (PEM) fuel cells used in automotive applications [14,15].

$$CH_3OH + H_2O \rightarrow CO_2 + 3H_2 \qquad (\Delta H^0 = +49.4\ kJ.mol^{-1}) \qquad (8)$$

$$CH_3OH + \tfrac{1}{2}O_2 \rightarrow CO_2 + 2H_2 \qquad (\Delta H^0 = -192.2\ kJ.mol^{-1}) \qquad (9)$$

Ethanol is often called a drinking alcohol as it is the prime ingredient in alcoholic beverages. It is used in antiseptic, in some antibacterial soaps and medical wipes. It is occasionally used to treat poisoning by other more toxic alcohols, in particular methanol and ethylene glycol. As ethanol is perfectly soluble in water, it is served as a solvent in making paints, permanent markers, and personal care products *etc*. Ethanol is also considered as a feedstock in synthesizing other organic compounds, for instance, ethyl halide, ethyl esters, ethyl amines, diethyl ether, and acetic acid.

In transportation sector, alcohols can be used directly as alternative fuels or as alternative fuel components due to many reasons, *e.g.*, reducing green house gases emission and toxic exhaust emission, enhancing overall energy efficiency, and minimizing the costs of fuel. Unlike gasoline and diesel, alcohols contain oxygen which helps increasing the combustion efficiency and, thus, reducing air pollution, *i.e.*, emissions of particulate matter, unburned carbons, carbon monoxide, as well as NO_x.

Without being reformed, methanol fuel is used in internal combustion engines for mobile propulsion in vehicles and portable machineries [16-18]. Methanol has a high octane value thereby it is blended with gasoline to enhance smoother burning in the engines. The resulting blend also has lower boiling temperature for better fuel vaporization in cold engines and no sulphur contamination which poisons the catalytic converter operations [19].

Ethanol is being used extensively as a fuel for motor vehicles, especially in Brazil and in the U.S. Like methanol, ethanol has a high octane rating thereby it is used as the octane enhancer in the E85 blend, with 85 % anhydrous ethanol and 15 % gasoline by volume, to power flexible-fuel vehicles commonly used in the U.S. and Europe. Bio-ethanol is being used to formulate a blend with diesel fuel, known as E-Diesel, composed of 88.7 % diesel fuel, 10% ethanol and 1.3 % additive. Ethanol is also used to synthesize an oxygenated fuel additive, namely ethyl *tert*-butyl ether (ETBE) *via* its reaction with isobutene. However, the use of MTBE and ETBE as the additives is being nowadays faded out due to water quality concerns.

Unfortunately, the presence of alcohols in fuel induces the corrosion to the metallic parts in the engines. In this context, methanol is more corrosive compared with ethanol. There is also limited miscibility between methanol and gasoline, due to the presence of water, which causes phase separation. Ethanol is an appropriate additive for petrol engines due to its high octane number but its low cetane number and its large amount of the heat of vaporization resists self-ignition in diesel engines [20]. Besides that, the instability of ethanol-diesel blends especially at low temperatures and high water contamination remains a great concern for ethanol-diesel blends application [21,22]. An alternative to ethanol as oxygenated additives for diesel fuel could be the compounds like acetals which are miscible in diesel fuel and show the good feature in terms of boiling points, viscosity and auto-ignition temperatures.

1.3 Synthesis of acetals from alcohols

In this study, we target the production of highly versatile acetals, namely *1,1*-dimethoxymethane (hereafter referred to as DMM) and *1,1*-diethoxyethane (hereafter referred to as DEE), from their corresponding alcohols, methanol and ethanol, respectively. A state of the art in the synthesis of both acetals is described in the following subsections.

1.3.1 Dimethoxymethane synthesis from methanol

The possible pathways of methanol reaction are demonstrated in Scheme 1-1 [23]. Different products are obtained depending on the catalyst, reaction temperature, and partial pressure of reactants, *i.e.*, oxygen and methanol. The redox-catalysed pathway leads to a sequence of oxidized species, namely formaldehyde (F), formic acid (FA) and carbon oxides (CO and CO_2), whereas the acid-catalysed pathway yields dehydration products, *i.e.*, dimethyl ether (DME), DMM and methyl formate (MF), respectively obtained from condensation of methanol with its aforementioned oxidation products. It is mentioned in the literature that formic acid is considered as an intermediate in the formation of MF or carbon oxides thus it is rarely observed in the product mixture [24,25]. The formation of hydrogen has not been reported when an oxygen-containing feed is employed. The significant amount of water is detected during the course of reaction.

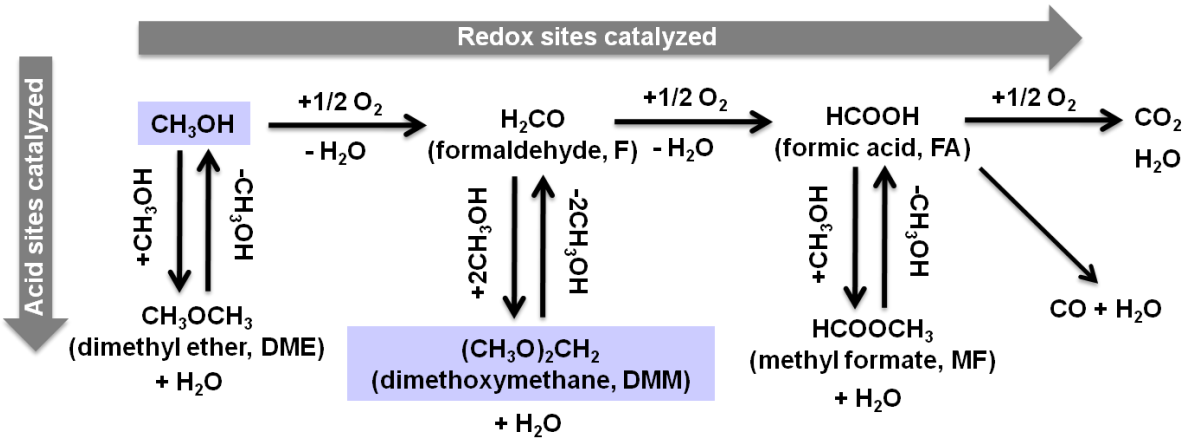

Scheme 1-1: Possible pathways of methanol reaction catalyzed by redox and acidic sites [23].

DMM or methylal is a symmetric dimetyl acetal of formaldehyde. It is a clear colourless liquid with a low boiling point, low viscosity, an excellent dissolving power and a pungent chloroform-like odour. It is also highly flammable and moderately irritating to eyes. The main properties of DMM are shown in Table 1-2.

Table 1-2: Main characteristics of dimethoxymethane [26].

Molecular formula	$C_3H_8O_2$
Molecular weight	76.09 $g.mol^{-1}$
Density	0.86 $g.mL^{-1}$ at 25 °C
Boiling point	42 °C
Melting point	-105 °C
Water solubility	soluble
Vapor pressure	43.98 kPa at 20 °C
Relative vapor density (air = 1.0)	2.63
Flash point	-18 °C
Auto-ignition temperature (°C)	-
Explosive limits (lower-upper)	1.6-17.6 vol. % in air

DMM is distinguished by its versatility for various applications. It is widely used as a solvent and as a starting material in the fragrance and pharmaceutical industries [27]. It is applied as a starting monomer in the synthesis of polyoxymethylene dimethylether (POMM), which could be used as a safe embalming agent in substitution of the currently used formaldehyde [28], a well-known human carcinogen. DMM and POMM are also considered as alternative fuels for low-temperature fuel cells, much safer than methanol, due to, *e.g.*, for POMMs lower volatility [29-32]. More importantly, DMM finds also an application as an oxygenated additive to diesel fuel, particularly helping in the reduction of particles emissions, of which the great harm to human health has been recently widely covered by the media [33,34].

Production of DMM at the industrial scale is being currently carried out in a sequential way *via* two consecutive steps: gas phase methanol partial oxidation to formaldehyde, which is followed, in a second dedicated reactor, by liquid phase acetalization of the so-obtained formaldehyde with methanol molecules [35-44]. Formaldehyde is manufactured in the industrial markets today by catalytic conversion of methanol using two major types of catalysts, *i.e.*, those are based on silver and iron molybdate [45-50]. Formaldehyde is produced in the silver-catalyzed process either by dehydrogenation (Eq. 10) or partial oxidation reaction of methanol (Eq. 11). The industrial plant operates at atmospheric pressure using a feed rich in methanol (50 % v/v) at 560-600 °C [47]. Methanol conversion per pass in the reactor is of 65-75 % and unconverted methanol is then separated from the reactive medium and recycled to achieve as high as 89 % yield in formaldehyde [51].

$$CH_3OH \rightarrow HCHO + H_2 \qquad (\Delta H^0 = +85\ kJ.mol^{-1}) \qquad (10)$$

$$CH_3OH + ½O_2 \rightarrow HCHO + H_2O \qquad (\Delta H^0 = -156\ kJ.mol^{-1}) \qquad (11)$$

Formaldehyde is produced only by methanol partial oxidation over iron molybdate catalysts. The process also operates at atmospheric pressure but with a much lower concentration of methanol, *i.e.*, 7 vol. % of methanol in air is fed into the reactor. An excess of air is used to ensure a maximum conversion of methanol and to avoid the explosive limits of methanol-air mixture which is located between 7-37 vol.% CH_3OH in air [47]. To assure the catalyst stability, the reaction temperature should not exceed 400 °C. This is also to limit side reactions, especially the dehydration of methanol to ether. The formaldehyde yield obtained from the iron molybdate catalyzed process is as high as 95 % with up to 98-99 % methanol conversion. In comparison to the silver catalyst, the iron molybdate is less sensitive to contamination by impurities in air, *i.e.*, CO_2, CH_4, and N_2O, and in methanol, *e.g.*, acetone. The average lifetime of iron molybdate catalyst is about 6 to 12 months which is longer than that of the silver catalyst that lasts typically only for 2-4 months [52].

In general, DMM is produced by a liquid phase condensation of formaldehyde and methanol over acidic catalysts. Since the early 70's a number of patents has been filed aimed at synthesizing DMM applying various types of solid catalysts. The Hiag-Werke AG used mineral acids, *e.g.*, H_2SO_4 and H_3PO_4, in a distillation column fed with methanol and formaldehyde. A maximum yield in DMM of 98 % is reported [53]. The VEB Leuna-Werke 'Walter Ulbricht' report the use of zeolites LZ40 as catalysts in an autoclave reactor and they claim that a selectivity to DMM of 90 % is achieved [54]. Shujuan mentions the feasibility of using HZSM-5 as a catalyst in the procedure for synthesis of DMM in an intermittent reactor at 20-100 °C [55]. In the patent filed by Asahi Chemical & Industry, Co., Ltd., alumina silicates are used for the liquid phase DMM formation from a mixture of methanol and formaldehyde and 99 % DMM yield is obtained [56]. They also report cation-exchanged Amberlite® 120B and sulfonated tetrafluoroethylene Nafion®-H resins as the active catalysts. Similar results are obtained by G. Lambiotte & Cie S.A with Amberlite® 15 wet resin [57] and by Asahi Chemical & Industry, Co., Ltd. using Amberlyst® 35 resin [58].

In the late 90's, the BP Corporation files a number of patents involving a two-steps consecutive process for preparation of polyoxomethylene dimethyl ether (POMM) from methanol and/or dimethyl ether, with DMM as a main product [37-59]. The first step consists

in the oxidation of methanol and/or DME to formaldehyde in the gas phase using the usual silver or copper containing catalysts, except in the [38] and [41] patents where tungsten and doped molybdenum oxides are applied respectively. In the second step the condensed formaldehyde is brought into contact with methanol and/or DME in a distillation column containing the acidic catalysts. Mostly, MFI zeolites are used at this stage nonetheless the acidic resins are also found active for DMM formation in the patents [37] and [60].

Synthesizing DMM *via* a single step direct route starting from methanol would obviously be preferred, thus minimizing not only the Capital Expenditure (CAPEX) and the production cost but also energy consumption besides reducing the environmental impact occurred along the two-steps process. In this respect, developing selective catalysts for the one step conversion of methanol to DMM is challenging, and has become a relatively widespread research subject in the recent years [61-80]. It has been reported that the direct reaction is strongly sensitive to the nature and strength of the catalytic active sites [23]. A schematic representation of the main products obtained from the oxidation reaction of methanol with respect to the acid and redox characters of active sites is depicted in Scheme 1-2. Tatibouët *et al.* [23] suggests that the formation of F requires a weak acidic center with low oxidizing power. If the site is more acidic, the residence time of F species becomes long enough to form an intermediate, dioxymethylene [81]. This intermediate can react further with methanol to form DMM. However, the oxidizing power of the active center cannot be too high that the dioxymethylene species is oxidized before its reaction with methanol. If the site is too acidic and possesses strong oxidizing power, the intermediate species are oxidized (i) into formate species which then reacts with methanol to form MF, or (ii) further oxidized in a greater extent to carbon oxides. The formation of DME highlights the highly acidic character. DME is a major product formed when the strong acid site with low oxidizing power is present.

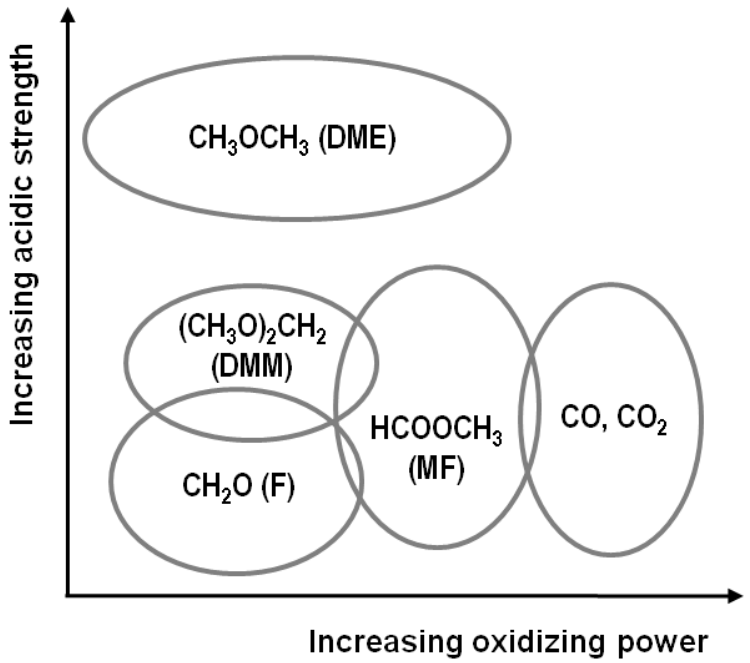

Scheme 1-2: Products obtained from the oxidation reaction of methanol depending on the properties of the active site adapted from [23].

Indeed, as shown in Scheme 1-2, an appropriate system for the direct synthesis of DMM should be a bifunctional catalyst in order to guide the reaction through the desired pathways leading to DMM. Various studies aimed at realising the direct synthesis of DMM from methanol over a variety of heterogeneous catalytic systems, *i.e.*, molybdenum-based catalysts [61] heteropolyacids (HPAs) [62], oxides of ruthenium [63] and of rhenium [64-69], vanadium-based catalysts [70-79], as well as amorphous mixed oxides of Mo, V, W, Cu, and Sb [80] can be found in the literature. In the studies reporting the use of bulk and supported 12-molybdophosphoric acid catalysts, up to 55 % of DMM selectivity is obtained at low methanol conversion of less than 20 % [61]. The presence of β-MoO_3 phase in the catalyst is claimed in the study to be relevant for the DMM formation. Liu *et al.* investigated the performances of supported $H_{3+n}V_nMo_{12-n}PO_{40}$ polyoxometallate Keggin clusters. They report a selectivity to DMM of 58 % at a methanol conversion of 68 % over 9.2 wt.% supported $H_4PVMo_{11}O_{40}/SiO_2$ [62]. Besides, after selective poisoning of surface protons by using an organic base, they are able to inhibit the formation of DME and thereby increase the selectivity of DMM to 80 % at 180 °C. The same authors, Liu *et al.*, further examined the performances of a completely different system, namely RuO_2 supported on SnO_2, ZrO_2, TiO_2, Al_2O_3 and SiO_2 prepared by incipient wetness impregnation method [63]. Catalytic performances were tested at low temperatures, *i.e.*, 27-127 °C, and atmospheric pressure in a

fixed-bed reactor. The so-obtained methanol oxidation rates and selectivities over supported RuO_2 catalysts compared at approximately 20 % conversion are listed in Table 1-3. At 120 °C, the oxidative dehydrogenation (ODH) turnover rates per exposed Ru atoms are about 1.5 times greater when RuO_2 is supported on SnO_2 than on ZrO_2 and TiO_2, and 2.5-4 times greater than when RuO_2 is supported on Al_2O_3 and SiO_2. The effect of supports on the ODH rates is ascribed to the effects of supports on RuO_x reducibility. Temperature-programmed reduction profiles show that the reduction peak temperatures increase by 30 °C as the support is changed from SnO_2 to ZrO_2, TiO_2, Al_2O_3, and SiO_2. The supports also influence the product selectivities on RuO_x-based catalysts. As shown in Table 1-3, acid function on Al_2O_3 and SiO_2 surfaces favors DMM formation with 57.4 and 56.1 % selectivities, respectively. SnO_2, ZrO_2, and TiO_2, of which the redox function is more pronounced, preferentially form methyl formate with 61, 71, and 70 %, respectively. These effects of supports on selectivity suggest that the secondary reaction of formaldehyde, which is a primary product from the ODH reaction, possibly occurs on the support surfaces or that the surfaces themselves can intercept the reaction intermediate required for further synthesis of DMM and MF. A maximum DMM selectivity of 67 % is, however, reported in this work over a 4.4 wt.% Ru/Al_2O_3 catalyst at low temperature (60 °C) using higher methanol pressure of 80 kPa. This observation is ascribed to that the reaction to form DMM is thermodynamically favored at low temperatures and the thermodynamic limitations are less severe when methanol partial pressure increases.

Table 1-3: Methanol oxidation rates and selectivities on supported RuO_2 catalysts adapted from [63].

Catalyst (Ru wt. %)	Ru surface density (Ru/nm^2)[a]	Reactants ($CH_3OH/O_2/N_2$, kPa)	Temperature (°C)	ODH turnover rate ($mol/g_{atom\ Ru\text{-}surf}.h$)[c]	Selectivity (%)		
					F	MF	DMM
RuO_2/TiO_2 (2.2 %)	3.1	4/9/1[b]	120	84.7	25.2	69.9	4.1
RuO_2/ZrO_2 (4.1 %)	2.1	4/9/1[b]	120	88.9	6.6	70.7	5.6
RuO_2/SnO_2 (4.1 %)	2.5	4/9/1[b]	120	142.3	20.0	60.7	15.5
RuO_2/SiO_2 (4.3 %)	1.1	4/9/1[b]	120	41.5	12.4	31.0	56.1
RuO_2/Al_2O_3 (4.4 %)	1.3	4/9/1[b]	120	71.0	11.6	30.1	57.4
RuO_2/SnO_2 (4.1 %)	2.5	80/18/2	60	19.9	1.6	57.3	40.8
RuO_2/Al_2O_3 (4.4 %)	1.3	80/18/2	60	9.5	9.4	23.4	66.8

[a] Based on the Ru content and the individual BET surface area; [b] With 96 kPa balance He; [c] Rate for primary methanol oxidative dehydrogenation to formaldehyde.

Iwasawa and co-workers focused their investigations on ReO_x compounds and Re-based mixed oxides supported on various solids, *i.e.*, TiO_2, SiO_2, V_2O_5, ZrO_2, α-Al_2O_3, α-Fe_2O_3, and γ-Fe_2O_3 [64]. The $SbRe_2O_6$ compound is reported for its good performance in DMM formation. It converts 6.5 % of methanol at 300 °C and provides as high as 92.5 % DMM selectivity [65]. The performances were determined in a fixed-bed reactor at atmospheric pressure. The catalyst was pretreated *in situ* under He flow at 300 °C for 1 h before catalytic reaction. The reactant mixture of CH_3OH/O_2/He was adjusted to 4.0/9.7/86.3 mol.% with 10 $L.h^{-1}.g_{cat}^{-1}$ space velocity. It is suggested that the performance of crystalline $SbRe_2O_6$ catalyst is correlated to the rhenium oxide connecting with Sb-O chains. No structural change in the bulk and surface of the catalyst is observed during and after reaction at 300 °C, with respect to the XRD, Raman, XPS, and SEM results. The performance of $SbRe_2O_6$ catalyst is also checked at higher temperature (400 °C). Interestingly, the conversion of methanol increases sharply to 86.2 % while keeping a high selectivity of 85.4 % towards DMM formation. Nevertheless, the surface area of $SbRe_2O_6$ (1 $m^2.g^{-1}$) and the loss of rhenium atoms through volatility under O_2 can be a disadvantage in its commercial applications.

The unique performances of supported Re oxide catalysts were examined by Yuan and Iwasawa [66]. Re oxide supported on TiO_2 (rutile), TiO_2 (anatase), V_2O_5, ZrO_2, α-Fe_2O_3, γ-Fe_2O_3, SiO_2, α-Al_2O_3, Sb_2O_3, Bi_2O_3, and MoO_3 were prepared by incipient wetness impregnation using an aqueous solution of NH_4ReO_4 and were calcined at 400 °C in He. The samples were further treated *in situ* at 300 °C for 1 h before use. Catalytic performances in methanol oxidation on supported Re oxides with 10 wt.% Re loading at 240 °C are summarised in Table 1-4. Among the tested catalysts, 10 wt.% Re/γ-Fe_2O_3 is found to be the most efficient one in DMM production with 91 % selectivity to DMM at 48 % conversion of methanol. It is suggested that the redox ability of Re oxides, $Re^{VI-VII} \leftrightarrow Re^{IV}$, is responsible for the catalytic performance, although appropriate Lewis acidity of the Re oxides is also necessary for the acetalization of formaldehyde with methanol to DMM. The oxide supports also prevent Re oxides from being sublimated and reduced to ReO_2 particles.

Table 1-4: Catalytic performances in methanol oxidation on supported Re oxides at 240 °C adapted from [66].

Catalyst	S_{BET} ($m^2.g^{-1}$)	CH_3OH conv. (mol.%)	Selectivity (mol.%)				
			HCHO	$CH_2(OCH_3)_2$	$(CH_3)_2O$	$HCOOCH_3$	CO_x
Re/TiO_2 (rutile)	5	53.7	1.9	83.1	0.7	9.1	5.2
Re/TiO_2 (anatase)	50	59.5	4.1	78.5	1.1	11.7	4.6
Re/V_2O_5	6	21.5	0.0	93.7	4.3	0.0	2.0
Re/ZrO_2	9	35.8	2.0	89.4	trace	7.6	1.0
Re/ α-Fe_2O_3	3	15.5	2.0	90.5	1.0	6.0	0.5
Re/γ-Fe_2O_3	16	48.4	2.4	91.0	1.0	4.6	1.0
Re/SiO_2	36	15.1	1.3	60.7	trace	11.9	26.1
Re/α-Al_2O_3	10	16.3	2.8	88.3	trace	5.9	2.9
Re/MoO_3	5	9.1	0.0	80.0	19.0	0.0	1.0

Experimental conditions: $CH_3OH/O_2/He$ = 4.0/9.7/86.3 mol.%, GHSV = 40 $L.h^{-1}.g_{cat}^{-1}$, atmospheric pressure, fixed-bed reactor; $CO_x = CO+CO_2$

Following the results of Iwasawa's group, Sécordel *et al.* [68] concentrated their study on supported TiO_2 (anatase) and SiO_2 oxorhenate system. The catalysts were prepared by oxidative thermal spreading of metallic Re^0 under dry condition, with the purpose to maintain the catalysts in the dehydrated conditions and thus preventing the volatilization of $HReO_4$. The supports were mixed with rhenium powder and the mixture was mechanically ground before *in situ* calcination under pure O_2 flow at 400 °C. The catalytic activity was measured in a fixed-bed reactor at atmospheric pressure. Typical reaction conditions, *i.e.*, $CH_3OH/O_2/He$ = 4/16/80 mol.% and GHSV of 26 $L.h^{-1}.g_{cat}^{-1}$, were employed. A maximum DMM selectivity of 77 % at 44 % methanol conversion is claimed over a Re/TiO_2 catalyst at 260 °C.

An attempt to use vanadium-containing catalysts has also been described by several groups. Fu *et al.* [70] demonstrated that the selectivity of DMM can be greatly increased by doping the traditional supported V_2O_5/TiO_2 catalyst with $Ti(SO_4)_2$ [71]. $Ti(SO_4)_2$ was added onto the V_2O_5/TiO_2 catalysts by incipient wetness impregnation method, followed by calcination at 400 °C. The catalytic tests were carried out in a glass reactor at atmospheric pressure using the feed comprises of 2 $mL.min^{-1}$ of CH_3OH, 6 $mL.min^{-1}$ of O_2, diluted in 30 $mL.min^{-1}$ of N_2. The catalysts were activated at 400 °C for 1 h in a flow of O_2/N_2 (6:30 $mL.min^{-1}$) prior to the tests.

The selectivity to DMM is greatly improved with the addition of $Ti(SO4)_2$ onto the V_2O_5/TiO_2 even at high conversion (Table 1-5). 88.6 % DMM selectivity is obtained at 60 % methanol conversion with the acid-modified $10\%V_2O_5/TiO_2$-$Ti(SO_4)_2$ catalyst whereas only 10.9 % selectivity is found at 40.7 % conversion for the V_2O_5/TiO_2 one. This suggests that the surface acidity of V_2O_5/TiO_2 is not strong enough to effectively catalyse the condensation reaction. Thereby, the production of a large amount of F as well as MF is observed in agreement with the assumptions of Tatiboüet *et al.* [23]. With the acid modification, the condensation of F with methanol is significantly promoted. A higher DMM selectivity of 92 % at 48 % methanol conversion is reported, however, over the V_2O_5/TiO_2-$Ti(SO_4)_2$ catalyst containing less amount of V_2O_5 (5 %). This performance is as good as that of 10 wt.% Re/γ-Fe_2O_3 cited in the work of Iwasawa group [66]. However, the V_2O_5/TiO_2-$Ti(SO_4)_2$ catalyst is more active than the supported Re/γ-Fe_2O_3. This is considering the fact that the rate of conversion of methanol over the supported vanadia is approximately 50 % higher although the reaction takes place at 80 °C lower temperature.

Table 1-5: Selective oxidation of methanol over V_2O_5/TiO_2 and V_2O_5/TiO_2-$Ti(SO_4)_2$ catalysts [70] in comparison with Re/γ-Fe_2O_3 catalyst [66].

Catalyst	S_{BET} ($m^2.g^{-1}$)	T(°C)	CH_3OH conv.(%)	Selectivity (%)				Rate[a]/mmol g^{-1} h^{-1}	
				DMM	F	MF	DME	CH_3OH	DMM
$10\%V_2O_5/TiO_2$	92	160	40.7	10.9	61.0	27.5	0.7	195	7.1
$10\%V_2O_5/TiO_2$-$Ti(SO_4)_2$	95	160	60.0	88.6	1.2	9.8	0.4	287	85
$5\%V_2O_5/TiO_2$-$Ti(SO_4)_2$	82	160	48.2	91.6	0.1	6.0	2.4	462	141
$10\%Re/\gamma$-Fe_2O_3	16	240	48.4	91.0	2.4	4.6	1.0	319	97

[a]Rate of conversion of methanol and formation of DMM based on the unit mass of V or Re.

Lu *et al.* [76] also prepared a series of supported V_2O_5/TiO_2 catalysts further modified with sulphuric acid for the selective oxidation of methanol. The V_2O_5/TiO_2 samples were typically prepared by incipient wetness impregnation of TiO_2 with aqueous NH_4VO_3 solution, followed by drying at 100 °C, and calcination at 420 °C. The sample was further impregnated with H_2SO_4 solution, followed by drying at 100 °C, and calcination at 400 °C. The influence of V_2O_5 and SO_4^{2-} contents in the catalysts on redox and acidic properties was examined as well as the performances in methanol reaction. The tests were carried out in a fixed-bed reactor at atmospheric pressure. The catalysts were first activated *in situ* in air at 400 °C for 1 h.

The molar ratio between methanol and oxygen in the feed was 3 and the space velocity was adjusted to 1200 h^{-1}.

The surface acidity increases significantly with the amount of SO_4^{2-} used in the acid modification. However, the acid strength is found to decrease simultaneously with V_2O_5 loading. The content of V_2O_5 should not exceed 15 % in order that the catalytically active vanadium species are highly dispersed on the V_2O_5/TiO_2 surface. As a compromise between the dispersion of vanadia species as well as the balance between redox and acid functions, the catalyst loaded with 15 wt.% V_2O_5 and 15 wt.% SO_4^{2-} is declared as the best catalyst in DMM formation. 93 % selectivity to DMM at 49 % methanol conversion at 150 °C is reached over this catalyst.

Supported vanadia catalysts were also of interest to Chen *et al.* [77] who studied performances of VO_x supported on TS-1 zeolite doping with SO_4^{2-} and PO_4^{3-} ions. The TS-1 zeolite was selected as a support due to its high surface area and excellent stability. The catalysts were prepared by incipient wetness impregnation of VOx/TS-1 with aqueous $(NH_4)_2SO_4$ or $(NH_4)_2HPO_4$ solutions. The selective oxidation of methanol was carried out in a fixed-bed reactor at atmospheric pressure with space velocity of 4000 h^{-1}. Despite the fact of using a reactant feed within the flammable region – *i.e.*, methanol/O_2/N_2 = 1/2.5/7.5 (v/v), the authors report a positive effect when adding SO_4^{2-} into VO_x/TS-1 catalyst that the so-obtained methanol conversion is significantly higher (46 % compared with 24 % for the unmodified catalyst) with essentially the same selectivity (81 % *vs.* 83 %). Addition of SO_4^{2-} ions facilitates the reduction of vanadia as evidenced in TPR profiles showing that the reduction peak temperature of the SO_4^{2-} doping VOx/TS-1 catalyst shifts to lower temperature compared to the undoped catalyst. The enhanced redox ability thus promotes the reaction of methanol to formaldehyde. Furthermore, the number of acid sites increases after the SO_4^{2-} addition with respect to pyridine infrared spectroscopy measurements. Therefore, this improvement in surface acidity helps promoting the acetalization reaction and increasing DMM formation.

Guo *et al.* prepared the V_2O_5/CeO_2 catalyst samples and applied in the selective oxidation of methanol [78]. The catalysts were prepared by the sol-gel method using NH_4VO_3, $Ce(NO_3)_3$, and citric acid as precursors. Their performances were tested in a fixed-bed reactor at atmospheric pressure using the feed comprised of $CH_3OH/O_2/Ar$ = 6/9.4/84.6 v/v. The catalysts were activated in a flow of 10% O_2-90 % Ar at 400 °C for 1 h prior to the tests.

At 160 °C, 90 % of selectivity to DMM at 17 % conversion of methanol is reported over the V_2O_5/CeO_2 catalyst loaded with 15 wt.% V_2O_5.

Developments of Sb-, V-, and Nb-containing catalysts for the oxidation of methanol were also described recently by Golinska-Mazwa *et al*. [79]. It is found that, by using a proper synthesis procedure for $SbVO_x$ mixed oxides and further modification with Nb species, it is possible to obtain a selective catalyst for DMM production. The authors synthesized $SbVO_x$ oxides catalysts with and without using Pluronic P123 as a template. The precursors of Sb ($(CH_3COO)_3Sb$ in tartaric acid) and V (aqueous NH_4VO_3) were added to the solution of Pluronic P123 in the template-assisted preparation. The catalysts were calcined at 540 °C in He. The use of template during the synthesis increases the surface area and pore volume of the final material. All the prepared catalysts contain rutile binary oxides $SbVO_4$ in which reducible oxovanadium species play a role on active centres in the methanol oxidation. Interestingly, the sample prepared in the presence of a template contains some amounts of $\alpha-Sb_2O_4$ phase. Sb_2O_4 is a p-type semiconductor thus the electron can transfer from vanadium species in $SbVO_x$ to Sb_2O_4 at the interface of these two phases. This electron transfer induces the formation of oxygen vacancies and thus promotes the chemisorption of O_2. The O^{2-} then spills over the interface and partially reoxidizes the vanadium species. This contributes to the increase in the catalytic activity (8 % *vs.* 26 %) as shown in Table 1-6. The catalyst synthesized in the presence of a template produces F as a major product, indicating the presence of weak acid/redox sites on the catalyst surface. Besides, significant amounts of MF and CO_2 are formed, indicating that stronger redox and medium acid centres are present on the surface. With the addition of niobium in the template-prepared catalyst, the catalytic performances are much improved. The conversion of methanol increases from 26 % on the Nb-free catalyst to 34 % on the $Nb/SbVO_x$(P123). The selectivity in DMM increases drastically (39 % *vs.* 4 %) at the expense of lower F selectivity (56 % *vs.* 27 %). This behavior is explained by the change in acidic strength resulting from Nb-V interaction and by a decrease in the amount of active oxygen on the $SbVO_x$ surface after the addition of Nb. The Nb-V interaction induces stronger F chemisorption on the surface. Thereby, the further interaction of F with methanol molecules is more favourable, facilitating the DMM formation.

Table 1-6: Steady-state conversions and selectivities obtained from Sb-V-Nb containing catalysts in methanol oxidation reaction adapted from [79].

Catalyst	CH_3OH conv. (%)	Selectivity (%)				
		F	DME	MF	DMM	CO_2
$SbVO_x$	8	40	46	3	11	Traces
$SbVO_x$(P123)	26	56	1	26	4	13
$Nb/SbVO_x$(P123)	34	27	1	4	39	29

Experimental conditions: fixed-bed reactor, atmospheric pressure, T = 150 °C (except that of $SbVO_x$ prepared without a template of which T = 200 °C), $CH_3OH/O_2/Ar$ = 4/8/88 mol.%, total flow = 40 $mL.min^{-1}$.

The use of amorphous oxide catalyst of the general formula $Mo_{12}V_3W_{1.2}Cu_{1.2}Sb_{0.5}O_x$, synthesized by a simple straightforward coprecipitation procedure, was reported by our team for the selective oxidation of methanol in gas phase [80]. Methanol reaction was carried out in a fixed-bed reactor at atmospheric pressure. The reaction feed was composed of 7.5 vol.% of CH_3OH, 8.5 vol.% of O_2 in He. The space velocity was adjusted to 22 $L.h^{-1}.g_{cat}^{-1}$. As high as 90 % DMM selectivity can be achieved at high methanol conversion of 68 % (280 °C), after preactivation of the $Mo_{12}V_3W_{1.2}Cu_{1.2}Sb_{0.5}O_x$ catalyst in pure oxygen at 340 °C for 1 h. The catalyst is also found promising for the industrial application as it can work in a wide range of reaction temperatures and methanol concentrations without a drastic loss in DMM selectivity.

1.3.2 Diethoxyethane synthesis from ethanol

The possible pathways of ethanol reaction are depicted in Scheme 1-3. The redox sites enable the production of partially oxidized species, *i.e.*, acetaldehyde (ACD) and acetic acid (AA), or totally oxidized species including CO and CO_2. Acid sites enable dehydration or condensation reactions yielding ethylene (ETH), diethyl ether (DETH), ethyl acetate (EA) and the target acetal *1,1*-diethoxyethane (DEE).

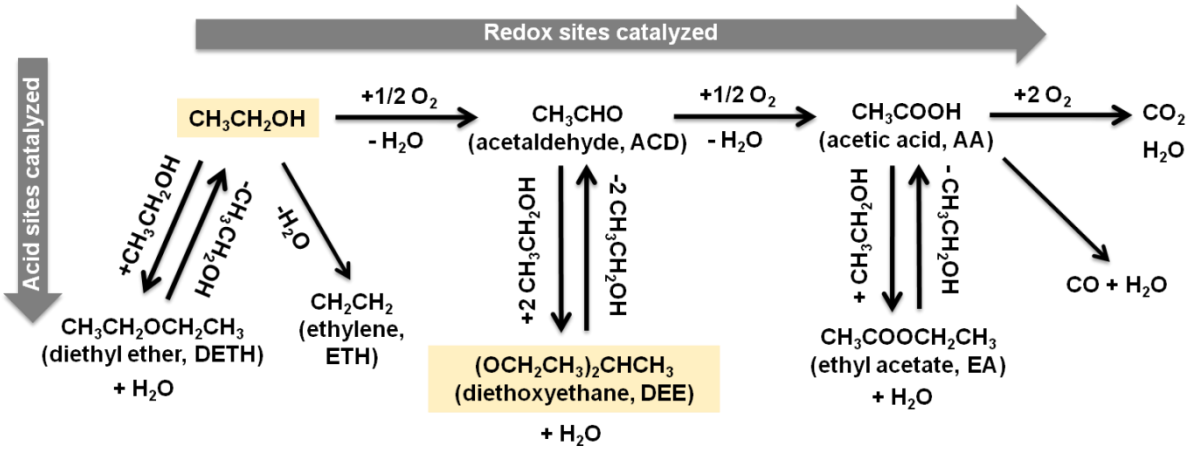

Scheme 1-3: Possible pathways of ethanol reaction catalyzed by redox and acidic sites.

DEE is considered a promising oxygenated additive to diesel blends [82-84], with the advantage of keeping or even increasing the cetane number [85] while being helpful in the efficient combustion of the resulting blend [57]. DEE can be incorporated into gasoline [86]. It can also be incorporated in ethanol fuel helping to decrease the auto ignition temperature [87]. DEE is an important raw material used for pharmaceutical products [88,89] and for synthetic perfumes, helping to increase the resistance to oxidation and therefore increases lifetime of the fragrances [90]. It is also an intermediate for the synthesis of polyacetal resins which are employed in exterior parts of automobiles, components of electric and office appliances, printers, and televisions [89,91].

Physically, DEE is a clear colourless liquid with a low boiling point, low viscosity, an excellent dissolving power and a pungent odour. Liquid DEE, as well as its vapour, is also highly flammable and irritating to eyes and skin. The main properties of DEE are shown in Table 1-7.

Table 1-7: Main characteristics of *1,1*-diethoxyethane adapted from [21,92].

Molecular formula	$C_6H_{14}O_2$
Molecular weight	118.17 $g.mol^{-1}$
Density	0.831 $g.mL^{-1}$ at 25 °C
Boiling point	102 °C
Melting point	-100 °C
Water solubility	5.0 $g.100mL^{-1}$
Vapor pressure	2.7 kPa at 20 °C
Relative vapor density (air = 1.0)	4.08
Flash point	-21 °C
Auto-ignition temperature	230 °C
Explosive limits (lower-upper)	1.65-10.4 vol. % in air

DEE is manufactured at the industrial scale by means of a two-step process in which acetaldehyde, which is first produced from ethanol or ethylene oxidation (step 1), is subsequently reacted with ethanol over an acid catalyst (step 2) [93]. Acetaldehyde is being produced industrially on a large scale *via* the Hoechst-Wacker process involving the oxidation of ethylene ($CH_2=CH_2$) by oxygen in water in the presence of tetrachloropalladate ($PdCl_2/CuCl_2$) catalyst [94,95]. However, the partial oxidation of ethanol is also considered as an alternative route for preparing acetaldehyde in the small volume of production. The commercial process for the oxidation of ethanol into acetaldehyde has been operated since the early 70's using a catalyst based on silver at temperatures between 370-450 °C.

The synthesis of DEE is typically conducted under conditions of homogeneous catalysis, with strong liquid inorganic acids like sulphuric and phosphoric acids as catalysts [96]. The use of these strong acids brings some disadvantages, *e.g.*, equipment corrosion at a high catalyst concentration and the difficulty in separation, due to the fact that the catalysts are dissolved in the reaction medium. To overcome these issues, application of heterogeneous catalysts is more desirable. The solid acid catalysts of various types from natural, laboratory, and commercial sources in the synthesis of DEE were summarized by Capeletti *et al.* [97] as shown in Table 1-8. After textural characterizations and acidity measurement, the performances of these catalysts were evaluated in the liquid phase acetalization of ethanol and acetaldehyde following the stoichiometric proportion under mild conditions (20 °C and atmospheric pressure). The authors conclude that all the catalysts are active. However the

resin Amberlyst® 15 resin, which exhibits the highest acidity and the lowest specific surface area, gives the best performance in terms of ethanol conversion of 50 % at equilibrium. In addition, an inhibitory effect of water formed in the reaction is reported, especially if it is adsorbed on the surface of the catalyst.

Table 1-8: Properties of acidic catalysts used in [97].

Catalyst	Surface area ($m^2.g^{-1}$)	Pore volume ($mL.g^{-1}$)	Acidity ($meq.g^{-1}$)
Polystyrene-polydivinylbenzene sulfonic resin (Amberlyst® 15), Rohm and Hass	45	0.360	4.7[a]
Acid-treated montmorillonite, Aldrich	345	0.564	0.273
Mordenite, Norton	436	0.210	0.649
Natural acid treated montmorillonite	235	0.262	0.640
Zeolite FCC catalyst, Fresh BR1160, Engelhard, UCS: 24.72 Å	342	0.259	0.540
Zeolite FCC catalyst, Isoplus 1000, Engelhard, UCS: 24.40 Å	336	n.a.	0.474
Amorphous FCC catalyst, HA-HPV, Ketjen 25 % Al_2O_3	454	0.688	0.382
Amorphous FCC catalyst, LA-LPV, Ketjen 12 % Al_2O_3	559	0.642	0.350
Equilibrium zeolite FCC catalyst, BR1160, Engelhard, UCS : 24.31 Å	175	0.213	0.065
Equilibrium zeolite FCC catalyst, Octavision, FCC S.A., UCS : 24.24 Å	151	0.120	0.160

[a]H+ milliequivalent g^{-1} of dry resin

Similar type of macroreticular resin namely Amberlyst® 18, with particle diameter of 265 µm, inner surface area of 30 $m^2.g^{-1}$, and ion-exchange capacity of 4.5 meq $H^+.g^{-1}$ of dry resin, was used by Silva and Rodrigues [98] as the catalyst in the liquid phase reaction of ethanol and acetaldehyde to produce DEE in a perfectly stirred batch reactor. Thermodynamic datas for the synthesis of DEE as well as the effect of temperature, initial molar ratio of reactants and pressure on reaction kinetics were described. A reaction mechanism and an equation rate with experimentally measured kinetic parameters were also reported. The thermodynamic equilibrium constant was measured in the temperature range of 20-60 °C. The reaction is found exothermic with the standard enthalpy, ΔH^0, at 25 °C of −10225.9 $J.mol^{-1}$ and the standard entropy (ΔS^0) of −33.395 $J.mol^{-1}.K^{-1}$, leading to the standard free energy (ΔG^0) of −269.3 $J.mol^{-1}$. Kinetic experiments show that the system pressure has no effect on the reaction rate at low temperatures (10-20 °C). The formation of DEE is not much affected by the initial ratio of ethanol and acetaldehyde however the greater equilibrium extent of acetal is observed for the stoichiometric ratio of 2. The proposed rate expression is based on Langmuir

adsorption isotherms. The activation energy of acetalization reaction is found to be 47.874 $kJ.mol^{-1}$.

It appears that the synthesis of DEE from ethanol and acetaldehyde is controlled by chemical equilibrium, leading to low conversions in conventional reactor systems. The equilibrium conversion is 59 % and the reaction is more favorable at low temperatures. The reactive mixture also exhibits three binary azeotropes (ethanol/water, ethanol/ DEE, and DEE/water) and one ternary azeotrope (ethanol/water/DEE). Thereby, the separation of products through conventional distillation is somewhat difficult. To overcome these obstacles, several methods have been proposed in literature [93] described hereafter.

In order to obtain an acceptable yield in DEE, the reaction equilibrium must be shifted towards the acetal formation. This can be accomplished, firstly, by using a large excess of one of reactants, usually ethanol. The surplus of reactant must then be extracted from the desired product in a purification step after reaction. Secondly, water must be eliminated by azeotropic distillation between a solvent and water. In this case, the boiling points of the constituents in the reaction medium must be compatible with the azeotrope and the solvent and water must be partially miscible. Alternatively, the use of innovative reactor systems which combine chemical reaction and products separation, *e.g.*, reactive distillation [99] and simulated moving-bed reactor (SMBR) [93,100], can be applied to remove the desired product from the reaction medium, to enhance the conversion of reactants above the equilibrium limit. However, the idea to operate reactive distillation in the production of DEE is not feasible. As the boiling points of DEE and water are really close (102 *vs.* 100 °C), one cannot ensure their separation in distillative columns. The SMBR technology, however, was successfully implemented in the synthesis of DEE from the reaction between ethanol and acetaldehyde by Silva and Rodrigues [93]. The DEE production and separation with 87 % purity at acetaldehyde conversion as high as 98 % using Amberlyst® 15 resin are achieved.

The addition of an organic solvent in the reaction mixture, in which DEE is highly soluble in the solvent and water is almost insoluble, has been proposed to displace the equilibrium towards acetal production and thus to increase the ethanol conversion. The use of solvents such as kerosene, toluene, carbon tetrachloride, benzene, hexane, etc. has been reported in the literature [101,102]. The synthesis of DEE from ethanol and acetaldehyde was studied by *Gomez et al.* [103] in a continuous flow fixed-bed reactor using Amberlyst® 15-wet resin as a catalyst. Catalytic performances were evaluated and compared under the absence and the

presence of *n*-hexane in the reactant feed. The results clearly point out that the addition of *n*-hexane to the feed mixture helps increasing the catalyst activity. The initial conversion of 59 % is obtained at 20 °C. The conversion remains stable for approximately 17 h and then continuously decreases to 25 % after 63 h of reaction. When the reactants-solvent feed is employed, the initial conversion is significantly higher, *i.e.*, 73 %. The conversion gradually decreases with time on stream, and reaches 61 % conversion after 65 h. This value is, however, obviously above the one obtained in the absence of solvent. The adverse effect of water formed during the reaction is diminished when *n*-hexane is added to the reactants mixture. Water mostly separates from the organic reaction phase thus the reversible reaction between DEE and water can be suppressed. However, the amount of DEE produced is not improved when the *n*-hexane was present.

Producing DEE *via* a one step process would enable lower production costs and be more environmentally favorable. The scientific literature concerning a direct synthesis of DEE from ethanol is scarce compared to those reported for the DMM synthesis. Only three publications [63,104,105] and one patent [106] have particularly reported the direct selective oxidation of ethanol aimed at producing DEE as a main product. Liu *et al.* [63] studied the gas phase selective oxidation of ethanol over RuO_2 supported on silica and tin oxides catalysts prepared by incipient wetness impregnation of SiO_2 and $Sn(OH)_4$ with aqueous solution of $Ru(NO)(NO_3)_3.xH_2O$. The freshly prepared samples were simply dried under ambient air at 125 °C overnight and then in dry air stream at 400 °C for 2 h before using in the tests. Ethanol reactions were carried out in gas phase using a fixed-bed reactor at atmospheric pressure and catalytic performances were checked at low temperatures, *i.e.*, 27-127 °C. The obtained ethanol oxidation turnover rates and selectivities on SnO_2 and SiO2 supported RuO_2 catalysts at about 10-15 % ethanol conversion are listed in Table 1-9.

Table 1-9: Ethanol oxidation rates and selectivites on RuO_2/SiO_2 and RuO_2/SnO_2 catalysts at about 10-15 % conversion[a] [63].

Catalyst	C_2H_5OH pressure (kPa)	ODH turnover rate[b] ($mol/g_{atom\ Ru\text{-}total}.h$)	Selectivity (%)[c]		
			ACD	EA	DEE
RuO_2/SiO_2 (1.1 Ru/nm^2)	4	30.1	97.1	0	2.9
RuO_2/SnO_2 (2.5 Ru/nm^2)	2	50.9	97.3	2.7	0
	4	73.2	93.4	2.0	4.6
	10	83.5	64.8	2.2	33.0
	20	86.1	30.8	1.2	68.0
	40	85.9	17.6	1.4	81.0

[a] Experimental conditions: with 9 kPa O_2, 1 kPa N_2, and balance He as a diluent; reaction temperature = 120 °C; [b] Rate for primary oxidative dehydrogenation of C_2H_5OH to acetaldehyde; [c]Acetaldehyde (ACD), ethyl acetate (EA) and diethoxyethane (DEE) were predominant products, no trace of neither diethyl ether and CO_x.

The authors claim that both RuO_2/SnO_2 and RuO_2/SiO_2 catalysts are active in the studied reaction. However, the oxidative dehydrogenation rates at the same partial pressure of ethanol (4 kPa) are higher when RuO_2 is supported on SnO_2 than on SiO_2, (73.2 *vs.* 30.1 $mol/g_{atomRu\text{-}total}.h$, respectively). They refer this superior activity to the ease of reducibility of RuO_2 domains on the SnO_2 support. The effect of ethanol pressures (2-40 kPa) on ODH rates and selectivities were investigated over RuO_2/SnO_2 catalyst. The conversion rates increase with pressure from 2 to 10 kPa (51 to 84 $mol/g_{atomRu\text{-}total}.h$) and reach a constant value from pressures of 10 to 40 kPa (84-86 $mol/g_{atomRu\text{-}total}.h$). The products shift from acetaldehyde (*i.e.*, 97.3 % at 2 kPa to 17.6 % at 40 kPa), formed in the primary ODH step, to DEE (*i.e.*, 0 at 2 kPa to 81 % at 40 kPa), formed via subsequent condensation reaction being favorable at higher ethanol pressures. The maximum DEE selectivity of 81% is obtained with 40 kPa ethanol partial pressure with a high ODH turnover rate of 86 $mol/g_{atomRu\text{-}total}.h$, corresponding to about10-15 % ethanol conversion at 120 °C.

The synthesis of DEE through a tandem aerobic oxidation-acetalization of ethanol using a $Pd(OAc)_2/Cu(OAc)_2$/paratoluene sulfonic acid was studied by Bueno *et al*. [104]. At 70 °C and under 10 atm of total pressure, a DEE selectivity of 92 % at 30 % ethanol conversion is reported. The reaction occurred in liquid phase in which the solution of 0.01 M of $Pd(OAc)_2$, 0.04 M of $Cu(OAc)_2$, 0.06 M of *p*-toluene sulfonic acid (*p*-TsOH), and 0.4 M of dodecane (internal standard) in 20 mL of ethanol was transferred into the reactor pressurized with oxygen to the desired amount of total pressure. In this way, ethanol was used as a solvent

instead of chloride solution which is normally applied in Wacker-type Pd/Cu catalytic system. The presence of *p*-TsOH helps stabilizing the active Pd^{II} species in the catalytic cycle. $Cu(OAc)_2$, as a co-catalyst, helps accelerating the *β*-hydrogen elimination step leading to acetaldehyde, which is considered as the rate limiting step for most Pd-catalyzed alcohol oxidation. Nevertheless, it is notable that, applying the homogeneous catalytic system retains some drawbacks. They are mainly due to the difficulty in catalyst recovery from reaction medium and the neutralization step needed at the end of reaction.

The liquid phase conversion of ethanol into DEE and butanol was studied by Marcu *et al.* [105] over Cu-Mg-Al mixed oxide catalysts obtained from layered double hydroxides (LDH) or hydrotalcite precursors. Performances were evaluated using 50 mL of ethanol in an autoclave at temperatures between 200-260 °C and autogenic pressure under stirring. A blank experiment in the absence of any catalyst at 200 °C gives the negligible conversion of ethanol (< 0.3 %) and, surprisingly, the formation of DEE at high selectivity of 86.1 %. With the Cu-free catalyst having the Mg/Al ratio of 3 ($MgAl_{(3)}O$), the conversion and selectivity to DEE remain unchanged (0.3 % and 87.5 %, respectively). When 5 atomic % of Cu is introduced in the catalyst ($Cu_5MgAl_{(3)}O$), the conversion increases up to 4 %, the selectivity to *n*-butanol suddenly increases to 40.3 % with the significant suppression of DEE selectivity to 35.9 %. The effect of Mg/Al ratio in the $Cu_5MgAl_{(y=1-5)}O$ catalysts was also checked. The results show that varying the ratio of Mg/Al has no influence on the conversion but slightly on selectivities to *n*-butanol and DEE. Influence of the Cu content on the catalytic performances was studied over $Cu_{(x=1-20)}MgAl_{(3)}O$ catalysts at 200 °C. An optimum conversion of 4.5 % is observed for the catalyst with 7 atomic % of Cu loading. The selectivity to butanol gradually decreases with increasing amount of Cu (42 % to 18 % from 1 to 20 at.% of Cu) whereas the selectivity to DEE exhibits a maximum value (~43 %) at 10 % Cu loading. When increasing the temperature from 200 to 260 °C, the conversion of ethanol increases with reaction temperature as expected (4 % to 9 %). The selectivity to *n*-butanol increases with temperature (40 % to 80 %, after 5 h) and time on stream (2.6 % to 11.1 % from 2 to 100 h, at 200 °C), at the expense of acetal DEE. The optimum yields are obtained for Cu loadings comprised between 5 and 10 atomic %.

Several examples of the production of DEE as a co-product or a by-product of the studied reaction can be found in literature [107-109]. Bae *et al.* [107] studied the dehydrochlorination of carbon tetrachloride, classified as the substantial ozone depleting material, in a medium of ethanol over platinum and palladium catalysts grafted on different supports, *i.e.*,

montmorillonite (Mont), activated carbon, Al_2O_3 and SiO_2-Al_2O_3. The supported Pt and Pd on Mont are reported as the best catalysts with respect to the relatively high conversions of CCl_4 and ethanol as well as the selectivities to chloroform ($CHCl_3$) and DEE. The catalysts were prepared by exchange of H-Mont with $(CH_3CN)_2PdCl_2$ or $(CH_3CN)_2PtCl_2$. The catalysts were loaded in a bomb reactor, in the desired amount of liquid reactants mixture of CCl_4, ethanol, and the internal standard of *n*-undecane. Molecular hydrogen with or without air was supplied to the reactor up to the desired reaction pressures. As shown in Table 1-10, 48.4 % conversion of CCl_4 is stated with 95.6 % selectivity to $CHCl_3$ for the Pt/Mont catalyst, along with 71.0 % DEE selectivity at 19.7 % ethanol conversion. The Pd/Mont catalyst exhibits 43.5 % CCl_4 conversion with 93.3 % selectivity to $CHCl_3$, along with a higher DEE selectivity of 77.4 % at slightly lower ethanol conversion (17.3 %). However, the Pt/Mont is less stable compared to the Pd/Mont considering larger amounts of metal leaching, *i.e.*, 7.56 wt.% of Pt is leached after reaction compared to 0.61 wt.% of Pd leaching only. The effect of molecular hydrogen, investigated on Pd/Mont, shows that the conversion of CCl_4 and selectivity to DEE from C_2H_5OH increases significantly with the increase in hydrogen pressure (Table 1-10). The role of ethanol in the reaction medium is described by the authors to accelerate the CCl_4 reaction and to increase the selectivity to $CHCl_3$. It also actively participates in the reaction to co-produce DEE. The adsorbed chlorine produced in the hydrochlorination reaction is protonated by ethanol giving acetaldehyde on Pd or Pt sites. Acetaldehyde then reacts with ethanol to form DEE *via* the aldol condensation on metal sites, as well as on acidic sites of the support. The protonation of adsorbed chlorine by ethanol also helps preventing HCl formation, suppressing the catalyst deactivation generally induced from the strongly adsorbed chlorine on carbonaceous species.

Table 1-10: Conversion and products distribution in liquid-phase hydrodechlorination of CCl_4 adapted from [107].

Catalyst	$P(H_2)$ MPa	CCl_4 Conversion (%)	Products distribution (mol.%)			C_2H_5OH Conversion (%)	Products distribution (mol.%)			
			$CHCl_3$	$C_2H_4Cl_{4-x}$ [a]	C_2Cl_6		DEE	ACD	EVE	DEC
2.8 wt.% Pd/Mont	3	43.5	93.3	1.3	5.4	17.3	77.4	12.1	8.8	1.7
	4.5[b]	33.7	91.4	1.5	7.5	15.1	79.3	11.0	9.4	0.3
	6[b]	35.5	91.2	1.5	7.1	13.3	83.6	10.7	5.2	0.5
2.5 wt.% Pt/Mont	3	48.4	95.6	0.9	3.57.3	19.7	71.0	7.6	18.9	2.5

Experimental conditions: T = 50 °C, CCl_4 = 64.5 mmol, C_2H_5OH = 217.4 mmol, *n*-undecane = 1.3 mmol, catalyst 0.1 g, reaction for 12 h; [a]C_2Cl_4 and C_2HCl_3 were the main products in $C_2H_4Cl_{4-x}$; [b]reaction for 6 h; *Abbreviations:* DEE = *1,1*-diethoxyethane, ACD = acetaldehyde, EVE = ethyl vinyl ethe, DEC = diethyl carbonate.

Production of ethylene and acetaldehyde by selective oxidation of ethanol using mesoporous V-MCM-41 catalysts was studied by Gucbilmez *et al.* [108]. The authors aimed at proposing a new process to obtain ethylene from bio-ethanol by oxidative catalytic dehydrogenation using vanadium incorporated MCM-41 type mesoporous catalysts. Selective oxidation experiments in gas phase were carried out at temperatures between 150-400 °C with O_2/ ethanol ratio in the feed stream varying between 0 to 2. The total flow rate was kept at 31.6 $mL.min^{-1}$. The major products are acetaldehyde and ethylene and CO_2 over the prepared V4b-MCM-41 catalyst (V/Si in MCM-41 = 0.04, S_{BET} = 1062 $m^2.g^{-1}$, V_{pore} = 1.09 $cm^3.g^{-1}$, d_{pore} = 3.20 nm). Small amounts of CH_4, acetic acid, ethyl acetate, diethyl ether, and DEE are observed, especially at low O_2/ethanol ratio and at low temperatures. At the same O_2/ethanol ratio of 0.5 in the feed composition, the conversion of ethanol raises from 24 % at 300 °C up to 99 % at 400 °C. A decrease in selectivities to acetaldehyde (49 % *vs.* 26 %) and to DEE (7 % *vs.* 1%) is observed in contrast to those of carbon dioxide (1 % *vs.* 3 %) and ethylene (28 % *vs.* 67%).

Santacesaria *et al.* investigated the oxidative dehydrogenation of ethanol over vanadium based catalysts prepared by grafting on titania-silica supports with different procedures [109]. They attempted to combine two advantages obtained from TiO_2 and SiO_2. TiO_2 in the form of anatase interacts strongly with V_2O_5 thereby favoring the dispersion of the active vanadia phase on the support. However, titania has some drawbacks which are limited surface area and lower resistance to sintering than other oxides. On the contrary, silica produces a weak interaction to V_2O_5 therefore V_2O_5 supported on silica shows high tendency to agglomerate

during calcination, leading to the formation of low dispersed active phases. By grafting SiO_2 with TiO_2, a newly formed support with high and thermostable specific surface area can be obtained, as well as a well-dispersed V_2O_5 catalyst.

The experiments were carried out at atmospheric pressure in a fixed-bed reactor at temperatures between 100-200 °C. A residence time of ethanol normally kept at 26.4 $g_{cat}.h^{-1}$. The reaction feed comprised 1.1 $mL.h^{-1}$ of ethanol, 7.7 $mL.h^{-1}$ of O_2, with 22 $mL.h^{-1}$ of He as a diluent. The results reveal two catalysts being selective to DEE formation, *i.e.*, supported vanadium on SiO_2 grafted with TiO_2 (V/TSMA) and supported vanadium on TiO_2 (V/TiO_2) catalysts, with the same amount of 6 wt.% V_2O_5 loading. The reactivity of V/TiO_2 catalyst is much higher than that of V/TSMA (85 % *vs.* 48 % at 120 °C). However, the grafted V/TSMA catalyst is more selective to DEE than the non-grafted V/TiO_2 catalyst (21 % *vs.* 15 %, with 48 % and 56 % selectivity to acetaldehyde, respectively). The authors also point out a positive effect of grafting that active vanadium species are dispersed more uniformly on the grafted support. This, in turn, has a positive effect on selectivity, although the catalyst is less active.

1.4 Choice of catalyst for the direct synthesis of dimethoxymethane and diethoxyethane

With respect to the reaction pathways postulated in Scheme 1-1 and Scheme 1-3, as well as the product distribution depending on the catalytic properties shown in Scheme 1-2, the appropriate system for the gas phase direct synthesis of acetals – *1,1*-dimethoxymethane (DMM) and *1,1*-diethoxyethane (DEE), from methanol and ethanol, respectively, must be a bifunctional catalyst with adequate balance between redox and acid sites of the proper respective strength. Regarding the bibliographic review we have conducted, it seems also that the catalyst should be an oxide or an active phase supported on an oxide support in order to obtain the thermal stability necessary to work in the temperature range of the target reactions (*i.e.*, 80 – 400 °C).

1.4.1 Iron molybdate catalysts

A bulk iron molybdate mixed oxides catalyst [110], which is being currently used in the industry for formaldehyde synthesis applying the reactant feeds with low methanol concentrations (*i.e.*, of less than 7.5 mol.%) [74,75,111,112], is an interesting candidate. Indeed, DMM is always detected as a by-product in the formaldehyde production, indicating the presence of an acid catalyzed function that should be tuned to focus the DMM selectivity

and the thermal stability of this catalyst has not to be demonstrated because the temperature range for industrial formaldehyde production seems to be coherent with the one envisage for DMM synthesis. Iron molybdate catalyst can also be interesting for the DEE production. This is owing to the similarities between ethanol and methanol oxidation reaction pathways which require presumably the same redox/acid catalytic functions.

The majority of literature dealing with iron molybdate catalysts focused on their use in the selective oxidation of methanol to formaldehyde. Industrial iron molybdate catalyst is composed by mixed oxides ($Fe_2(MoO_4)_3$ and MoO_3), generally with a large excess of Mo. The ratio between Mo and Fe can exceed 5 in the industrial iron molybdate catalysts, however, usually they present Mo/Fe ratios between 2.3 and 5 [49]. A surplus of molybdenum is introduced to compensate the loss of volatile reduced molybdenum atoms during the oxidation reaction, with the help to extend the lifetime of the catalyst.

Adkins and Peterson were the first to mention the use of iron molybdate mixed oxides as an active catalyst in formaldehyde production from methanol [113]. In their work, the FeMo mixed oxides were prepared by coprecipitation of ferrous iron malate, ammonium molybdate, and ammonium nitrate solutions. The porous steel was added to the mixing solution then water was evaporated. Afterwards the catalyst coated pellets were dried for several hours at 60 °C and calcined at 360-370 °C in a slow flow of dry air for 1 h. Later on Kerr and coworkers prepared iron molybdates by coprecipitating sodium molybdate solution with ferric chloride solution [114]. The method of preparation developed by Kerr *et al.*, as cited by Pernicone [115], allows one to vary the relative concentrations of Mo and Fe parent solutions to obtain the catalysts with a reproducible Mo/Fe molar ratio of 2. The Kerr's method is also feasible to prepare Fe-W-O mixed oxides catalyst with a W/Fe molar ratio of 2, simply by substituting the molybdate with a tungstate solution. Thereby the catalytic activities of iron molybdate and iron tungstate catalysts can be compared directly.

In laboratory scales many researchers prefer to use ammonium molybdate and iron nitrate as Mo and Fe sources, respectively. This is to avoid the contamination of catalyst poisons such as sodium and chlorine [116,117]. According to Popov *et al.*, the activity of iron molybdate decreased drastically by a factor of 10 to 12 when adding the sodium salts during its preparation [118]. The presence of sodium decreased the surface acidity that helps preventing the competitive adsorption between methanol and water. Nonetheless the industrial iron

molybdate catalysts are still prepared from ammonium molybdate and ferric chloride solutions.

A number of parameters are known to influence the quality of the final catalysts including the concentration of parent solutions, temperature and time during precipitating, pH of the resulting solution after precipitation, as well as temperature and time for calcinations [117]. Pernicone referred in his work that the catalyst activity depends strongly on the final pH [115], in agreement with Wilson [119] who also found that the surface area of catalysts depends mainly on the concentration of ammonium molybdate solution. Boreskov and coworkers [120,121] believed that the Mo/Fe ratio was a critical factor to the activity and selectivity of the FeMo mixed oxides system. They claimed the optimum activity for atomic ratio of 1.7 for the selective methanol oxidation to formaldehyde reaction, in agreement with Sun-Kuo *et al*. [122], while Acosta *et al*. [123] claimed the ratio of 2.4.

Arruana and Wanke [124] found an increase of 30 % in the activity of Fe/Mo oxide catalysts calcined at temperatures in the range of 257-547 °C (*i.e.*, 530-820 K) under air flow during the first 18 h, ascribing to the formation of Mo rich surface layers. The activity then declined when extended the thermal treatment to 572 h, possibly due to the sublimation of Mo. In a similar context, Trifirò *et al*. [125] studied the variations of Fe_2O_3-MoO_3 catalyst with the temperature of calcinations and confirmed the decrease of surface area and a severe decrease in catalytic activity.

The coprecitation techniques in aqueous solution are the most common ways to prepare the non-supported iron molybdate catalysts. The subsequent precipitate is then washed, dried, and usually calcined at temperatures in the range of 300-600 °C. However, this method of preparation is not the only way to synthesize FeMo mixed oxides catalyst. Several alternatives have been reported in the literature. In the work of Popov *et al*. Mo rich iron molybdate catalysts were prepared by centrifugal milling of a paste composed of iron oxalate and molybdic acid [126]. Klafkowski prepared Fe-Mo-O mixed oxides by impregnation of *iso*-$Fe(OH)_3$ or γ-FeOOH with an aqueous solution of ammonium paramolybdate [127]. The impregnated samples were dried at 120 °C for 3 h before calcination. Soares *et al*. [128] prepared the iron molybdate catalysts *via* a sol-gel method in which iron solution was slowly added to Mo solution without precipitation. They pointed out in this work that the surface areas of catalysts prepared by sol-gel techniques were higher than those prepared by coprecipitation. Later on they reported the preparation of Mo rich iron molybdate by the

sol-gel like technique using iron nitrate and molybdenum hexacarbonyl solutions in a medium of propionic acid [117]. In addition to the higher surface area obtained, the sol-gel like catalyst was more tolerant to surface reduction and surface Mo loss by MoO_3 sublimation. Wach and Brands developed the *in situ* preparation of iron molybdates in a fixed bed packed with particles of MoO_3 and Fe_2O_3 oxides in the absence of water. They claimed that performances of the obtained catalysts were equivalent to those of an industrial catalysts tested in the same conditions [129-131]. Beale *et al*. successfully developed a one-step hydrothermal method to prepare poorly crystalline Mo_5O_{14} and an amorphous $Fe_2(MoO_4)_3$ type precursor which then transformed to high surface area mixed oxides of $Fe_2(MoO_4)_3/MoO_3$ above calcinations temperature of 300 °C [116]. In their work, appropriate amounts of iron nitrate nonahydrate and ammonium heptamolybdate were mixed and well-stirred to obtain the gel like solution. The mixture was heated in a Teflon-lined autoclave at 150 °C for 24 h. The resulting precipitate was separated and dried at 60 °C overnight before calcination. The authors also claimed that this mixed phase sample showed a higher selectivity for formaldehyde production than a conventional sample prepared *via* coprecipitation. The preparation of iron molybdate thin films catalysts was suggested recently in the work of Ulrich and coworkers [132] as a model catalyst for the selective methanol oxidation to formaldehyde reaction. A well-ordered thin Fe-Mo oxide films were prepared by Mo deposition onto a thin Fe_3O_4 (111) film grown on Pt(111) single crystal and oxidation at elevated temperatures. Lately Jin *et al*. [133] synthesized iron molybdate catalysts comprising $Fe_2(MoO_4)_3$ nano-particles anchored onto MoO_3 nano-rods applied for the same reaction. MoO_3 nano-rods were impregnated with iron nitrate solution *via* the incipient wetness method. The nano-structured $Fe_2(MoO_4)_3/MoO_3$ was found to have comparable performances under the tested reaction conditions to the conventional coprecipitation catalyst.

Methanol oxidation over iron molybdate catalysts is carried out industrially in fixed bed reactors where it can be tricky to maintain the uniform temperature distribution. Several authors have proposed the use of fluidized bed reactors to minimize the hot spots of the catalytic bed. The non-supported FeMo catalysts are not applicable in fluidized bed reactors due to their weak resistance in mechanical abrasion. Two preparation techniques are generally used to prepare the supported iron molybdate catalysts: (i) incipient wetness and (ii) spraying the support material with a solution of Mo and Fe precursors in the presence of citric acid [134]. Studies on Mo-Fe-O supported over Al_2O_3 and SiO_2 revealed that supported catalysts were less active than non-supported ones [134-137]. In this case, the interaction between

support material and active Mo-Fe-O phase was a crucial factor. This interaction could alter the nature of the catalyst, for instance, modify the electronic properties of Fe species on the surface. Cairati *et al*. also reported that the increase in the surface area of the supports had an adverse effect on the catalytic behavior and this effect is more significant for alumina than for silica [138]. However, what could be promising for possible fluidized bed reactor operation is to use silica as the support material and minimize its interaction with the mixed oxides, due to its high surface area, by using a high content of the active Mo-Fe-O phase. This concept was realized by Diaz *et al*. [139]. The silica supported Mo-Fe and Mo-Fe-P mixed oxides were prepared in the presence of citric acid as a chelating agent. The prepared catalysts presented good performances in fluidized bed reactors, with high activity and selectivity towards formaldehyde both at low and high methanol conversions.

1.5 References

[1] R.J. Farrauto, C. Bartholomew, Introduction to Industrial Catalytic Processes, Chapman & Hall, London, 1997.

[2] J.B. Hansen, Handbook of Heterogeneous Catalysis, vol.4, fourth ed., Wiley–VCH, New York, 1997, 1856.

[3] D.L. Klass, Biomass for Renewable Energy, Fuels and Chemicals, Academic Press, San Diego, 1998.

[4] G.W. Huber, S. Iborra, A. Corma, Chem. Rev. 106 (2006) 4044.

[5] http://www.nacatsoc.org/21nam/data/papers/Paper1981.pdf, verified January 10, 2013.

[6] A. Kumar, D.D. Jones, M.A. Hanna, Energies 2 (2009) 556.

[7] C. Wyman, in Encyclopedia of Energy; Cleveland, C. J., Ed.; Elsevier: London, 2004; Vol. 2.

[8] A. Aden, M. Ruth, K. Ibsen, J. Jechura, K. Neeves, J. Sheehan, B. Wallace, L. Montague, A. Slayton, J. Lukas, Report No. NREL/TP-510-32438; National Renewable Energy Laboratory: Golden, CO, 2002; http://www.osti.gov/bridge, verified on January 10, 2013.

[9] J.E. Lodgsdon, in Ethanol Enclycopedia of Chemical Technology, fourth ed., Longman, New York, vol.9, 1994, 812.

[10] Report of the European Commission: Summary of the economy's hydrogen.

[11] P.L. Spath, D.C. Dayton, Report No.NREL/TP-510-34929; National Renewable Energy Laboratory, Golden, CO, 2003; http://www.osti.gov/bridge, verified on January 10, 2013.

[12] A.S. Arico, S. Srinivasan, V. Antonucci, Fuel Cells 1 (2001) 133.

[13] R. Dillon, S. Srinivasan, A.S. Arico, V.J. Antonucci, J. Power Sources 127 (2004) 112.

[14] S.G. Chalk, J.F. Miller, F.W. Wagner, J Power Sources 86 (2000) 40.

[15] C. Song, Catal. Today 77 (2002) 17.

[16] T.B. Reed, R.M. Lerner, Science 182 (1973) 1299.

[17] R.F. Klausmeier, I.F. Billick, Energy Fuels 7 (1993) 27.

[18] M. Specht, F. Staiss, A. Bandi, T. Weimer, Int. J. Hydrogen Energy 23 (1998) 387.

[19] http://www.methanol.org/Energy/Transportation-Fuel/Fuel-Blending-Guidelines/Blenders-Product-Bulletin-(Final).aspx, verified on January 10, 2013.

[20] H. Kim, B. Choi, Renewable Energy 10 (2008) 2222.

[21] F. Frusteri, L. Spadaro, C. Beatrice, C. Guido, Chem. Eng. J. 134 (2007) 239.

[22] D.-G. Li, H. Zhen, L. Xincai, Z. Wu-gao, Y. Jian-guang, Renewable Energy 30 (2005) 967.

[23] J.-M. Tatibouët, Appl. Catal. A: Gen. 148 (1997) 213.; J.M. Tatibouet, J. E. Germain, J. Catal. 72 (1981) 375; J.-M. Tatibouët, H. Lauron-Pernot, J. Mol. Catal. A: Chem. 171 (2001) 205.

[24] E. Tronconi, A. S. Elmi, N. Ferlazzo, P. Forzatti, G. Busca, P. Tittarelli, Ind. Eng. Chem. Res. 26 (1987) 1269.

[25] M. Ai, J. Catal. 54 (1978) 426.

[26] Dimethoxymethane safety data sheet, product number D134651, http://www.sigmaaldrich.com, verified January 10, 2013.

[27] C. Doucet, L. Germanaud, J.-L. Couturier, J.-L. Dubois, J.-M. Sage, EP Pat., 1914293, 2008.

[28] WO Pat., 090294, 2008.

[29] Q. Sun, A. Auroux, J. Shen J. Catal. 244 (2006) 1.

[30] R. Chetty, K. Scott, J. Power Sources 173 (2007) 166.

[31] D. Devaux, H. Yano, H. Uchida, J-L. Dubois, M. Watanabe, Electrochim. Acta, 56 (2011) 1460.

[32] F. Vigier, C. Coutanceau, J. M. Léger, J.L Dubois, J. Power Sources, 175 (2008) 82.

[33] J.C. Ball, C. Lapin, J. Buckingham, E. Frame, D. Yost, M. Gonzalez, E. Liney, M. Natarajan, J. Wallace, S. A. E. Trans. Section 4 110 (2001) 2176.

[34] M. Matti Maricq, R.E. Chase, D.H. Podsiadlik, W.O. Siegl, E.W. Kaiser, S. A. E. Trans. Section 4 107 (1998) 1504.

[35] D. Arnold, B. Hierholzer, H. Wloch, K.-F. Mück, EP Pat., 704442, 1996; J. Bhalchandra Vinayak, W. John Raymond, US Pat., 5959456, 1999; WO Pat., 018209, 1993.

[36] S. Satoh, Y. Tanigawa, US Pat., 6379507, 2002.

[37] G.P. Hagen, M.J. Spangler, US Pat., 6160174, 2000.

[38] G.P. Hagen, M.J. Spangler, US Pat., 6437195, 2002.

[39] G.P. Hagen, M.J. Spangler, US Pat., 6166266, 2000.

[40] US Pat., 003/0171534.

[41] G.P. Hagen, M.J. Spangler, US Pat., 6350919, 2002.

[42] G.P. Hagen, M.J. Spangler, US Pat., 6392102, 2002.

[43] G.P. Hagen, M.J. Spangler, US Pat., 6265528, 2001.

[44] G.P. Hagen, M.J. Spangler, US Pat., 6160186, 2000.

[45] G. Reuss, W. Disteldorf, O. Grundler, A. Hilt, in Ullmann's Encyclopedia of Industrial Chemistry, 5th Edition, VCH Publishers, Vol. A11, 1992, 619.

[46] H.R. Gerberich, A.L. Stautzenberger, W.C. Hopkins, Formaldehyde. In Encyclopedia of Chemical Technology, 3rd Edition; H. F. Mark, J.J. McKetta, D.F.A. Othmer, Eds.; Standen Editors John Wiley & Sons, Inc.: USA; Vol. 11, 1983, 231.

[47] J.R. Fair, R.C. Kmetz, Formaldehyde. In Encyclopedia of Chemical Processing and Design; J.J. McKetta, W.A. Cunningham, Eds.; Marcel Dekker, Inc.: USA; Vol. 23, 1985, 350.

[48] A.R. Chauvel, P.R. Curty, R. Maux, C. Petitpas, Hydr. Proc. 51 (1973) 179.

[49] A.B. Stiles, T.A. Koch, Oxidation Catalysts. In Catalyst Manufacture, 2nd Edition; Editor Marcel Dekker: New York; 197, 1995, Chap.20.

[50] A.P.V. Soares, M.F. Portela, A. Kiennemann, Catal. Rev. 47 (2004) 125.

[51] M. Muhler, Handbook of Heterogeneous Catalysis; G. Ertl, H. Knözinger, J. Weitkamp, Eds.; VCH: Germany; Vol. 5, 1997, 2274.

[52] http://www.lookchem.com/Chempedia/Chemical-Technology/Organic-Chemical Technology/3055.html, verified on January 10, 2013.

[53] DT Pat., 2202070, 1972.

[54] DD Pat., 245868, 1985.

[55] CN Pat., 1301688.

[56] J. Masamoto, J. Ohtake, M. Kawamura, EP Pat., 0327343, 1989.

[57] G. Lambiotte, CH Pat., 688041, 1997.

[58] S. Satoh, Y. Tanigawa, US Pat., 6379507, 2002.

[59] G.P. Hagen, M.J. Spangler, US Pat., 5959156, 1999.

[60] G.P. Hagen, M.J. Spangler, US Pat., 6437195, 2002.

[61] M. Fournier, A. Aouissi, C. Rocchiccioli-Deltcheff, J. Chem. Soc., Chem. Commun., 1994, 307; C. Rocchiccioli-Deltcheff, A. Aouissi, M.M. Bettahar, S. Launay, M. Fournier, J. Catal. 164 (1996) 16; C. Rocchiccioli-Deltcheff, A. Aouissi, S. Launay, M. Fournier, J. Mol. Catal. A: Chem. 114 (1996) 331.

[62] H. Liu, E. Iglesia, J. Phys. Chem. B 107 (2003) 10840; H. Liu, E. Iglesia, J. Catal. 223 (2004) 161.

[63] H. Liu, E. Iglesia, J. Phys. Chem. B 109 (2005) 2155.

[64] Y. Yuan, H. Liu, H. Imoto, T. Shido, Y. Iwasawa, Chem. Lett. (2000) 674; Y. Yuan, T. Shido and Y. Iwasawa, Chem. Commun. (2000) 1421.

[65] Y. Yuan, H. Liu, H. Imoto, T. Shido, Y. Iwasawa, J. Catal. 195 (2000) 51; Y. Yuan, K. Tsai, H. Liu, Y. Iwasawa, Top Catal. 22 (2003) 9.

[66] Y. Yuan, Y. Iwasawa, J. Phys. Chem. B 106 (2002) 4441.

[67] A. Tougerti, S. Cristol, E. Berrier, V. Briois, C. La Fontaine, F. Villain, Y. Joly, Phys. Rev. B 85 (2012) 1.

[68] X. Sécordel, A. Yoboué, S. Cristol, C. Lancelot, M. Capron, J.-F. Paul, E. Berrier, J. Solid State Chem. 184 (2011) 2806.

[69] O.A. Nikonova, M. Capron, G. Fang, J. Faye, A.-S. Mamede, L. Jalowiecki-Duhamel, F. Dumeignil, G. A. Seisenbaeva, J. Catal., 279 (2011) 310.

[70] Y. Fu, J. Shen, Chem. Commun. (2007) 2172.

[71] J. Liu, Y. Fu, Q. Sun, J. Shen, Microporous Mesoporous Mater. 116 (2008) 614.

[72] J. Liu, Q. Sun, Y. Fu, J. Shen, J. Colloid Interface Sci. 335 (2009) 216; H. Zhao, S. Bennici, J. Shen, A. Auroux, J. Mol. Catal. A: Chem. 309 (2009) 28; W. Li, Y. Sun, Catal. Commun. 11 (2010) 396; H. Zhao, S. Bennici, J. Shen, A. Auroux, J. Therm. Anal. Calorim. 99 (2010) 843; H. Guo, D. Li, D. Jiang, W. Li, Y. Sun, Catal. Lett.135 (2010) 48; H. Zhao, S. Bennici, J. Shen, A. Auroux, J. Catal. 272 (2010) 176; H. Zhao, S. Bennici, J. Cai, J. Shen, A. Auroux, A, Catal. Today 152 (2010) 70.

[73] Q. Sun, Y. Fu, J. Liu, A. Auroux, J. Shen, Appl. Catal. A: Gen. 334 (2008) 26.

[74] E. Tronconi, A. S. Elmi, N. Ferlazzo, P. Forzatti, G. Busca, P. Tittarelli, Ind. Eng. Chem. Res., 26 (1987) 1269.

[75] G. Deo, I. E. Wachs, J. Catal. 146 (1994) 323.

[76] X. Lu, Z. Qin, M. Dong, H. Zhu, G. Wang, Y. Zhao, W. Fan, J. Wang, Fuel 90 (2011) 1335.

[77] S. Chen, S. Wang, X. Ma, J. Gong, Chem. Commun. 47 (2011) 9345.

[78] H. Guo, D. Li, C. Chen, Z. Fan, Y. Sun, Chinese Journal of Catalysis 33 (2012) 813.

[79] H. Golinska-Mazwa, P. Decyk, M. Ziolek, J. Catal. 284 (2011) 109.

[80] S. Royer, X. Sécordel, M. Brandhorst, F. Dumeignil, S. Cristol, C. Dujardin, M. Capron, E. Payen, J.-L. Dubois, Chem. Commun. 7 (2008) 865.

[81] G. Busca, J. Lamotte, J.C. Lavalley, V. Lorenzelli, J. Am. Chem. Soc., 109 (1987) 5197; G. Busca, Catal. Today, 27 (1996) 457.

[82] M. Natarajan, E.A. Frame, T. Asmus, W. Clark, J. Garbak, M.A. Gonzalez, E. Liney, W. Piel, J.P. Wallace III, SAE Tech. Pap. Ser., 2001, 2001-01-3631.

[83] B.E. Hallgren, J.B. Heywood, SAE Tech. Pap. Ser., 2001, 2001-01-0648.

[84] A.S. Cheng, R.W. Dibble, B.A. Buchholz, SAE Tech. Pap. Ser., 2002, 2002-01-1705.

[85] DE Pat. 2911411, 1980.

[86] C. Kohlpaintner, M. Schulte, J. Falbe, P. Lappe, J. Waber, In: Ullmann's Encyclopedia of Industrial Chemistry, 6th edition, Wiley-VCH, 1999.

[87] V.M.T.M. Silva, A.E. Rodrigues, AIChE J. 48 (2002) 625.

[88] F.A.J. Meskens, Synthesis 7 (1981) 501.

[89] US Pat., 5527969, 1996.

[90] US Pat., 5321006, 1994.

[91] US Pat., 5362918, 1994.

[92] *1,1*-Diethoxyethane safety data sheet, product number W200220, http://www.sigmaaldrich.com, verified January 10, 2013.

[93] V.M.T.M. Silva, A.E. Rodrigues, AIChE J. 51 (2005) 2752.

[94] R. Jira, Angew. Chem. Int. Ed. 48 (2009) 9034.

[95] R. Jira in Applied Homogeneous Catalysis with Organometallic Compounds, 2nd ed. (Eds.: B. Cornils, W. A. Herrmann), Wiley-VCH, Weinheim, 2002, p. 386, 1323.

[96] DE Pat., 4404515A1, 1995.

[97] M.R. Capeletti, L. Balzano, G. de la Puente, M. Laborde, U. Sedran, Appl. Catal. A: Gen. 198 (2000) L1.

[98] V.M.T.M. Silva, A.E. Rodrigues, Chem. Eng. Sci. 56 (2001) 1255.

[99] S.P. Chopade, M.M. Sharma, React. Func. Polym. 34 (1997) 37; S.P. Chopade, M.M. Sharma, React. Func. Polym. 32 (1997) 53; M.M. Sharma, React. Func. Polym. 26 (1995) 3; N. Calvar, B. González, A. Dominguez, Chem. Eng. Process 46 (2007) 1317; A.D. Dhale, L.K. Myrant, S.P. Chopade, J.E. Jackson, D.J. Miller, Chem. Eng. Sci. 59 (2004) 2881.

[100] A.K. Kolah, S.M. Mahajani, M.M. Sharma, Ind. Eng. Chem. Res., 35 (1996) 3707.

[101] F.F. Cristófoli, J. Espinosa, P.A. Aguirre, in First World Conference of Biomass for Energy and Industry. James and James Science Publishers, Sevilla, 2001, pp.657-660.

[102] DE Pat., 3403426 A1, 1985.

[103] M.F. Gomez, L.A. Arrúa, M.C. Abello, J. Chem. Technol. Biotechnol. 79 (2004) 391.

[104] A.C. Bueno, J.A. Gonçalves, E.V. Gusevskaya Appl. Catal. A: Gen. 329 (2007) 1.

[105] I.-C. Marcu, D. Tichit, F. Fajula, N. Tanchoux, Catal. Today 147 (2009) 231-238.

[106] US Pat., 20050059839A1, 2005.

[107] J.W. Bae, E.J. Jang, D.H. Jo, J.S. Lee, K.H. Lee, J. Mol. Catal. A: Chemical 206 (2003) 225.

[108] Y. Gucbilmez, T. Dogu, S. Balci. Ind. Eng. Chem. Res. 45 (2006) 3496.

[109] E. Santacesaria, A. Sorrentino, R. Tesser, M. Di Serio, A.J. Ruggiero, J. Mol. Catal. A: Chemical 204-205 (2003) 617.

[110] J.-L. Dubois, M. Brandhorst, M. Capron, C. Dujardin, WO Pat., 2007/034264, 2007.

[111] J. Gornay, X. Sécordel, M. Capron, G. Tesquet, P. Fongarland, E. Payen, J.-L. Dubois, F. Dumeignil, Oil & Gas Science and Technology 65 (2010) 751.

[112] I.E. Wachs, US Pat., 6875724, 2005.

[113] H. Adkins, W.R. Peterson, J. Am. Chem. Soc. 53 (1931) 1512.

[114] P.F. Kerr, A.W. Thomas, A.M. Langer, The American Mineralogist, 48 (1963) 14.

[115] N. Pernicone, J. Less-Comm.- Metals, 36 (1974) 289.

[116] A.M. Beale, S.D.M. Jacques, E. Sacaliuc-Parvalescu, M.G. O'Brien, P. Barnes, B.M. Weckhuysen, Appl. Catal. A: General, 363 (2009) 143.

[117] A.P.V. Soares, M.F. Portela, Catal. Rev. Sci. Eng. 47 (2005) 125.

[118] B.I. Popov, L.N. Shkuratova, N.G. Skorokhova, React. Kinet. Catal. Lett. 3 (1975) 463.

[119] J.H. Wilson, Raman Spectroscopy Studies of Iron/Molybdenum Oxide Catalysts for the Oxidation of Methanol to Formaldehyde, University of Wisconsin-Madison Ph.D. Thesis, 1986.

[120] G.K. Boreskov, Kinet. Katal. 6 (1965) 1052; G.D. Kolovertnov, G.K. Boreskov, V.A. Dzisko, B.I. Popov, D.V. Tarasova, G.C. Belugina, Kinet. Catal. (Engl. Transl.), 6 (1965) 950.

[121] G.K. Boreskov, G.D. Kolovertnov, L.M. Kefeli, L.M. Plyasova, L.G. Karakchiev, V.N. Mastikhin, V.I. Popov, V.A. Dzis'Ko, D.V. Tarasova. Kinet. Catal. (Engl. Transl.) 7 (1965) 125.

[122] M.R. Sun-Kuo, S. Mendioroz, J.L.G. Fierro, J.M. Palacios, A. Guerrero-Ruíz, J. Mater. Sci. 30 (1995) 496.

[123] G. Acosta, C. Guzman, I. De La Torre, E. Martinez, 72nd Annual Meeting of the American Institute of Chemical Engineers, San Francisco, CA, USA, 1979.

[124] J. Arruano, S. Wanke, Canad. J. Chem. Eng. 53 (1975) 301.

[125] F. Trifirò, S. Notarbartolo, I. Pasquon, J. Catal. 22 (1971) 324.

[126] B.I. Popov, A.V. Pashis, L.N. Shuratova, React. Kinet. Catal. Lett. 30 (1986) 129.

[127] W. Klafkowski, React. Kinet. Catal. Lett., 6 (1977) 425.

[128] A.P.V.Soares, M.F. Portela, A. Kiennemann, Stud. Surf. Sci. Catal. 110 (1997) 807.

[129] I.E. Wachs, L.E. Briand, US Pat. 287021, 1999.

[130] I.E. Wachs, L.E. Briand, US Pat. 6331503B1, 2001.

[131] I.E. Wachs, L.E. Briand, US Pat. 6624332B2, 2003.

[132] J.J. Ulrich, J. Sainio, Y. Lei, D. Edwards, R. Davies, M. Bowker, S. Shaikhutdinov, H.-J. Freund, Surf. Sci. 605 (2011) 1550.

[133] G. Jin, W. Weng, Z. Lin, N.F. Dummer, S.H. Taylor, C.J. Kiely, J.K. Bartley, G.J. Hutchings, J. Catal. 296 (2012) 55.

[134] C.G. Hill Jr., J. Wilson III, J. Mol. Catal. 67 (1991) 57.

[135] L. Cairati, L. Di Fiori, P. Forzatti, I. Pasquon, F. Trifirò, Ind. Chem. Proc. Des. Dev. 19 (1980) 561.

[136] P. Forzatti, React. Kinet. Catal. Lett. 20 (1982) 213.

[137] C.G. Hill Jr., J.H. Wilson III, J. Mol. Catal. 63 (1990) 65.

[138] L. Cairati, M. Carbucicchio, O. Ruggeri, Stud. Surf. Sci. Catal. 3 (1979) 279.

[139] A.P.S. Dias, V.V. Rozanov, J.C.B. Waerenborgh, M. F. Portela, Appl. Catal. A: General 345 (2008) 185.

Chapter 2

Catalysts preparation and experimental techniques

2.1 Catalysts preparation

The preparation of catalysts applied in the selective oxidation of methanol and ethanol to acetals, *1,1*-dimethoxymethane (DMM) and *1,1*-diethoxyethane (DEE) is detailed in the following subsections. A procedure to obtain a bifunctional iron molybdate mixed oxide catalyst is described, as well as the preparation of iron molybdates with tungsten and aluminium modification, aimed at enhancing the catalyst acidity. The preparation of single oxides of MoO_3 and Fe_2O_3 as Fe-free and Mo-free catalysts is also given.

2.1.1 Iron molybdate mixed oxide

Iron molybdate mixed oxide catalysts were prepared by coprecipitation of aqueous solutions of ammonium molybdate tetrahydrate ($(NH_4)_6Mo_7O_{24}.4H_2O$) and iron chloride hexahydrate ($FeCl_3.6H_2O$), according to a procedure described by Pernicone *et al*. [1,2]. Following this procedure of synthesis, the catalyst formulation can be specifically optimized by systematically tuning different synthesis parameters that can have influences on the catalytic activity, for instance, concentration of the precursor's solutions, ratio between Mo and Fe, and calcination temperature.

2.1.1.1 Preparation of molybdenum and iron precursors

An aqueous solution of 250 mL with 10 g of $(NH_4)_6Mo_7O_{24}\cdot 4H_2O$ (AHM; Fluka, 99 %) was first prepared leading to a 4 wt.% AHM precursor solution. The obtained transparent solution was magnetically stirred and heated to a temperature comprised between 50 and 60 °C. This AHM solution, which was initially at pH around 5, was acidified with concentrated HCl acid to reach pH close to 1, under stirring and heating. We have to notice that the solution should remain transparent. Meanwhile, 75 mL (approximately 1/3 by volume of the Mo precursor solution) of a 10 wt.% Fe precursor solution was prepared dissolving 7.5 g of $FeCl_3\cdot 6H_2O$ (Sigma-Aldrich, 98 %) in the needed water volume was prepared as a 10 wt.% Fe precursor solution. The $FeCl_3$ solution was magnetically stirred while being heated to the same temperature as of the AHM solution (50-60°C). The theoretical Mo/Fe molar ratio was equal to 2 by using these amounts of Mo and Fe precursors.

2.1.1.2 Precipitation

The solution of $FeCl_3$ was continuously added to the AHM solution with a feeding burette under vigorous stirring at a temperature kept between 50-60°C. A lower precipitation

temperature could implicate problems of filtration afterwards. The speed of addition was roughly 3.33 $mL.s^{-1}$. The obtained yellowish precipitate was maintained under agitation for 1 h in its mother liquor. It is suggested to add the $FeCl_3$ solution in the AHM one because the precipitation of iron in the form of $Fe_2(MoO_4)_3$ needs an excess of molybdenum.

2.1.1.3 Decantation, filtration, and drying

After agitation, the decantation process takes place until obtaining a clear solution. This top solution was removed and the precipitate was rinsed with distilled water in the same volume of the discarded solution. This operation was repeated until chloride concentration was less than 2000 ppm. The presence of excess chloride ion was crucial as it decreased the acidity of catalyst. The reference solution of 2000 ppm was prepared by dissolving 3.297 g of NaCl in one litre of distilled water. 5 mL of the discarded solution and 5 mL of the reference solution were placed in different volumetric flasks of 25 mL. 2 mL of calibrated $AgNO_3$ acidified by nitric acid was added in each flask. The intensity of the white $AgCl_{(s)}$ precipitate obtained from the discarded solution was compared to that of the reference. The yellowish precipitate was filtered when the discarded solution is less intense. Otherwise, the precipitate was washed with water before performing again the decantation. After filtration, the precipitate cake was dried at 100-110°C overnight.

2.1.1.4 Calcination

The recovered solid after drying was weighed and mixed with stearic acid ($CH_3(CH_2)_{16}COOH$; Sigma-Aldrich, 95 %) in a quantity equivalent to 1 % of the dried solid mass. The mixture was crushed in a mortar before being pelletized with an IR press. The obtained pellets were further sieved to gather particles with a diameter comprised between 2 and 3 mm. These particles were subsequently calcined in air (0.3 $L.min^{-1}$) with a heating rate of 1°C.min^{-1} until 350 °C for 1 min and of 2°C.min^{-1} until 450 °C for 2 h. The calcined catalysts were subsequently sieved to particles of 250-500 μm diameters before use in catalytic measurements.

The catalysts were named according to their composition and theoretical molar ratio of the single components. For example, the iron molydate mixed oxide with a molar Mo/Fe ratio of 2.5 was named FeMo2.5.

2.1.2 Iron molybdate mixed oxide with tungsten and aluminium modifications

The FeMoW mixed oxide catalysts were prepared by substituting certain amount of W into Mo portion of the FeMo catalyst. The coprecipitation method was also applied here. Ammonium heptamolybdate tetrahydrate ($(NH_4)_6Mo_7O_{24}.4H_2O$, AHM, 4 wt.% of Mo) was dissolved in water and was kept heating at temperatures between 50-60 °C under stirring. In a meantime, the precursors solution of Fe and W were separately prepared by dissolving appropriate amount of ferric chloride ($FeCl_3.6H_2O$, 10 wt.% of Fe) and ammonium metatungstate monohydrate ($(NH_4)_6H_2W_{12}O_{40}.H_2O$, AMT, 4 wt.% of W; Sigma-Aldrich, 99.99 %) in water. The solutions were also kept stirring and heating at the same temperature as that of AHM solution. The AHM solution (pH~5) was acidified with HCl to reach a pH around 1. The AMT solution was then continuously poured into the AHM solution under vigorous stirring, following with the iron chloride solution by the feeding burette. The obtained yellowish precipitate was maintained under agitation for 1 h in its mother liquor before being decanted, dried, and calcined following the same procedures as those applied for the synthesis of unmodified FeMo catalyst.

The FeMoW catalysts were named according to the percentage of W substituting in the FeMo formulation. The FeMo catalyst in which 10 wt.% of Mo was replaced by W was named $FeMoW_{10\%}$, for instance.

Table 2-1: Amount of precursor used in syntheses of FeMoW mixed oxides catalysts.

Catalyst	Mass of precursor (g)			Volume of precursor (mL)		
	AHM[a]	$FeCl_3.6H_2O$[b]	AMT[c]	AHM	$FeCl_3.6H_2O$	AMT
$FeMoW_{10\,\%}$	9	7.5	1.09	225	75	11.4
$FeMoW_{15\,\%}$	8.5	7.5	1.81	212.5	75	18.9
$FeMoW_{20\,\%}$	8	7.5	2.48	200	75	26

[a]4 wt.% $(NH_4)_6Mo_7O_{24}.4H_2O$ solution; [b]10 wt.% solution; [c]4 wt.% $(NH_4)_6H_2W_{12}O_{40}.H_2O$

The FeMoAl mixed oxides catalysts were prepared by replacing the portion of Fe of the FeMo catalyst by certain amount of Al. The synthesis procedures were similar to those applied for the FeMoW mixed oxides catalyst. The exceptions were that aluminum nitrate nonahydrate ($Al(NO_3)_3.9H_2O$, 10 wt.% of Al; Sigma-Aldrich, ≥ 98 %) was used as an Al precursor and the aluminum nitrate solution was first poured in the solution of ferric chloride before the mixture was continuously poured in the AHM solution using the feeding burette.

The FeMoAl catalysts were named according to the percentage of Al substituting in the FeMo formulation. For example, the FeMo catalyst in which 10 wt.% of Fe was replaced by Al was named $FeMoAl_{10\%}$.

Table 2-2: Amount of precursor used in syntheses of FeMoAl mixed oxides catalysts.

Catalyst	Mass of precursor (g)			Volume of precursor (mL)		
	AHM[a]	$FeCl_3.6H_2O$[b]	$Al(NO_3)_3.9H_2O$[c]	AHM	$FeCl_3.6H_2O$	$Al(NO_3)_3.9H_2O$
$FeMoAl_{10\ \%}$	10	6.75	1.25	250	67.5	16.5
$FeMoAl_{20\ \%}$	10	6	2.29	250	60	9

[a]4 wt.% $(NH_4)_6Mo_7O_{24}.4H_2O$ solution; [b]10 wt.% solution; [c]10 wt.% $Al(NO_3)_3.9H_2O$ solution

2.1.3 Fe_2O_3 and MoO_3 single oxides

Single oxide of Fe_2O_3 is prepared by calcination of commercial Fe_2O_3 (Merck, 99 %) was treated in air for 2 h at 350 °C, with a heating rate of 2 °C.min^{-1}. To prepare the single oxide of MoO_3, the Mo precursor, AHM, is calcined at 450 °C, with a heating rate of 2 °C.min^{-1} for 6 h in air. The calcined Fe_2O_3 and MoO_3 powders are similarly sieved to particles of 250-500 μm diameters before measuring their catalytic performances.

2.2 Characterization methods

The characterization techniques used to study the solid surface and properties of the prepared catalysts are presented in the following subsections.

2.2.1 Elemental analysis

2.2.1.1 Inductive coupled plasma with mass spectrometry (ICP-MS)

Elemental analysis of the calcined samples to determine experimental quantities of iron and molybdenum in percentage atomic weight was carried out by ICP-MS using a Thermo-Fischer X7 ICP-MS device. The experiments were performed at the Central Analyses Centre of the CNRS at Solaize, France.

2.2.1.2 Inductive coupled plasma with atomic emission spectrometry (ICP-AES)

Quantities of iron and molybdenum in the calcined samples were measured by ICP-AES using a Vista-Pro spectrometer (VARIAN). 200 mg of catalyst was dissolved in the mixture of 2.5 mL of nitric acid and 5 mL of hydrochloric acid and heated at 120 °C until the solid was completely dissolved. After cooling the solution, acidifying water was added to a total volume

of 100 mL. The solution was then diluted 10 times before the analysis. The volume of 0.25 mL of the aforementioned solution was taken and the acidifying water was added to a 25 mL total volume. For the elemental identification, the characteristic wavelength at 238.204 and 259.94 nm were used for Fe and those at 277.539 and 281.615 nm were applied for Mo.

2.2.2 X-Ray diffraction

In order to follow the crystallization of the different phases, the freshly prepared samples (*i.e.*, the non-calcined) were subjected to X-Ray diffraction analyses with increasing temperature from 50 °C to 500 °C (increasing temperature rate of 10 °C.min^{-1}) under air flow. The diffractograms were collected on a D8 Advance diffractometer (Brüker AXS) equipped with a Cu Kα radiation (λ=1.5406 Å) as X-ray source. The diffractograms were recorded for 2θ values comprised between 10 and 60° using a 0.02° step with an integration time of 1.5 s. X-ray patterns of the catalysts after calcination were collected on the same apparatus at ambient temperature in static air and were recorded in the same 2θ interval. Phase interpretation of XRD patterns was carried out by comparison with the Joint Committee on Powder Diffraction Standards (JCPDS) database registered in the EVA X-ray diffraction analysis software.

2.2.3 Differential thermal analysis and thermogravimetric analysis (DTA-TGA)

Thermogravimetric analysis (TGA) was applied to the freshly prepared sample before calcination to monitor any loss of its mass as a function of temperature. TGA technique can be coupled with differential thermal analysis (DTA) where the amount of heat generated or absorbed by the sample was measured as a function of increasing temperature. TGA analyses were performed using a Thermobalance TA Instruments SDT2960. DTA analyses were carried out in a Thermobalance SETARAM SETSYS. The catalysts were heated from room temperature to 600 °C with an increasing temperature rate of 5 °C.min^{-1} under air flow in both analyses.

2.2.4 Nitrogen adsorption

The specific surface areas of the calcined catalysts were determined using the single-point BET (Brunauer, Emmett, Teller) method [3], with N_2 adsorption at liquid N_2 temperature and subsequent desorption at room temperature. The samples were outgassed at 200 °C for 30 minutes prior to analysis in order to remove physisorbed water at the catalyst surface.

2.2.5 Low energy ion scattering (LEIS)

Elemental identification of the atoms located on the outer surface of the samples (top atomic layer), as well as the in-depth distribution of the subsurface (0-10 nm), was analysed by Low-Energy Ion Scattering (LEIS). In a LEIS measurement, a beam of noble gas ions of known mass (m_1) and energy (E_i) of few keV (below 10 keV), typically $^4He^+$ or $^{20}Ne^+$, are directed perpendicularly towards a sample surface. The incident ions then collide with the surface atoms, with mass m_2, before being back-scattered. The energy of the scattered ions (E_f) is monitored and is used to derive the mass of surface atoms by the laws of conservation of energy and momentum:

$$E_f = E_i \left(\frac{4m_1 m_2 cos^2(\theta)}{(m_1+m_2)^2} \right) \quad (1)$$

where θ is the fixed and narrowly defined scattering angle. Determination of surface elemental identification is thus given by the correlation between E_i or E_f and m_2.

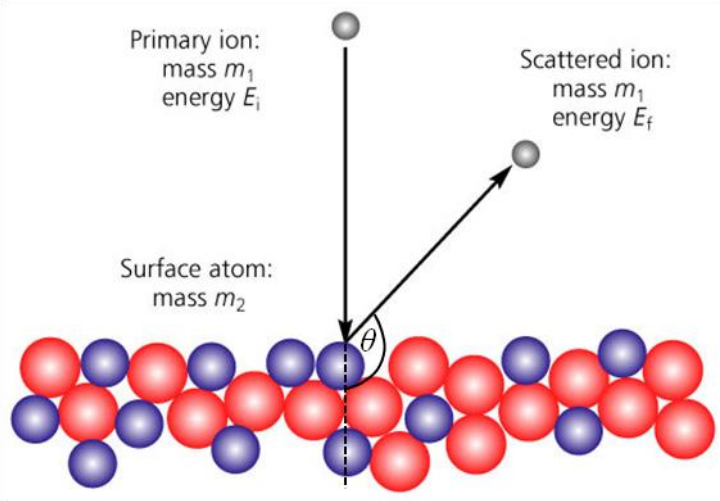

Figure 2-1: Schematic illustrating the low-energy ion scattering (LEIS) adapted from [4].

The LEIS spectra were recorded on a Qtac^{100} spectrometer (ION TOF GmbH, Figure 2-2), described in [5].The instrument uses a double toroidal energy analyser which collects the scattered ions for a given scattering θ of 145° from all azimuth angles, thereby increasing the sensitivity. The LEIS spectra of the calcined samples were obtained using 3 keV $^4He^+$ scattering. Assuming a sputter yield of 0.1 atoms per He-ion under a 4 nA target current, only 3.0 x 10^{13} atoms.cm^{-2} were sputtered from the sample surface during the analysis.

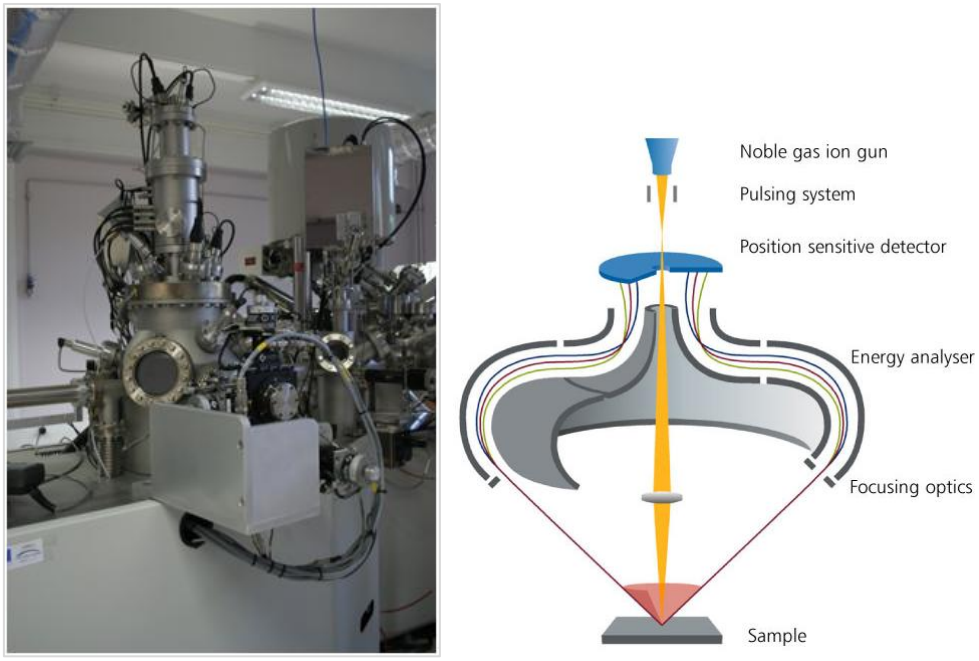

Figure 2-2: (left) Photograph of the Qtac[100] (ION TOF GMBH) apparatus. (right) Schematic of the Qtac[100]. The double toroidal analyzer gives a linear dispersion in energy on the detector, thus enabling parallel detection. Using a pulsed ion beam and time-of-flight filtering, the ions are also mass selected [5,6].

2.2.6 X-Ray photoelectron spectroscopy (XPS)

The catalysts surface, including the elemental composition and the chemical and electronic state of each element in the surface, was investigated by X-ray photoelectron spectroscopy (XPS). XPS spectra are obtained by irradiating a material with a beam of X-rays (*hv* energy) under ultra-high vacuum (UHV) conditions while simultaneously measuring the kinetic energy (E_{kin}) and number of electrons which escape from the top 10 nm of the sample being analyzed. The spectrum is a plot of the number of electrons detected versus the binding energy (E_b) of these electrons detected. Each element provides a characteristic set of XPS peaks at characteristic binding energy values, which are used to identify the element that exists on the surface. The characteristic peaks correspond to the electron configuration within the atoms, *e.g.*, 1s, 2s, 2p, etc. The amount of element within the analyzed area (or volume) is related to the number of detected electrons in each of the characteristic peaks. To determine the atomic concentration, the main XPS signal is corrected by dividing area (number of electrons detected) by the corresponding photoemission cross-section and by the transmission function of the spectrometer and normalized over all of the elements detected. The principle of XPS and a basic component of an XPS system are illustrated in Figure 2-3.

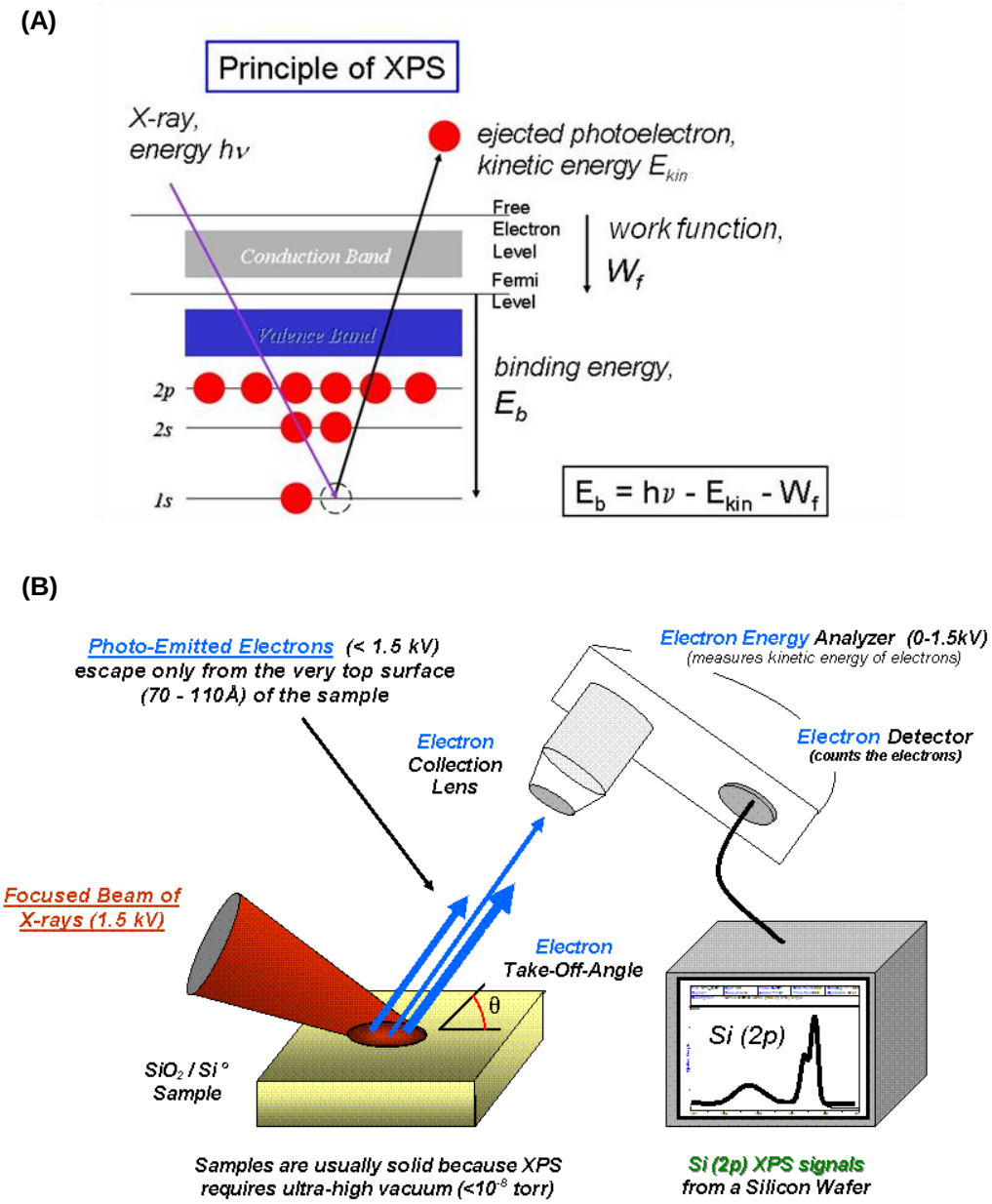

Figure 2-3: (A) Principle of XPS [7] and (B) basic component of an XPS system [8].

In this thesis, the XPS analyses were performed with a VG ESCALAB 220XL spectrometer (Thermo) (Figure 2-4A) using the Al Kα radiation (1486.6 eV) in the large area lens mode. The surface composition was obtained from measurement of the Mo 3d, Fe 2p, C 1s, and O 1s levels, obtained at a 40 eV pass energy. The C 1s binding energy for the C-(C, H) bond was fixed at 285.0 eV as an internal reference. The measurements were carried out under vacuum (around 10^{-7} Pa). The simulation of the experimental photopeaks was carried out using the CasaXPS software [9]. The non-pre-treated catalyst was first analysed under its freshly

prepared form by XPS before being analysed again after pre-reduction in a dedicated treatment chamber (Figure 2-4B) placed under methanol-rich helium atmosphere (20 mol.% methanol) at 255 °C, without intermediate re-exposure to the air. The second measurement was then performed after pre-treatment in oxygen and methanol flow in He ($CH_3OH/O_2/He$ = 20/16/64 mol.%, air condition) in order to perform partial oxidation reaction.

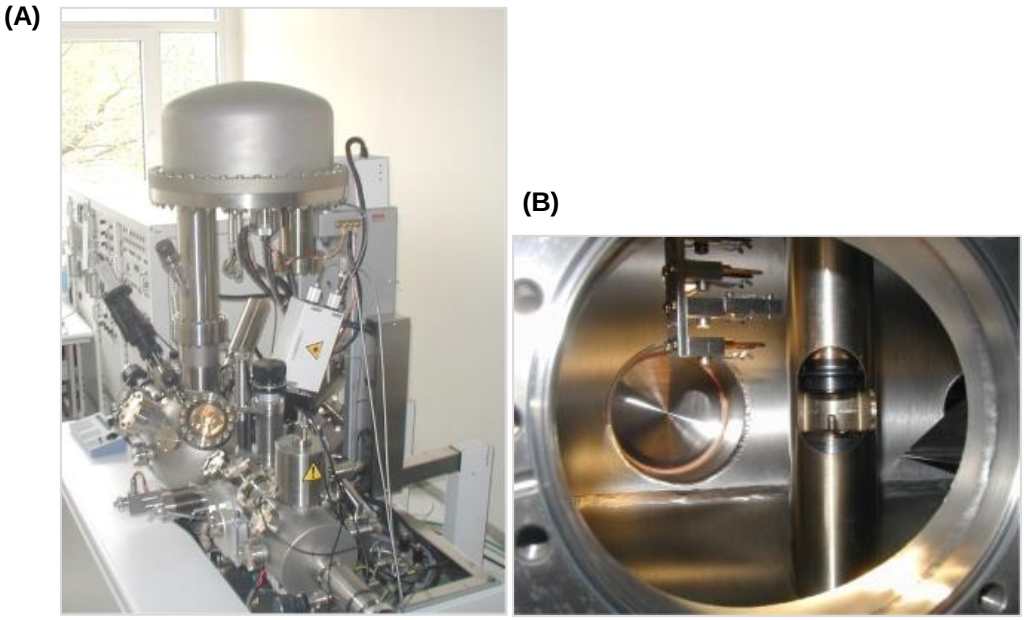

Figure 2-4: (A) Photograph of the VG ESCALAB 220XL apparatus. (B) *In situ* catalysis cell of preparation chamber, where the catalyst was treated under specified under specified condition before being transferred *in situ* towards the analysis chamber.

2.2.7 Electron paramagnetic resonance (EPR)

Electron Paramagnetic Resonance spectroscopy (EPR), also called Electron Spin Resonance (ESR), is a technique used to study chemical species that possess one or more unpaired electrons. When the compound with unpaired electrons is exposed to microwave radiation at fixed frequency, the energy levels accessible to the unpaired electronic spin are split by that field in two energy levels: low-energy state with $M_s = -1/2$ and the high-energy state with $M_s = +1/2$. By increasing the external magnetic field, the energy difference between the two states is widened until it matches, or is resonant with, the energy of the applied microwave frequency. This phenomenon is called the Zeeman effect. At this point, electrons are promoted from the low-energy state to the high-energy one. These electron transitions are observed as the partial adsorption of the microwave intensity. Since the adsorption is fairly broad, an accurate measure of the spacing between the peaks is usually obtained by examining the first-derivative spectrum. Therefore, the EPR spectra (Figure 2-5) are recorded as the rate

of change of adsorption, or the derivative of the imaginary part of the molecular magnetic susceptibility with respect to the external static magnetic field in arbitrary units ($d\chi''/dB$), versus the magnetic field strength [10].

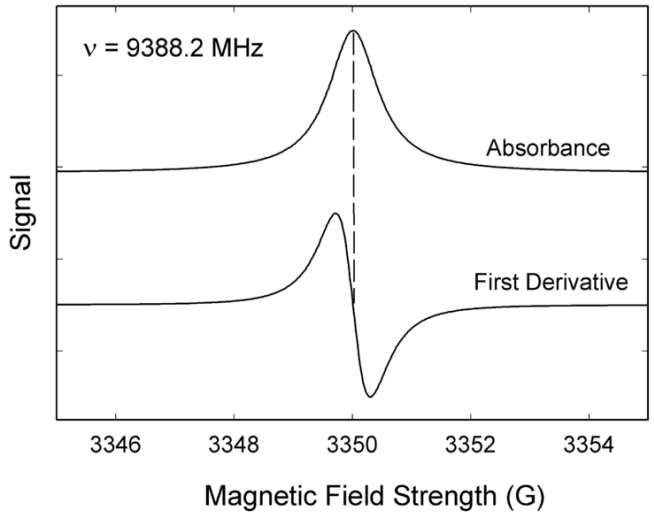

Figure 2-5: Comparison of adsorption spectrum and EPR spectrum [11].

A fingerprint used for the compound identification is the proportional g-factor (also called the electron Landé factor), which contains the chemical information that lies in the interaction between the electron and the electronic structure of the molecule. The g-factor ($g_e + \Delta g$) is determined at the centre of the derivative signal according to the equation:

$$hv = (g_e + \Delta g)\beta B \qquad (2)$$

where h is Planck's constant, v is the microwave frequency, β is the Bohr magneton, and B is the strength of the magnetic field.

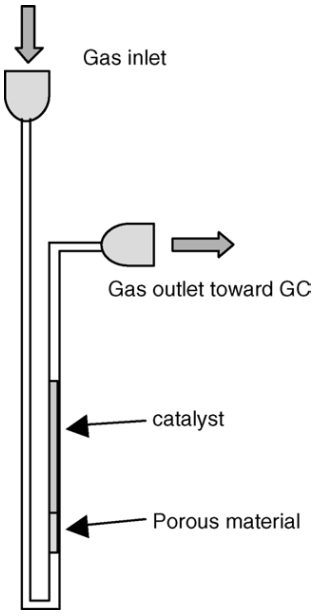

Figure 2-6: Cell dedicated to the EPR experiments [12].

In this thesis, *In situ* Electron Paramagnetic Resonance (EPR) spectra were collected with an X-Band BRUKER ELEXYS E580 spectrometer operating at a 100 kHz modulation frequency and a 2 G modulation amplitude. The microwave power was set to 1 mW. A specially designed cell used for the EPR measurements in *in situ* or *operando* conditions was described in Figure 2-6 [12]. This cell consists of a U-tube containing a filter where the catalyst is located. The gas mixture of methanol, oxygen, and helium flows from the bottom and the products are then analyzed on-line by the µ-gas chromatograph. The fresh catalyst was firstly placed in a cell inserted in a dual cavity at room temperature under vacuum. The treatment temperature was gradually increased to 255 °C. Afterwards a reactant mixture (CH_3OH/O_2/He = 20/16/64 mol.%) was introduced in the EPR cell reactor. For iron molybdate mixed oxides compounds, the active electron and nuclear spins for EPR measurements are listed in Table 2-3. For the Mo^V species the electron is localized in d^1 orbital and as *g* value is governed by the electronic structure, the *g* value attempt for such species will be lower than the free electron *g* value of 2.0023. In the case of Fe^{III}, the electron configuration d^5 will provide a *g* value higher than 2 but also depending on spin state. Effectively Fe^{III} can exhibit a high spin state $S = 5/2$ or low spin state of $S = 1/2$ depending on the ligand field geometry of the complex.

Table 2-3: Nuclear spins and EPR patterns [13].

Metal	Valency	Isotope	Spin (abundance)	EPR lines
Fe	III	54, 56, 57, 58	0 + 1/2 (2 %)	1 + 2 (2 %)
Mo	V	92, 94, 95, 96, 97, 98, 100	0 + 5/2 (25 %)	1 + 6 (4 %)

2.2.8 Temperature-programmed desorption of ammonia (NH_3-TPD) coupled with mass spectroscopy (MS)

The acidity of the fresh catalysts was evaluated by NH_3-TPD using a Micromeritics Autochem 2920 apparatus coupled with a mass spectrometer Omnistar. The freshly prepared catalyst were outgassed under a helium flow of 40 $mL.min^{-1}$, while being heated from room temperature to 250 °C with a heating rate of 10 $°C.min^{-1}$.The final temperature was kept 30 minutes to ensure total elimination of physisorbed water molecules and then cool down to room temperature under He. Adsorption of NH_3 was then performed at room temperature using a 30 $mL.min^{-1}$ flow of 10 % of NH_3 in He for 30 min before the sample was purged with pure He (50 $mL.min^{-1}$) for 2 h to remove physisorbed NH_3. Desorption of NH_3 was then performed applying a heating rate of 10 $°C.min^{-1}$ from room temperature to 600 °C under a He flow of 10 $mL.min^{-1}$ and remained at this temperature for 1 h. In another set of experiments, the samples were also partially reduced with pure H_2 (40 $mL.min^{-1}$) at 280 °C for 1 h before being subjected to TPD experiments, in order to check the acidic properties of reduced catalysts. The recorded NH_3 signals were fitted using the DMFit software [14].The peak area was then calculated and correlated with the amount of adsorbed NH_3 on the basis of the pulsed NH_3 injection experiments.

2.3 Description of catalytic tests

2.3.1 Selective oxidation reaction of methanol

A schematic diagram of the reactor setup used to perform the selective oxidation reaction of methanol in gaseous phase is described in Figure 2-7.

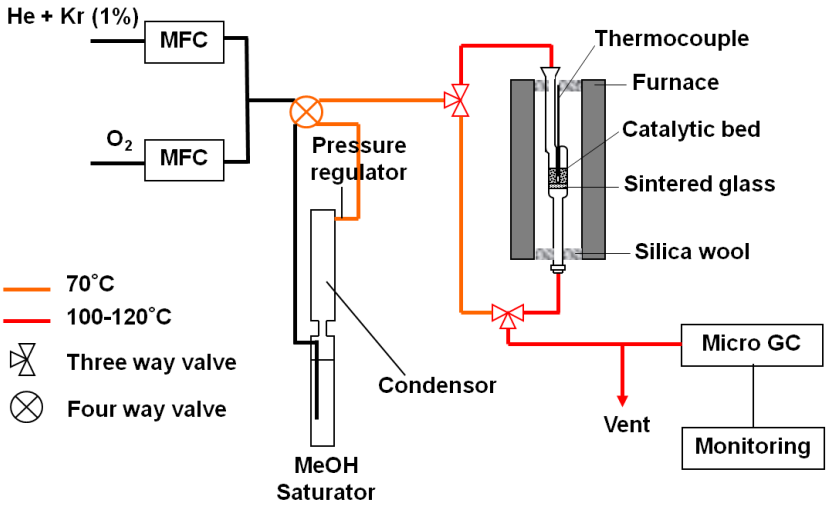

Figure 2-7: Schematic diagram of methanol setup.

At first, a gaseous mixture of He (with 1 % of Kr) and O_2 was passed through a saturator filled with methanol. The flow rates of He and O_2 were controlled by mass flow controllers (Brooks 5850 TR). Helium was employed as the carrier gas and to dilute the reactants. A condenser connected to a refrigerated bath (HAAKE model DC 10) allowed controlling the temperature to adjust the partial pressure of methanol. The temperature was measured at the top of the condenser with a K-type thermocouple. The partial pressure of methanol was set by means of the equation:

$$\ln(P) = A + \frac{B}{T} + C * \ln(T) + D * T^2 \qquad (3)$$

where T is temperature (K); P is partial pressure of methanol (Pa); A, B, C, and D were coefficients of Antoine's equation: A = 81.768, B = -6876, C = -8.7078, and D = $7.19*10^{-6}$ [15]. A difference between saturator and condenser temperatures between 35-40 °C was required for a stable methanol concentration.

The reaction feed comprising the desired concentrations of methanol and O_2 diluted in He was then introduced in a fixed-bed reactor placed in a heating furnace (ERALY). The furnace

temperature was determined by a K-type thermocouple connected to a MICROCOR II R-type controller. The reaction temperature was thus measured by another K-type thermocouple inserting in a thermocouple well in contact with the catalytic bed. The top and bottom ends of the furnace were insulated with glass wool to minimize the heat dispersion. The reaction products were analysed by an online gas micro-chromatograph (SRA 3000 μ-GC, Agilent technologies) equipped with two columns, Plot U (30 μm film thickness, 320 μm inner diameter, and 3 m length) and molecular sieves (5 Å pore opening, 12 μm film thickness, 320 μm inner diameter, and 10 m length), and two thermal conductivity detectors (TCDs). The first TCD module was used to analyse O_2, and CO while the second module was applied for formaldehyde, dimethyl ether, methanol, methyl formate, dimethoxymethane, and CO_2 analyses. The stainless steel tubing of the apparatus was constantly heated to prevent methanol condensation. The tubing after the exit of reactor was heated to 120 °C to avoid paraformaldehyde formation, especially after reaction at high temperature.

The reactor was by-passed and the concentrations of methanol and O_2 in the reaction feed were checked prior to the test. When the desired amount of reactants was stabilized, the feed was sent to the reactor. The catalytic tests were carried out at atmospheric pressure at different temperatures between 230-290 °C. The reactor was loaded with 150 mg of catalyst diluted with the same amount of carborundum (250 μm), to compensate for the heat release from the reaction. Unless specified, the catalysts were directly used after their calcinations, without any pretreatment. The reaction feed was carefully chosen outside the explosive zone of the mixture (Figure 2-8) [16]. It consisted of 40/13/47 mol% of CH_3OH/O_2/He. The gas hourly space velocity (GHSV), defined as the volumetric flow rate of the feed gas per gram of the catalyst per hour, was adjusted to 16 $L.h^{-1}.g_{cat}^{-1}$, with the total flow of methanol/O_2/He of 40-42 $mL.min^{-1}$. The reaction products were analysed every 20 minutes until stabilization (measurements at the steady state).

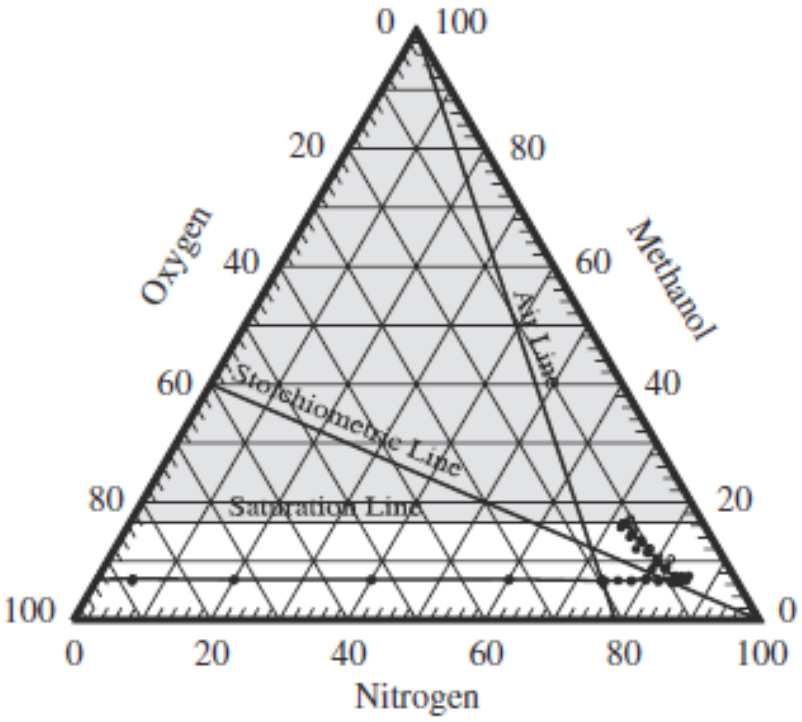

Figure 2-8: Flammability diagram for methanol [16].

2.3.2 Selective oxidation reaction of ethanol

A schematic diagram of the reactor setup in performing the selective oxidation reaction of ethanol in gaseous phase is described in Figure 2-9.

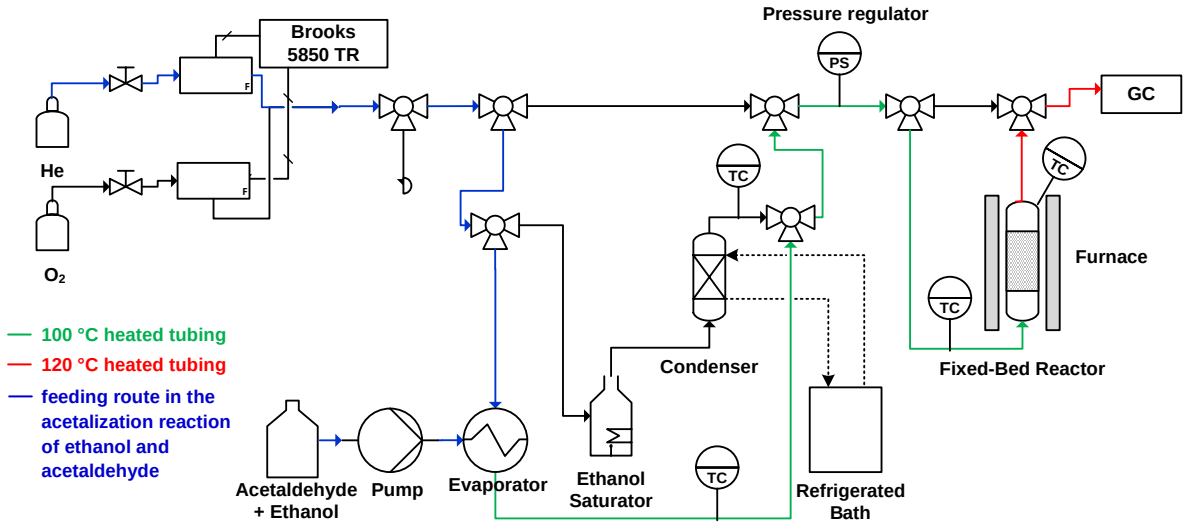

Figure 2-9: Schematic diagram of ethanol setup.

Similar to methanol reaction, a gaseous mixture of He and O_2 was passed through a saturator filled with ethanol. The flow rates of He and O_2 were controlled by mass flow controllers (Brooks 5850 TR). A condenser was connected to a refrigerated bath (Thermo Electron), which allowed controlling the temperature to adjust the partial pressure of ethanol. The temperature was measured at the top of the condenser with a K-type thermocouple. The partial pressure of ethanol was set by means of the equation:

$$\ln(P) = A + \frac{B}{T} + C * \ln(T) + D * T^2 \quad (4)$$

where T is temperature (K); P is partial pressure of ethanol (Pa); A, B, C, and D were coefficients of Antoine's equation: A = 74.75, B = –7164.3, C = –7327, and D = $3.134*10^{-6}$ [15]. A difference between saturator and condenser temperatures between 35-40 °C was necessary for a stable concentration of ethanol.

The reaction feed with the desired concentrations of ethanol, O_2, and He was then introduced in a fixed-bed reactor placed in a heating furnace controlled by a temperature controller (Vertex VTA810). The furnace temperature was determined by a K-type thermocouple connected to a MICROCOR II R-type controller. The reaction temperature was thus measured by the K-type thermocouple sticked to the reactor wall where the catalytic bed was located. The top and bottom ends of the furnace were also insulated with glass wool to minimize the heat dispersion.

The reactor was loaded with 150 mg of catalyst diluted with 600 mg of carborundum (250 μm), to compensate for the heat release from the reaction which is highly exothermic compared to the one with methanol. The reaction feed highly concentrated of ethanol was selected in order to maximize the acetal formation. The feed composition was also carefully chosen outside the explosive region of the mixture (Figure 2-10) [16], consisted of 30.8/7/62.2 mol% of ethanol/O_2/He. The gas hourly space velocity (GHSV) was initially adjusted to 26 $L.h^{-1}.g_{cat}^{-1}$, with the total flow of ethanol/O_2/He of 65 $mL.min^{-1}$.

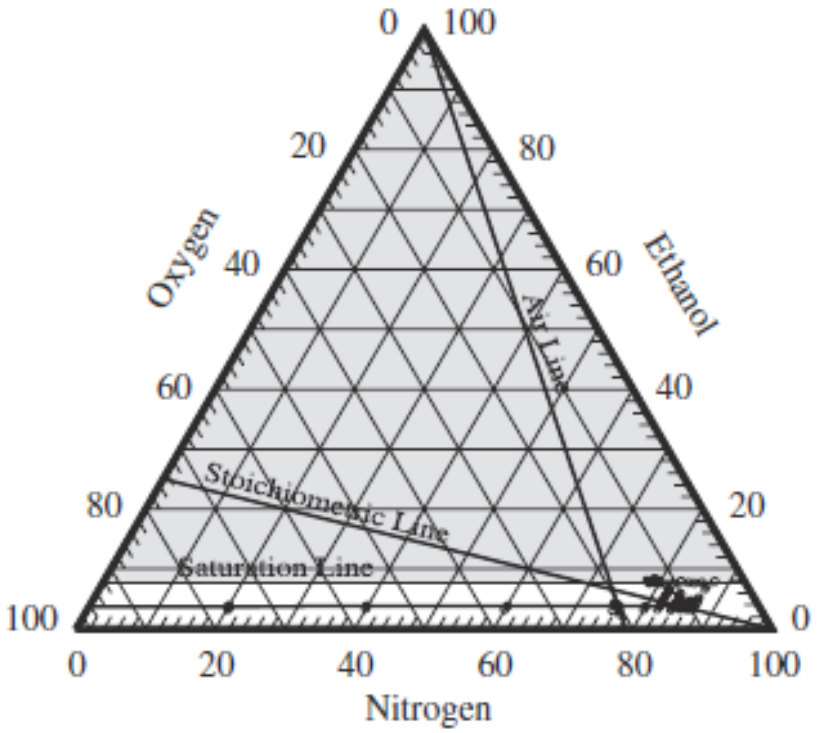

Figure 2-10: Flammability envelope for ethanol [16].

Prior to the test, the reactor was by-passed and the concentrations of ethanol and O_2 in the reaction feed were checked. When the desired amount of reactants was stabilized, the feed was sent to the reactor. The catalytic tests were carried out at atmospheric pressure at different temperatures between 200-250 °C. The effluent gas mixture was analysed every 30 minutes by an online gas chromatograph (Thermo Trace GC Ultra) comprised of two furnaces. A central oven, maintained at 100 °C, was equipped with two columns – a packed column (HaysepQ, 80-100 mesh) and a capillary column (PS255, 30 m-0.32 mm-film micron). A molecular sieve and injection loops were located in an auxiliary oven heated to 120 °C. The GC was equipped with TCD and FID detectors, with He as a carrier gas. The TCD detector was used to analyse lighter molecules, *i.e.*, CO, CO_2, N_2, O_2, H_2O, and ethylene. The FID detector was used to analyse heavier molecules, *i.e.*, ethanol, diethyl ether, acetaldehyde, acetic acid, ethyl acetate, and diethoxyethane. The stainless steel tubing of the apparatus was constantly heated to prevent the condensation of both ethanol (78.4 °C boiling point) and diethoxyethane (102 °C boiling point).

Unlike the methanol reaction, the influence of catalyst pretreatment was also studied. The catalyst was pretreated in the 60 $mL.min^{-1}$ flow of O_2 and He (20/80 mol.%) at 340 °C (10

°C.min^{-1} increasing temperature rate) for 15 h. Afterwards, the temperature of the catalytic bed was lowered close to the desirable reaction temperature while maintaining the catalyst in the same flow condition.

2.3.3 Acetalization reaction of ethanol and acetaldehyde

A schematic diagram of the acetalization reaction of ethanol and acetaldehyde is also depicted in the aforementioned Figure 2-9. The reaction was carried out in the absence of oxygen. Instead of using the saturator-condenser system, the mixture of ethanol and acetaldehyde, with a stoichiometric molar ratio of 2:1, was supplied to the fixed-bed reactor by means of a metering pump (Agilent 1260 Quaternary Infinity Pump VL). The mixture was then diluted with He, sending *via* the flow controller, before being evaporized and sending to the reactor. The reactor was filled with 150 mg of the catalyst (250-500 μm) was mixenbd well with 600 mg of carborundum (SiC, 250 μm). The tests were carried out at slightly higher than atmospheric pressure (1.35 bar) at temperatures between 80-120 °C. The space velocity was employed at 26 L.h^{-1}.g$_{cat}^{-1}$, with the total flow of ethanol/acetaldehyde/He of 65 mL.min^{-1}. Analyses of reaction products were performed similar to those described for the selective oxidation reaction of ethanol (*cf.* subsection 2.3.2).

2.3.4 Products analysis

Catalytic performance indicators were expressed in terms of conversions, product selectivities, and yields. The conversions (X) of methanol, ethanol, and oxygen were calculated using the following equations:

$$X_{MeOH} = \frac{(n_{MeOH,in} - n_{MeOH,out})}{n_{MeOH,in}} \quad (5)$$

$$X_{EtOH} = \frac{2*(n_{EtOH,in} - n_{EtOH,out})}{2*n_{EtOH,in}} \quad (6)$$

$$X_{O_2} = \frac{n_{O_2,in} - n_{O_2,out}}{n_{O_2,in}} \quad (7)$$

where n is the amount of the reactant (either alcohol or oxygen) in moles before and after reaction.

In this work, the selectivity to product B is defined as the total number of carbon atoms of the product B divided by the total number of carbon atoms of the alcohol being converted as follow:

$$S_B = \frac{n^o_{carbon} * n_B}{n^o_{carbon} * (n_{alcohol,in} - n_{alcohol,out})} \quad (8)$$

It is notable that methanol and ethanol contain one and two carbon atoms, respectively. For the selective oxidation of methanol, the selectivities to formaldehyde (F), dimethyl ether (DME), methyl formate (MF), and dimethoxymethane (DMM) were calculated as follows:

$$S_F = \frac{n_F}{n_{MeOH,in} - n_{MeOH,out}} \quad (9)$$

$$S_{DME} = \frac{2 * n_{DME}}{n_{MeOH,in} - n_{MeOH,out}} \quad (10)$$

$$S_{MF} = \frac{2 * n_{MF}}{n_{MeOH,in} - n_{MeOH,out}} \quad (11)$$

$$S_{DMM} = \frac{3 * n_{DMM}}{n_{MeOH,in} - n_{MeOH,out}} \quad (12)$$

For the selective oxidation of ethanol, the selectivities to acetaldehyde (ACD), diethyl ether (DETH), ethylene (ETH), acetic acid (AA), ethyl acetate (EA), and diethoxyethane (DEE) were calculated using the equations:

$$S_A = \frac{2 * n_{ACD}}{2 * (n_{EtOH,in} - n_{EtOH,out})} \quad (13)$$

$$S_{ETH} = \frac{4 * n_{DETH}}{2 * (n_{EtOH,in} - n_{EtOH,out})} \quad (14)$$

$$S_E = \frac{2 * n_{ETH}}{2 * (n_{EtOH,in} - n_{EtOH,out})} \quad (15)$$

$$S_{AA} = \frac{2 * n_{AA}}{2 * (n_{EtOH,in} - n_{EtOH,out})} \quad (16)$$

$$S_{EA} = \frac{4 * n_{EA}}{2 * (n_{EtOH,in} - n_{EtOH,out})} \quad (17)$$

$$S_{DEE} = \frac{6 * n_{DEE}}{2 * (n_{EtOH,in} - n_{EtOH,out})} \quad (18)$$

The yield of product *B* was defined as the total number of carbon atoms of the product B being produced from the reaction divided by the initial number of carbon atoms of the alcohol before reaction:

$$Y_B = \frac{n^0_{carbon} * n_B}{n^0_{carbon} * n_{alcohol,in}} * 100 \quad (19)$$

or else, Eq. 19 can be deduced to, $Y_B = X_{alcohol} * S_B$ (20)

In any experiment, the carbon balance was verified by calculating the ratio of the total number of carbon atoms in the carbonaceous products, including the unconverted alcohol, to the number of carbon atoms in the alcohol feed. Indeed, the analysis was considered as reliable when the carbon balance was close to 100. It is notable that the carbon balance in any experiment reported in this thesis, which underlines accuracy of the measurements, was comprised between 90 and 110 %.

$$B_{C,MeOH} = \frac{\left(n_F+2*n_{DME}+3*n_{DMM}+2*n_{MF}+n_{CO}+n_{CO_2}+n_{MeOH}\right)_{out}}{n_{MeOH,in}} \quad (21)$$

$$B_{C,EtOH} = \frac{\left(2*n_{ACD}+4*n_{DETH}+2*n_{ETH}+2*n_{AA}+6*n_{DEE}+4*n_{EA}+n_{CO}+n_{CO_2}+n_{EtOH}\right)_{out}}{2*(n_{EtOH,in})} \quad (22)$$

2.4 References

[1] N. Pernicone, F. Lazzerin, G. Liberti, G. Lanzavecchia, J. Catal. 14 (1969) 293.

[2] N. Pernicone, J. Less-Comm.- Metals, 36 (1974) 289.

[3] S. Brunauer, P.H. Emmett, E. Teller, J. Am. Chem. Soc. 60 (1938) 309.

[4] H.H. Brongersma, T. Grehl, E.R. Schofield, R.A.P. Smith, Platinum Metals Rev., 54 (2010) 81.

[5] H.H. Brongersma, T. Grehl, P.A. van Hal, N.C.W. Kuijpers, S.G.J. Mathijssen, E. R. Schofield, R.A.P. Smith, H.R.J. ter Veen, Vacuum 84 (2010) 1005.

[6] http://www.platinummetalsreview.com/images/articles/54/2/Smith-54-2-apr10-f4.jpg, verified on January 10, 2013.

[7] http://www.ifw-dresden.de/institutes/ikm/organisation/dep-31/methods/x-ray photoelectron-spectroscopy-xps, verified on January 10, 2013.

[8] http://en.wikipedia.org/wiki/File:System2.gif, verified on January 10, 2013.

[9] N. Fairley, www.casaxps.com, verified on January 10, 2013.

[10] R. Biswas, H. Kühne, G.W. Brudvig, V. Gopalan, Science Progress, 84 (2001) 45.

[11] http://en.wikipedia.org/wiki/File:EPR_lines.png, verified on January 10, 2013.

[12] M. Brandhorst, S. Cristol, M. Capron, C. Dujardin, H. Vezin, G. Lebourdon, E. Payen, Catal. Today 113 (2006) 34.

[13] W.R. Hagen, Dalton Trans., 2006, 4415.

[14] D. Massiot, F. Fayon, M. Capron, I. King, S. Le Calvé, B. Alonso, J-O. Durand, B. Bujoli, Z. Gan, G. Hoatson, Magn. Reson. Chem. 40 (2002) 70.

[15] Component plus 2.0.0.4 software, Prosim S.A.

[16] M.R. Brooks, D.A. Crowl, J. of Loss Prevention in the Process Industries, 20 (2007) 144.

Chapter 3

Results and discussion: 1,1-dimethoxymethane synthesis from methanol

Parts of this chapter are published in:

K.-a. Thavornprasert, M. Capron, L. Jalowiecki-Duhamel, O. Gardoll, M. Trentesaux, A.-S. Mamede, G. Fang, J. Faye, N. Touati, H. Vezin, J.-L. Dubois, J.-L. Couturier, F. Dumeignil, Appl. Catal. B: Environ., http://dx.doi.org/10.1016/j.apcatb.2013.01.043

3.1 Introduction

In this chapter, the experimental results and their discussion are concentrated on the direct conversion of methanol aimed at *1,1*-dimethoxymethane (DMM) formation. We begin with preliminary characterizations of the tested solids, *i.e.*, iron molybdate (FeMo) mixed oxides, MoO_3, and Fe_2O_3 catalysts. In this context, differential scanning calorimetry and thermogravimetric analyses (DSC-TGA) were used to investigate any change due to temperature in the amount of heat generated or adsorbed by the non-calcined sample and the loss of its mass, respectively. The calcined catalyst composition was examined using elemental analysis including inductively-coupled plasma (ICP) coupled with either mass spectroscopy (MS) or with atomic emission spectroscopy (AES). Powder X-ray diffraction (XRD) was relevant for analyzing different mixed oxides phases being formed after the catalyst calcination. The specific surface area of the calcined catalysts was determined as well by nitrogen adsorption.

Performances of those aforementioned catalysts evaluated in a fixed-bed rector at atmospheric pressure under different reaction conditions are described afterwards. The reactivity of the catalysts in the partial oxidation of methanol is indeed dependent on several factors, *e.g.*, reaction temperature, oxygen concentration, as well as the composition of the catalysts. Influence of these parameters on the catalytic performance was then analyzed and discussed herein the chapter.

Following the catalytic measurements section, intensive characterizations on FeMo mixed oxides catalyst system aiming to investigate their relevant catalytic properties and to correlate these functions to the catalytic behavior in the direct synthesis of DMM from methanol. Temperature-programmed desorption of ammonia (NH_3-TPD) as well as more sophisticated characterization methods including low energy ion scattering (LEIS), X-ray photoelectron spectroscopy (XPS), and *in situ* electron spin resonance (EPR) were applied for this purpose. The so-obtained results could therefore give us reliable hints to propose a model of the active site for this catalytic system in the studied reaction.

3.2 Preliminary characterizations of FeMo mixed oxides and single oxides (MoO_3 and Fe_2O_3) catalysts

The dried FeMo mixed oxides samples were analyzed by DSC and TGA measurements in order to study the thermal effect on the catalyst before calcination. Figure 3-1 presents a DSC curve of the FeMo3.75 sample before calcination; the DSC experiment of this sample is characteristic of the series. The curve shows endothermic peaks between 80 °C and 200 °C, that can be ascribed to the elimination of physisorbed water for temperatures lower than 125°C, to dehydration for the temperature range between 125 and 200 °C [1] and to the decomposition of NH_4^+ present in the Mo precursor ($(NH_4)_6Mo_7O_{24}.4H_2O$). It was reported that the dehydration occurs with the formation of an amorphous anhydrous iron molybdate, which then decomposes and crystallizes at higher temperatures giving a mixture of mixed oxide phases [2]. The crystallization is evidenced by two intense exothermic DSC peaks between 380 °C and 430 °C. The loss of water and decomposition of the anhydrous iron molybdate in the same range of temperatures is also observed by TGA analysis (Figure 3-2). With respect to these results, the calcination should be performed at a temperature higher than 250 °C to assure complete decomposition of the catalyst precursor. According to Pernicone [2], the highest surface area is also obtained after crystallization at 370 °C where the traces of water are completely vanished. It is notable that other samples in the series of FeMo mixed oxides catalyst exhibit the same aforementioned characteristics.

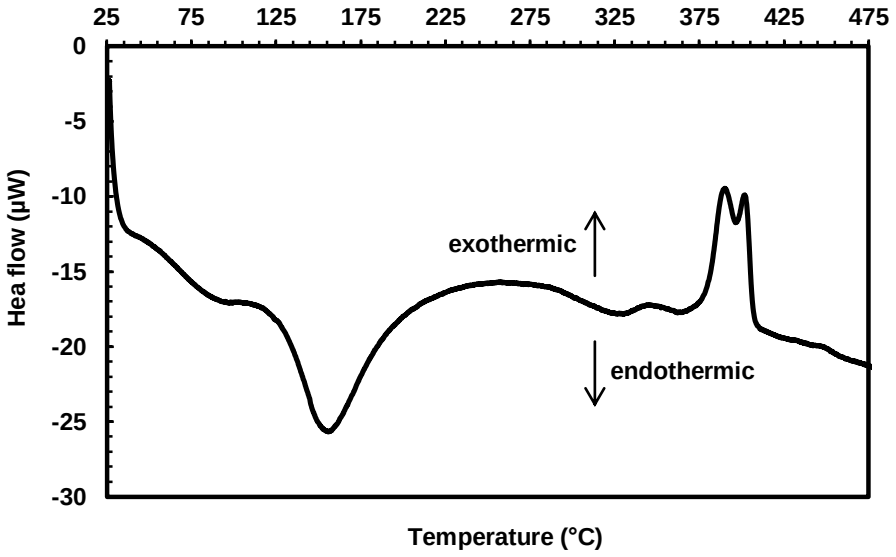

Figure 3-1: DSC curve of the non-calcined FeMo3.75 sample.

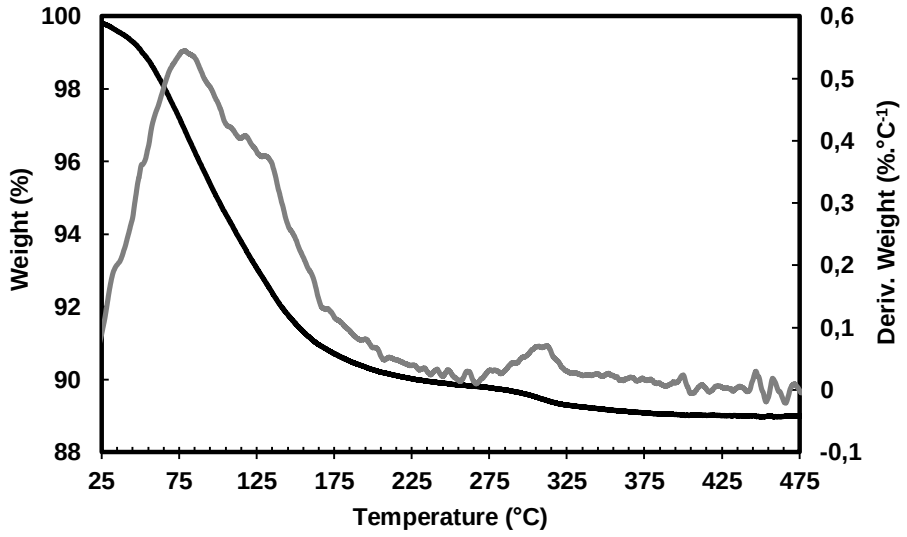

Figure 3-2: TG (in black) and DTG (in grey) curves of the non-calcined FeMo3.75 sample.

Table 3-1: Physical properties of the calcined catalysts ($T_{calcined}$ = 450 °C) prepared with different Mo/Fe nominal atomic ratios and single oxides (Fe_2O_3 and MoO_3).

Catalyst	S_{BET} ($m^2.g^{-1}$)	Mo/Fe ratio		Fe/M_T	Amount of crystalline phase (rel. %)	
		ICP-MS	ICP-AES		$Fe_2(MoO_4)_3$	MoO_3
FeMo2.5	2	2.5	2.6	0.283*	87	13
FeMo3.0	7	2.8	2.8	0.260*	77	23
FeMo3.5	11	3.5	3.6	0.222*	80	20
FeMo3.75	10	3.4	3.4	0.228*	64	36
FeMo4.0	5	-	3.9	0.205	52	48
Fe_2O_3	2	-	-	1	100 rel.% Fe_2O_3	
MoO_3	4	-	-	0	100 rel.% MoO_3	

* From ICP-MS measurements.

The calcined catalysts were characterized by X-ray diffraction (XRD) to determine the different phases of mixed oxides appearing after calcinations. It has been reported that the iron molybdate mixed oxide catalysts consist of two or three crystalline phases depending on the synthesis parameters [3-5]. XRD patterns of the calcined FeMo catalysts exhibit characteristic peaks of ferric molybdate ($Fe_2(MoO_4)_3$, JCPDS#83-1701) and molybdite (MoO_3, JCPDS#05-0508) phases, as shown in Figure 3-3. The respective amount of each main phase present in the catalysts was determined from their diffractograms using the Eva

software (Table 3-1). FeMo2.5, FeMo3.0, FeMo3.5, FeMo3.75 and FeMo4.0 samples are constituted of $Fe_2(MoO_4)_3$ with 87, 77, 80, 64 and 52 rel.% and MoO_3 with 13, 23, 20, 36 and 48 rel.%, respectively. Their specific surface areas obtained from the nitrogen adsorption experiments are summarised in Table 1 with 2, 7, 11, 10 and 5 $m^2.g^{-1}$, respectively. The ICP-MS (or ICP-AES) atomic composition of the samples are also given in terms of Mo/Fe atomic ratios, with values of 2.5, 2.8, 3.5, 3.4 and 3.9, respectively – corresponding to Fe/M_T values, (where M_T = Fe + Mo), of 0.283, 0.260, 0.222, 0.228 and 0.205. It is notable that the relative amount of MoO_3 phase present in the catalyst reasonably increases with the Mo/Fe atomic ratio. Nonetheless, no significant correlation could be observed between the specific surface areas – which remained low in any case, less than or equal to 11 $m^2.g^{-1}$ – and the Mo/Fe ratio. The single oxides, Fe_2O_3 and MoO_3, exhibited pure hematite (Fe_2O_3, JCPDS#89-8104, Figure 3-4) and pure molybdite (MoO_3, JCPDS#76-1003, Figure 3-5) phases, respectively. Their specific surface areas obtained from the nitrogen adsorption experiments were of 2 and 4 $m^2.g^{-1}$.

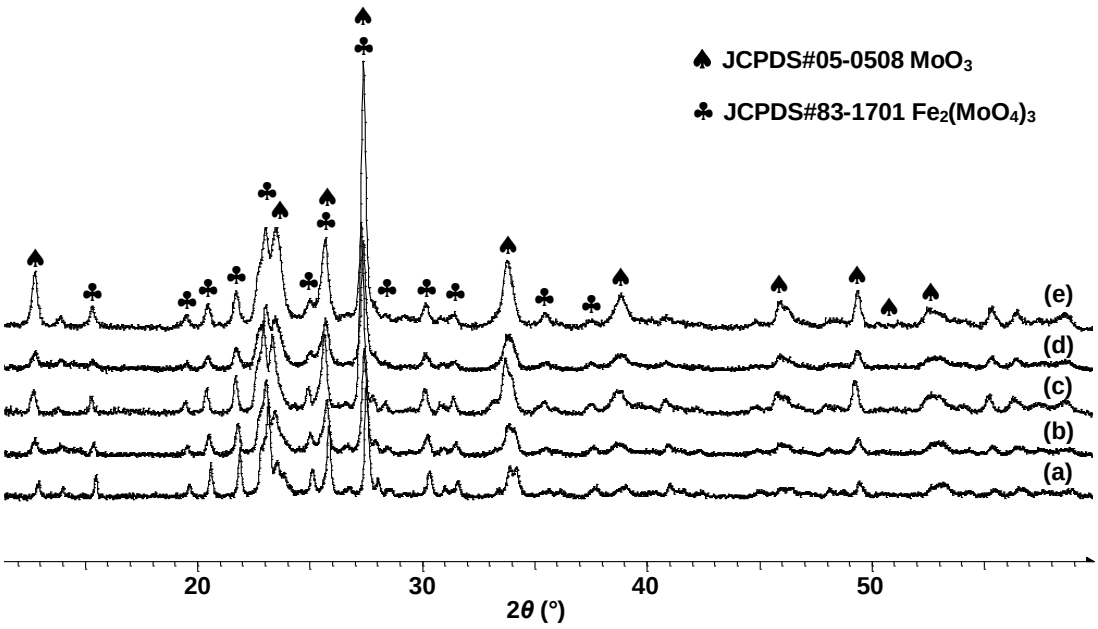

Figure 3-3: XRD patterns of the FeMo catalysts after calcination at 450 °**C** in air for 2 h: FeMo2.5 (a), FeMo3.0 (b), FeMo3.5 (c), FeMo3.75 (d) and FeMo4.0 (e).

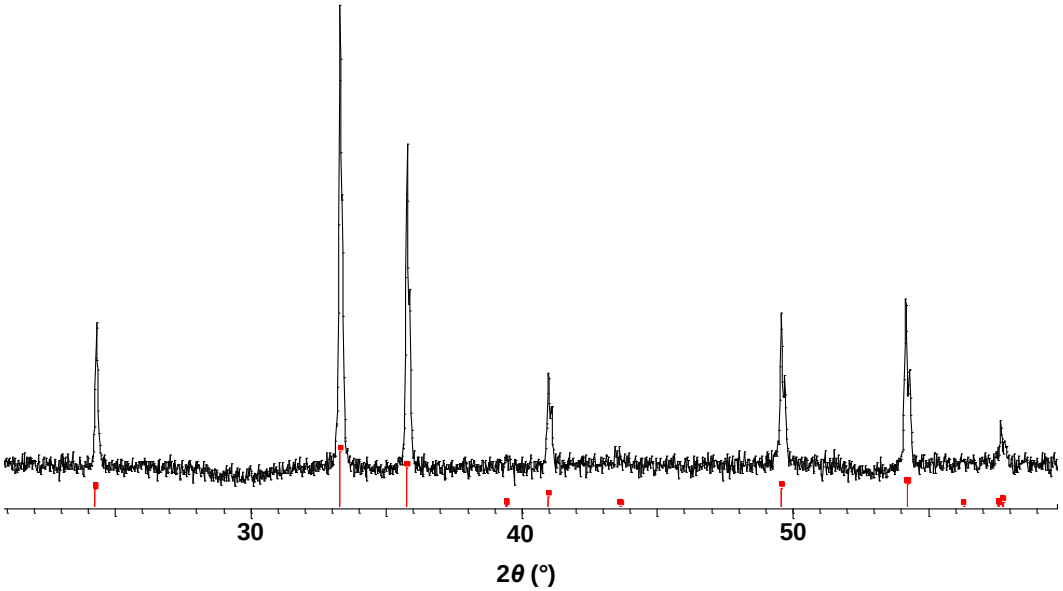

Figure 3-4: XRD patterns of Fe_2O_3 obtained after pretreatment in air at 350 °C for 2 h.

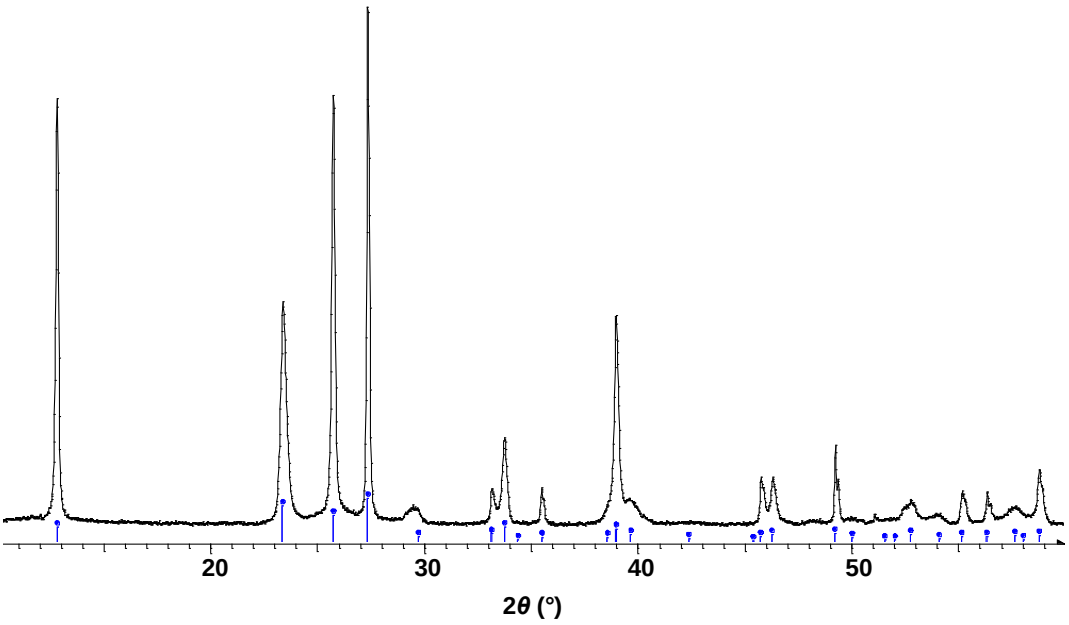

Figure 3-5: XRD patterns of MoO_3 obtained after calcination at 450 °C in air for 6 h.

3.3 Catalytic measurements

3.3.1 Effect of reaction temperature

The FeMo3.75 catalyst was tested in the partial oxidation reaction of methanol at different temperatures (230 °C, 255 °C, 270 °C, and 285 °C) in order to study the influence of temperature on the catalytic performance and to optimize the temperature where the best yield in DMM could be achieved. Catalytic performance indicators, *i.e.*, methanol conversion, products selectivities, and DMM yield, at the steady state as a function of reaction temperature are shown in Figure 3-6.

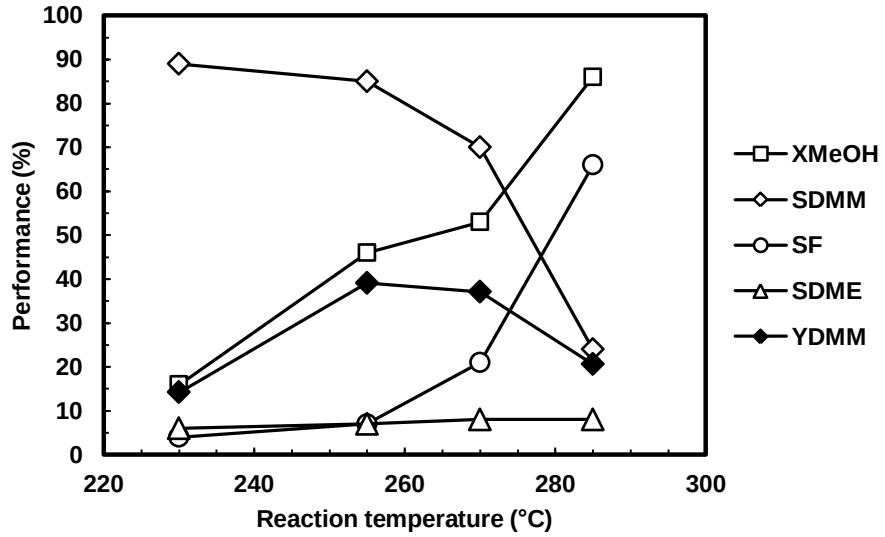

Figure 3-6: Steady state performance over FeMo3.75 catalyst as a function of reaction temperature; reaction conditions: $CH_3OH/O_2/He$ = 40/13/47 mol.%, O_2/CH_3OH = 0.325, GHSV = 16 $L.h^{-1}.g_{cat}^{-1}$, $m_{catalyst}$ = 150 mg.

With increasing temperature, the conversion of methanol certainly increases almost linearly from 16 % at 230 °C to 86 % at 285 °C. The major products of reaction are formaldehyde (F), DMM, and dimethyl ether (DME). A small amount, *i.e.*, less than 2 %, of methyl formate (MF) and carbon oxides (CO and CO_2) are observed. The selectivity to DME remains constant, *i.e.*, approximately 7 %, in any tested reaction temperature. The DMM selectivity gradually decreases with temperature from 89 % (230 °C) to 85 % (255 °C) and 70 % (270 °C), then decreases drastically to 24 % at 285 °C. In contrast, F selectivity increases with temperature from 4 % (230 °C) to 7 % (255°C) and 21 % (270 °C), then increases sharply to 66 % at 285 °C. As one can see that the selectivity to DMM decreases with increasing conversion of methanol, especially at high temperatures. The increase in conversion, indeed,

lead to a depletion of methanol in the reaction medium, which then suppress/limit the DMM formation. The high temperature could also facilitate the desorption of methoxy groups adsorbed on the catalyst surface in the form of F. Otherwise, the oxidation reaction of methanol becomes more thermodynamically favorable than the consecutive acetalization to form DMM when increasing temperature. The best yield in DMM of 39 % is clearly obtained at 255 °C with 46 % of methanol conversion and 85 % of DMM selectivity. This optimum reaction temperature will be further employed to study the effect of oxygen concentration in the reaction feed described in the following subsection.

3.3.2 Effect of oxygen content in the reaction feed

The FeMo3.75 catalyst is tested in the reaction of methanol carried out with the reaction mixture containing different concentrations of oxygen. The reaction feed is composed of 40 mol.% of methanol and *x* mol.% of oxygen, diluted in helium, where *x* = 7, 8.5, 13, and 19 – corresponding to O_2/CH_3OH ratios of 0.175, 0.2, 0.325, and 0.5, respectively. This range of feed composition was chosen in order to be safely out of the flammability zone (*cf.* Figure 2-8 in Chapter 2). The catalytic performance indicators – methanol conversion, products selectivities, and DMM yield – at the steady state are plotted as a function of oxygen concentration in the feed in Figure 3-7.

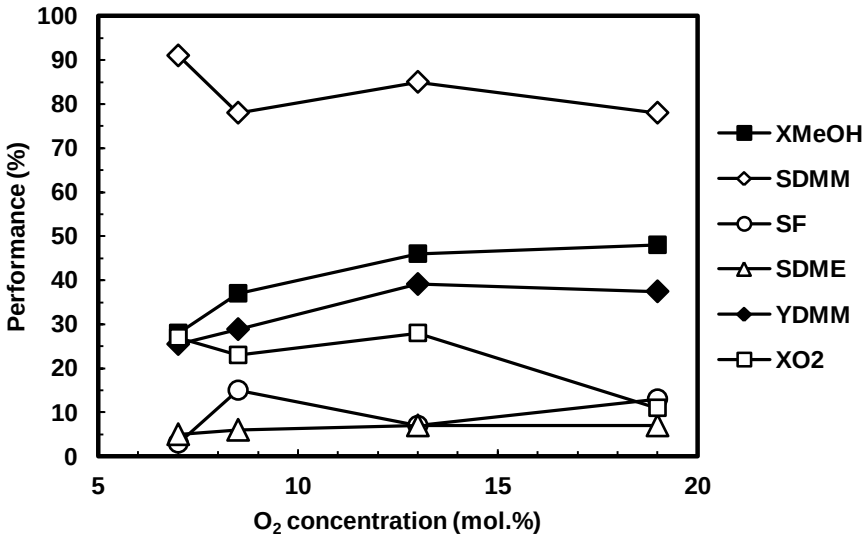

Figure 3-7: Steady state performance over FeMo3.75 catalyst as a function of oxygen concentration in the feed; reaction conditions: GHSV = 16 $L.h^{-1}.g_{cat}^{-1}$, $m_{catalyst}$ = 150 mg, *T* = 250-255 °C, time on stream = 12 h for each point.

The conversion of methanol increases with oxygen content in the reactive mixture from 28 % (7 mol.% O_2) to 48 % (19 mol.% O_2), in contrast with the conversion of O_2, which decreases from 27 % to 11 %, respectively. DMM, F, and DME are maintained as the major products of reaction, with the observation of a small amount of MF and carbon oxides (less than 2 %). The selectivity to DME remains constant, *i.e.*, approximately 6 %, in any varied oxygen concentration. In general, the DMM selectivity gradually decreases with increasing amount of oxygen in the feed from 91 % (7 mol.% O_2) to 78 % (19 mol.% O_2) however no drastic loss in DMM yield is evidenced. Contrary to DMM, the selectivity to F tends to increase with oxygen content from 7 % (7 mol.% O_2) to 13 % (19 mol.% O_2). Relatively high DMM selectivity (85 %) and methanol conversion (45 %) is obtained at 13 mol.% of oxygen in the reaction medium, leading to the highest DMM yield of 39 %.

3.3.3 Effect of catalyst composition

It is obvious that the composition of the material plays a role in the catalytic activity, in order to evaluate this parameter we have synthesized a series of catalysts by changing the Mo/Fe ratio. The Figure 3-8 presents the catalytic performances at 255 °C at the steady state over the FeMo mixed oxides samples with different Mo and Fe loadings using the reaction mixture comprised of $CH_3OH/O_2/He$ = 40/13/47 mol.%, which were proven to be the optimal reaction temperature and feed composition for DMM production, respectively. One can see from the figure that during the reaction, the methanol conversion gradually increases with time on stream before stabilizing (Figure 3-8A). FeMo3.75 exhibits the highest conversion of 46 %. FeMo3.0 and FeMo3.5 catalysts show similar methanol conversions (*ca.* 35 %), whereas FeMo4.0 gives a conversion of 19 %. The lowest conversion is however observed over FeMo2.5 (17 %), possibly due to its particularly low specific surface area (2 $m^2.g^{-1}$). Irrespective of the sample, the same trend is observed concerning DMM selectivity evolution, which gradually increases with time on stream before stabilizing after 4 ~ 5 h (Figure 3-8B). The highest DMM selectivity is observed over FeMo2.5 (93 %), certainly linked with the low conversion of this sample. At low methanol conversion, the quantity of methanol which can react with oxidized intermediates (formaldehyde, methoxy groups, *etc.*) is still high and this could facilitate the DMM formation, leading to the high DMM selectivity. Likewise, a high selectivity to DMM of 89 % is obtained with FeMo4.0, which also exhibits a rather low conversion (19 %). A considerably high DMM selectivity of 85 % is however still observed over FeMo3.0, FeMo3.5 and FeMo3.75 catalysts. As a consequence of its high conversion, FeMo3.75 with a Mo/Fe bulk atomic ratio of 3.4 presents the highest yield in DMM (Figure

3-8C). This sample is also the one that exhibited a relatively large amount of MoO_3 phase (36 %) together with a relatively high specific surface area (10 $m^2.g^{-1}$) in comparison to the other samples (*cf.* subsection 3.2, Table 3-1).

The performance indicators (methanol conversion, DMM selectivity and DMM yield) are also reported relative to the proportion of Fe in the samples. In Figure 3-9, these parameters are plotted *vs.* Fe/M_T. Clearly, an optimal DMM yield of 50 % might be extrapolated for a Fe/M_T ratio of about 0.24 (Mo/Fe = 3.2) (Figure 3-9B). The performances of the Fe_2O_3 and the MoO_3 samples, thus with Fe/M_T = 1 and 0, respectively, are also added for comparison. A stable conversion of 7 % is obtained over Fe_2O_3 without any DMM formation. This sample is selective to methyl formate (80 %) and formaldehyde (20 %), which show a low amount of active sites with probably different acidic properties. On the other hand, MoO_3 exhibits a high selectivity to DMM of 80 % at the same methanol conversion of 7 %. This suggests that even if MoO_3 has a low amount of active sites, it possesses the intrinsic properties to yield DMM (*i.e.*, redox and acidic properties), which are then boosted in the presence of Fe in the mixed oxide, with a synergetic effect on conversion. Figure 3-9B shows a close-up of Figure 3-9A for Fe/M_T ratios between 0.2 and 0.3. This figure evidences that high DMM yields are obtained in a very narrow range of Fe contents, *i.e.*, 30 to 40 % yields in DMM are achieved with the Fe/M_T ratios between 0.22 and 0.26.

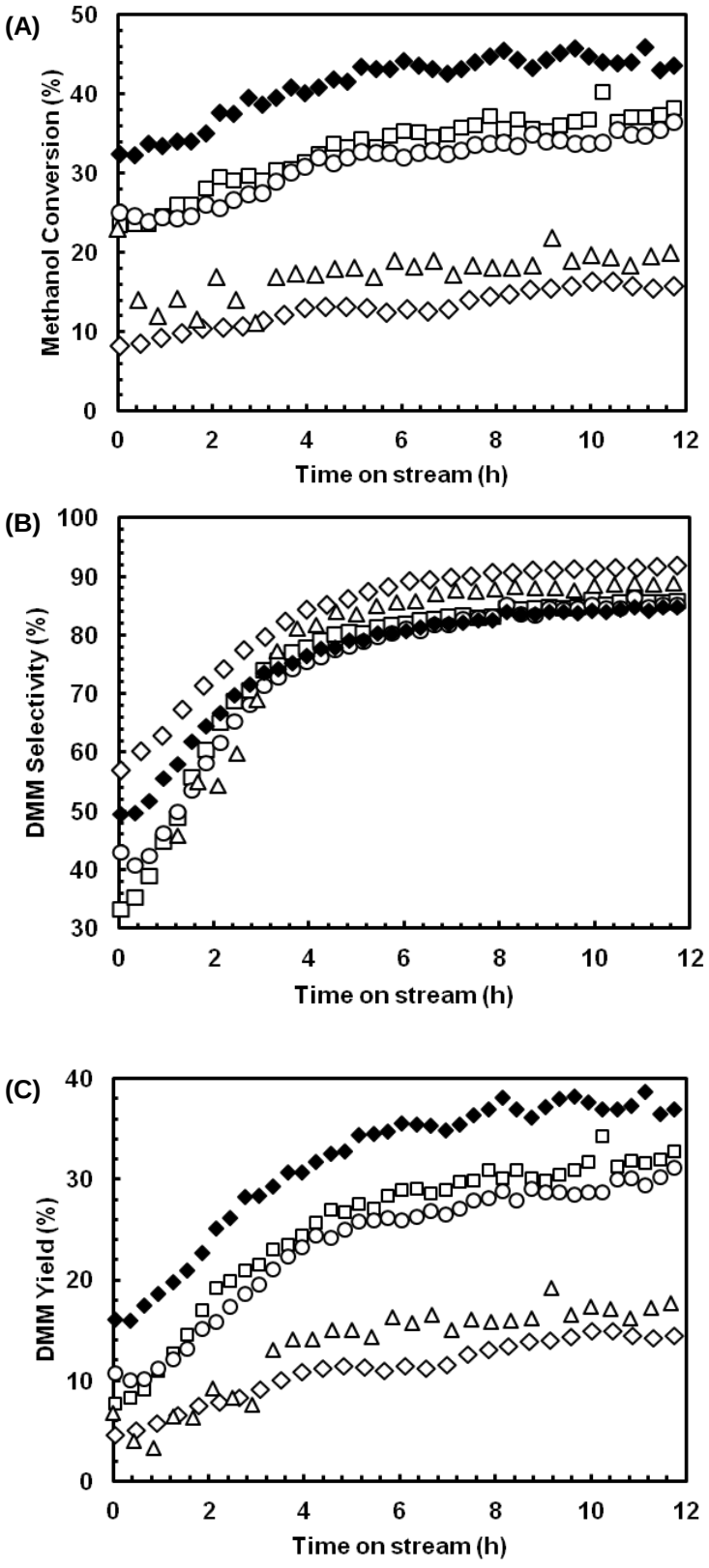

Figure 3-8: Methanol conversion versus time on stream (A), DMM selectivity (B), and DMM yield (C) observed over FeMo2.5 (◇), FeMo3.0 (□), FeMo3.5 (○), FeMo3.75 (◆) and FeMo4.0 (△) catalysts; reaction conditions: $CH_3OH/O_2/He$ = 40/13/47 mol.%, O_2/CH_3OH = 0.325, GHSV = 16 L. $h^{-1}.g_{cat}^{-1}$, $m_{catalyst}$ = 150 mg, *T* = 255 °C.

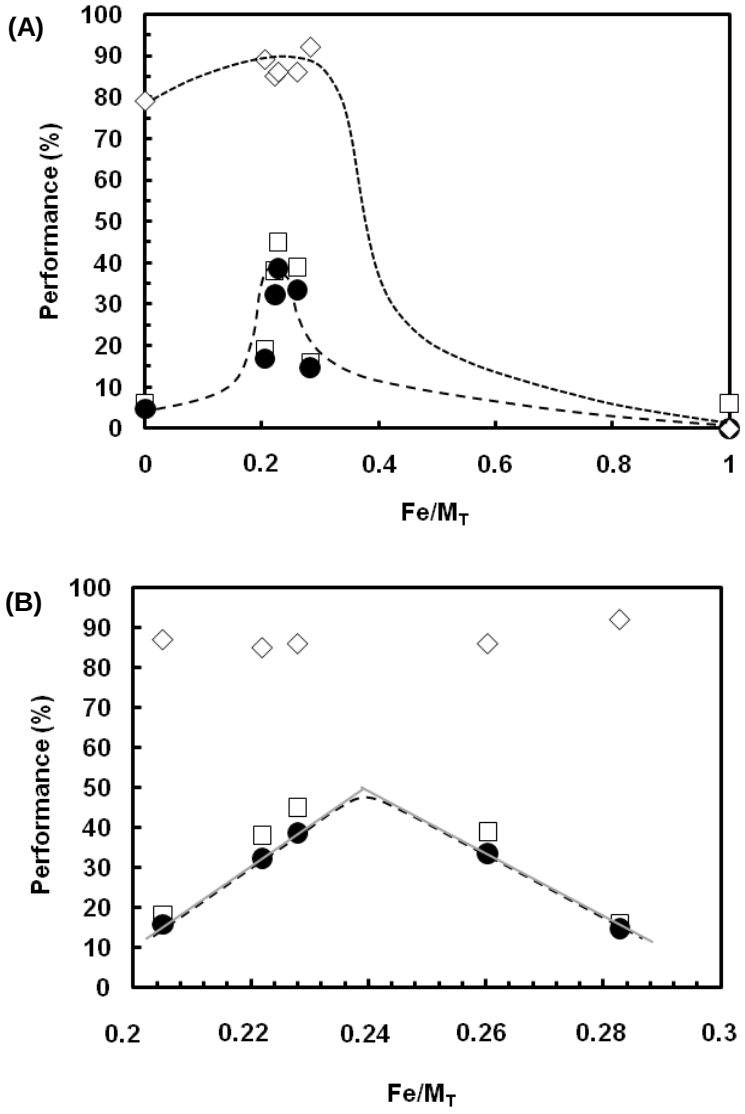

Figure 3-9: (A) Steady state performance as a function of the Fe/M_T molar ratio (with Fe + Mo = M_T); Methanol conversion (□), DMM selectivity (◇), and DMM yield (●); (B) Zoom-in results for Fe/M_T ratios between 0.2 and 0.3; reaction conditions: $CH_3OH/O_2/He$ = 40/13/47 mol.%, O_2/CH_3OH = 0.325, GHSV = 16 $L.h^{-1}.g_{cat}^{-1}$, $m_{catalyst}$ = 150 mg, time on stream = 12 h for each point.

3.4 Intensive characterizations

As mentioned before, the present work aims at investigating the redox and acid properties of the FeMo mixed oxide system and correlating these properties to the catalytic behavior. The excellent performances of this particular catalyst can be explained using advanced characterization methods as those proposed hereafter.

3.4.1 Low-energy ion scattering

Evolution of the catalyst surface was investigated by the LEIS measurement. The LEIS spectra recorded in static conditions (*i.e.*, less than 1 % of a monolayer was sputtered during one spectrum) of iron molybdate mixed-oxides with different Mo/Fe ratios are presented in Figure 3-10A. They reveal that both Mo and Fe species are exposed at the outermost atomic layer of the catalysts. The atomic composition of the samples given in terms of Mo/Fe atomic ratios, determined by LEIS are of 4.0, 2.4, 4.1, 2.7 and 3.0, respectively for FeMo2.5, FeMo3, FeMo3.5, FeMo3.75, and FeMo4 catalysts (Table 3-2). These values are quite different from those obtained by ICP-MS (or ICP-AES) reported in Table 3-1, meaning that it exists a non-homogeneous distribution of the different atoms (*i.e.*, Mo and Fe) within the matrix between the bulk and the surface of the catalysts. In particular, the catalyst giving the highest DMM yield (FeMo3.75) presents a surface Mo/Fe ratio of 2.7 by LEIS, which is slightly lower than the bulk one determined by ICP-MS (Mo/Fe = 3.4). LEIS sputtering series were recorded on this catalyst to determine the evolution of relative quantities of Mo and Fe species present at the outermost surface layer. The evolution of the relative intensities of Mo, Fe and O peaks with the He^+ ion fluence from 3keV $^4He^+$ LEIS spectra of the FeMo3.75 catalyst is depicted in Figure 3-10B. Along the sputtering experiments, the intensity of Mo peak is significantly higher than those of Fe and O peaks, suggesting that surface contaminants preferentially interacted with Mo species on the surface. Development of Mo/Fe ratio from $^4He^+$ LEIS spectra of the FeMo3.75 catalyst with the He^+ ion fluence is presented in Figure 3-11. At the beginning of the experiment, the outer monolayer exhibits a Mo/Fe ratio of 2.4. The Mo concentration increases with progressive exposure of the second atomic layer till a Mo/Fe ratio of around 4. Assuming a surface layer of 10^{15} atoms.cm^{-2}, an estimated depth of around 0.7 monolayer is eroded after the successive LEIS analyses. In other words, 30 % of the outer layer remains after these sputtering experiments and 70 % of the underneath layer is consecutively revealed. An average Mo/Fe ratio of 3.6 can then be estimated, taking into account the values of Mo/Fe determined at the beginning (Mo/Fe = 0.3*2.4) and at the end

(Mo/Fe = 0.7*4) of the successive experiments. This so-obtained averaged Mo/Fe ratio is thus in a good agreement with that determined from elemental analysis (Mo/Fe = 3.4) – the bulk ratio that would probably be revealed in case of the complete erosion of the outermost surface layer.

Table 3-2: Atomic composition of calcined catalysts in terms of Mo/Fe ratios determined by LEIS.

Catalyst	FeMo2.5	FeMo3.0	FeMo3.5	FeMo3.75	FeMo4.0
Mo/Fe ratio	4.0	2.4	4.1	2.7	3.0

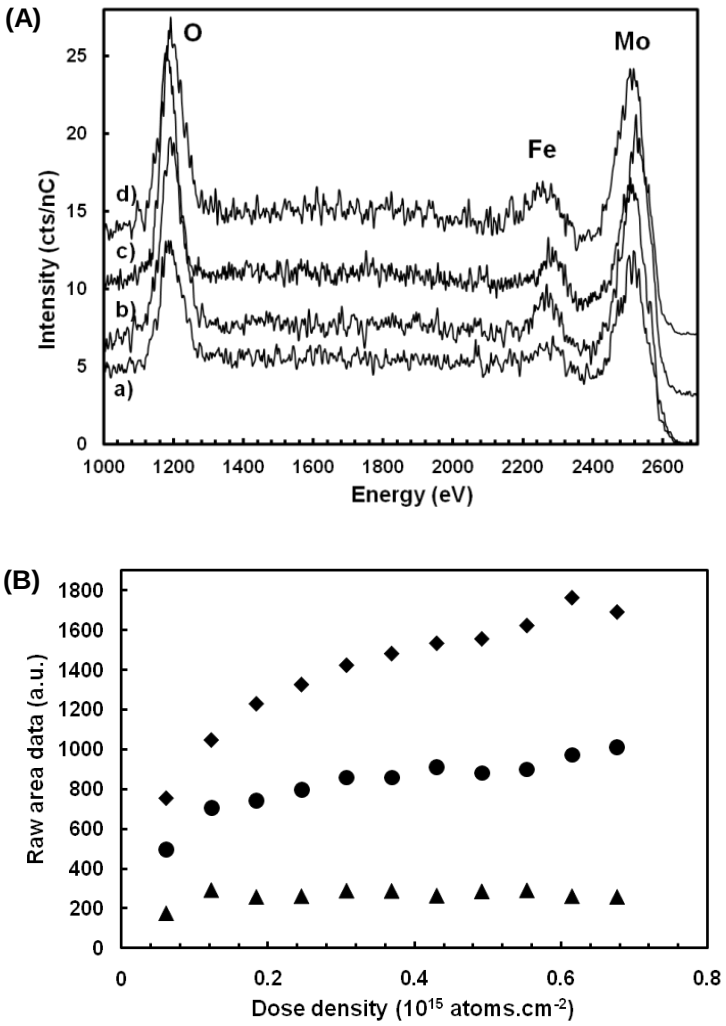

Figure 3-10: (A) 3 keV $^4He^+$ LEIS spectra of iron molybdates: FeMo2.5 (a), FeMo3.0 (b), FeMo3.5 (c), and FeMo3.75 (d); (B) Evolution of relative intensities of Mo (◆), Fe (▲) and O (●) peaks with the He^+ ion fluence from 3keV $^4He^+$ LEIS spectra of FeMo3.75 catalyst during sputtering experiments.

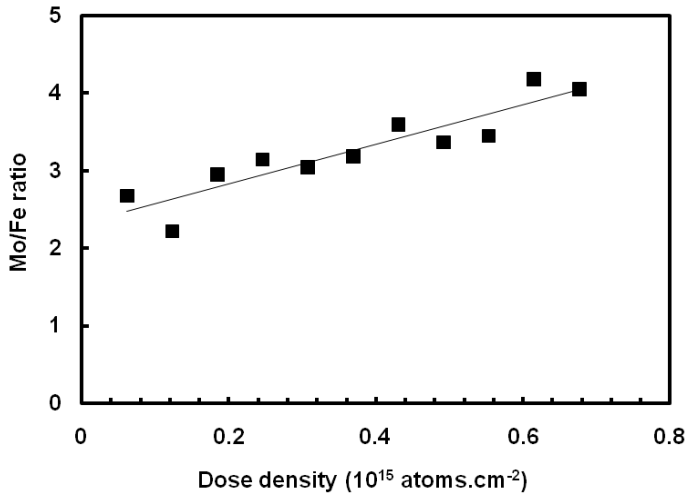

Figure 3-11: Evolution of the Mo/Fe ratio from 3 keV $^4He^+$ LEIS spectra of FeMo3.75 catalyst with the He^+ ion fluence.

3.4.2 X-ray photoelectron spectroscopy

Surface composition and oxidation state were inferred from X-ray photoelectron spectroscopy (XPS measurements). FeMo3.0 catalyst is chosen as a representative of the catalysts in the studied series. This catalyst is considerably reactive with significant conversion and selectivity (35 % and 85 %, respectively). It also presents relatively high amount of $Fe_2(MoO_4)_3$ phase (77 %), which is useful to reliably observe any change occurring on Mo and Fe centres. Figure 3-12 presents an evolution of the XPS Fe 2p spectra of FeMo3.0 after different treatment conditions. The shape and positions of the Fe 2p photopeaks, assigned to Fe atoms in the fresh catalyst (Figure 3-12A), correspond only to Fe^{III} species [6]. Indeed, the Fe $2p_{3/2}$ peak located at 711.2 eV presents a characteristic asymmetry due to multiplet splitting of high spin Fe^{III} ions [7] and it has an associated satellite peak located at around 8 eV at higher energy. After exposure to the CH_3OH/He mixture for 60 min, a new set of components appears at lower Binding Energy (BE) on the Fe 2p signal (Figure 3-12B). They are attributed to the formation of Fe^{II} species. Indeed, the BE for Fe $2p_{3/2}$ is of 709.0 eV associated with a satellite peak at higher energies with a variation of around 6 eV. Thus, Fe^{III} centers are partially reduced under the flow of CH_3OH/He before reaching a surface composition of 46 % of Fe^{II} and 54 % of Fe^{III} at the end of the treatment (Table 3-3). When oxygen is further added to the pre-treatment gas mixture, the proportion of Fe^{II} decreases to 29 % (Figure 3-12C). This evidences the partial re-oxidation of Fe^{II} by molecular oxygen on the surface or by the Mars-van Krevelen mechanism involving an O species migration.

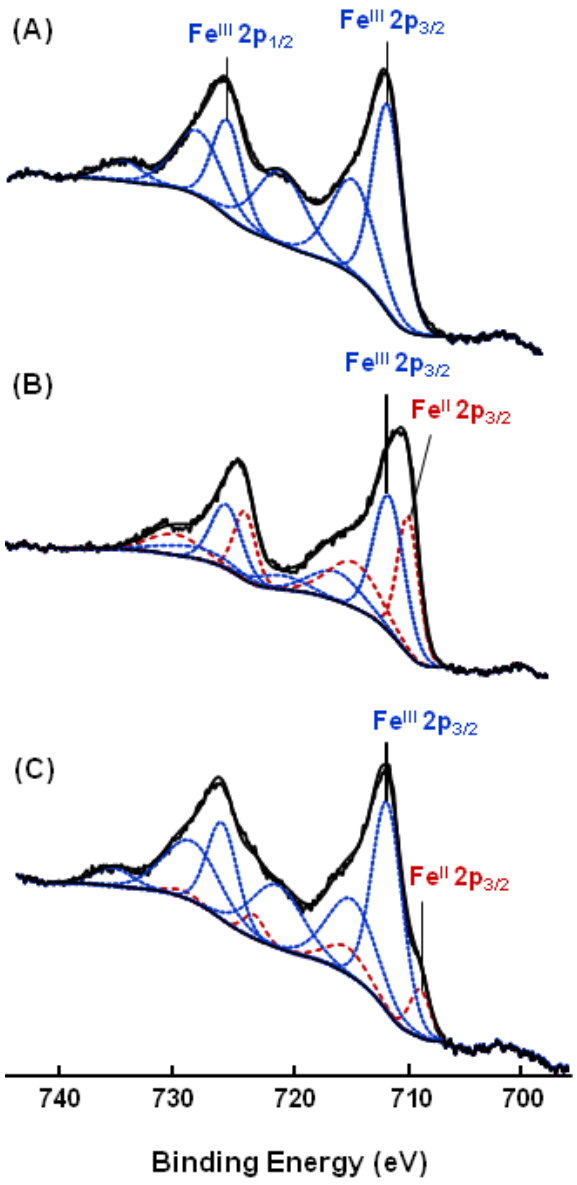

Figure 3-12: XPS analyses of the Fe 2p level for the FeMo3.0 sample under different conditions: Fresh catalyst (A), CH_3OH/He after 60 min (B), and CH_3OH/O_2/He after 60 min (C).

On the contrary, no significant change in BE values for Mo centres are observed. A Mo 3d doublet located at 232.3 and 236.3 eV is present in Figure 3-13, corresponding to the characteristic BE values of Mo $3d_{5/2}$ and Mo $3d_{3/2}$ for Mo^{VI} species, respectively [8]. However, a slight shift of 0.4 eV is observed for both peaks when the catalyst is exposed to the mixture of CH_3OH/He. This shift to lower BE (231.6 eV) for Mo $3d_{5/2}$ cannot be explained by a partial reduction of Mo^{VI} as the BE values of Mo 3d for Mo^{V} species have been reported in literature with a difference of 1.6 eV from those of Mo^{VI} [9]. Moreover, an increase in the peak width (FWHM) of Mo $3d_{5/2}$ peak (0.8 eV) is observed, associated with a slight shift to lower BE of this peak, when placing the catalyst under the reducing atmosphere

(CH_3OH/He). Based on this observation, while the oxidation degree of Mo (in iron molybdate) remained VI, its environment is disturbed that could be explained by the removal of some oxygen species and the creation of anionic vacancies without reducing the oxidation degree.

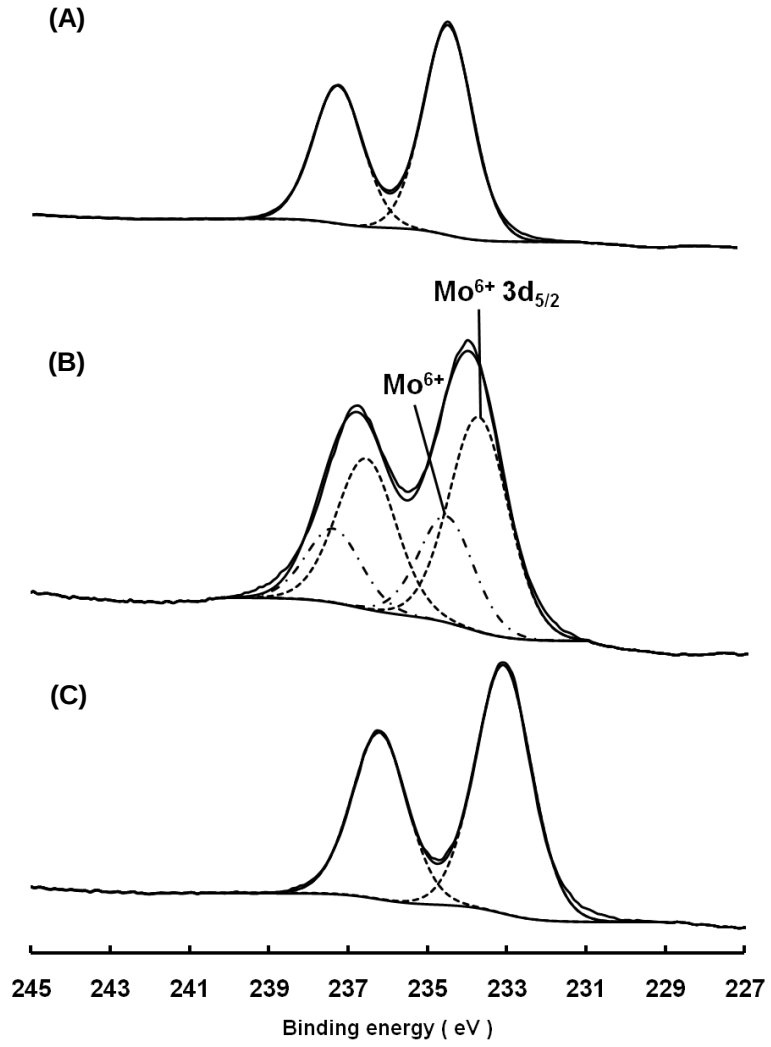

Figure 3-13: XPS analyses of the Mo 3d level for the FeMo3.0 sample under different conditions: Fresh catalyst (A), CH_3OH/He after 60 min (B), and CH_3OH/O_2/He after 60 min (C).

At the same time, the C 1s energy domain presents a significant increase in the contribution of the C-O component located at 286.5 eV (Figure 3-14B), which was attributed to the formation of methoxy groups (CH_3O-) [10], due to the dissociative adsorption of methanol at the surface of the catalyst. Also, it has to be noted that the fresh catalyst shows the characteristic feature of surface contamination by carbon (Figure 3-14A). The combined changes observed on Mo and C suggests that the methoxy groups are presumably linked with Mo atoms. The position of the Mo $3d_{5/2}$ photopeak shifts back to its initial value (232.6 eV) when the oxygen flow is

introduced into the feed mixture. This could evidence the desorption of methoxy groups from the surface and/or their surface reaction.

Table 3-3: XPS analysis results after one hour on stream with FeMo3.0 sample after different *in situ* treatments at 255°C in 20 mol. % of methanol in air.

Treatment condition	**Binding Energy (eV)**		**Peak width (FWHM)**		**Relative atomic conc. of Fe $2p_{3/2}$ species (%)**		**Mo/Fe XPS atomic ratio**
	Mo $3d_{5/2}$ (Mo^{VI})	**Fe $2p_{3/2}$ (Fe^{III})**	**Mo $3d_{5/2}$ (Mo^{VI})**	**Fe $2p_{3/2}$ (Fe^{III})**	**Fe^{III}**	**Fe^{II}**	
Fresh catalyst	232.3	711.2	1.9	4.3	100	-	3.0
Air (O_2/He)	232.0	712.2	1.6	4.8	100	-	5.1
CH_3OH/He	231.6	709.0	2.4	4.3	54	46	4.8
CH_3OH/O_2/He	232.6	712.2	1.6	3.9	71	29	3.4

The surface atomic composition changes according to the different treatment conditions (Table 3-3), especially after treating the catalyst under air and CH_3OH/He conditions, where Mo enrichment on the surface is observed, with atomic Mo/Fe ratios of 5.1 and 4.8, respectively. When considering the catalyst placed in the flow of CH_3OH/O_2/He, the Mo/Fe ratio variation is not so significant even if a partial reduction of the solid occurs as evidenced by the presence of Fe^{II}. The Mo/Fe ratio of 3.4 is determined after the treatment in the presence of the reactants mixture. The so-obtained value is close to that of the fresh catalyst (Mo/Fe = 3.0). It is also notable that for the fresh catalyst, the atomic Mo/Fe ratio at the surface measured by XPS is in a good agreement with that determined by ICP-MS (Mo/Fe = 2.8, Table 3-1), meaning that the bulk and the surface measured by XPS has essentially the same composition.

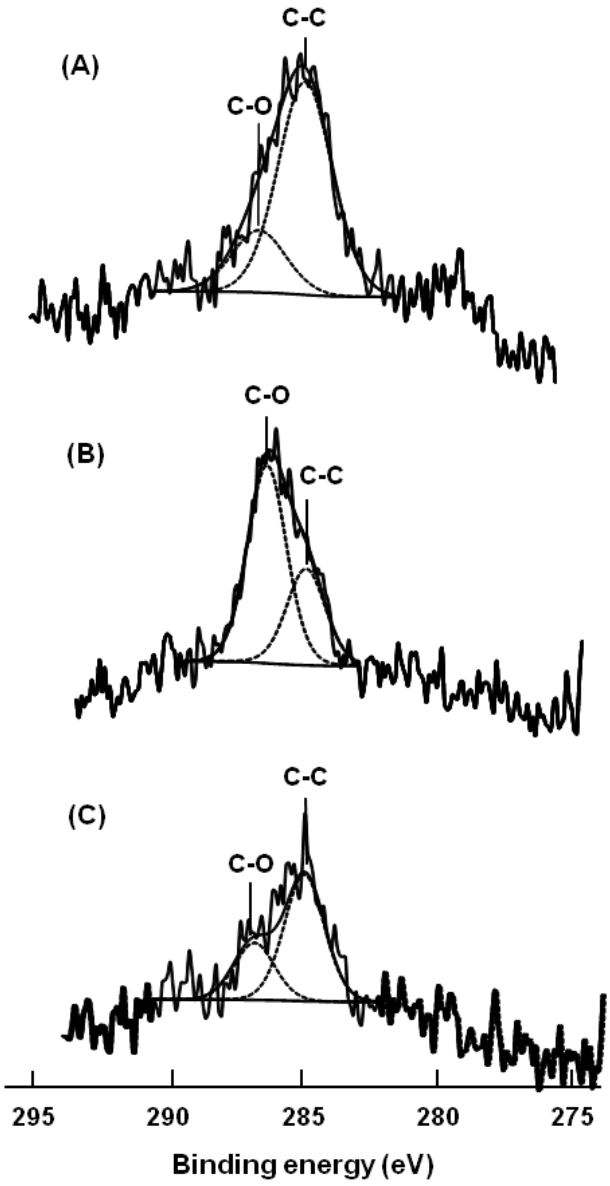

Figure 3-14: XPS analyses of the C 1s level for the FeMo3.0 sample under different conditions: Fresh catalyst (A), CH_3OH/He after 60 min (B), and CH_3OH/O_2/He after 60 min (C).

3.4.3 Electron paramagnetic resonance

In situ EPR experiments were carried out at 255 °C with the best catalyst, namely FeMo3.75, in the presence of 20 mol.% of CH_3OH in air. Figure 3-15 reveals a major peak located at $g = 2.002$, characteristic of Fe^{III} in an octahedral environment, in agreement with the $Fe_2(MoO_4)_3$ crystal structure [11-13]. A minor peak, with less intensity, appears at $g = 4.17$, which is characteristic of Fe^{III} species in a tetrahedral environment and can be assigned to surface defects. The intensity of the Fe^{III} signal also decreases with analysis time in the presence of the reactants mixture. Quick reduction of Fe^{III} to Fe^{II} species is evidenced when

starting the treatment followed by a slower reduction process (Figure 3-16). In agreement with the XPS results, there is no evidence of any presence of Mo^{V} species. An experiment under drastic reducing conditions (20 mol.% of CH_3OH in Ar at 255 °C) has also been performed with the aim at forcing total reduction of the catalyst. Only a decrease in the Fe^{III} quantity is observed with time on stream, whereas Mo centers remain in the Mo^{VI} state, indicating that the reduction of the catalyst is indeed exclusively owing to the reduction of iron species. The same observation was also reported by Gesmundo *et al.* as studies on the iron molybdate catalyst showed that Fe^{III} were reduced by methanol to Fe^{II}, however, Mo^{V} only appeared after extensive reduction of Fe^{III}. These Mo^{V} centers were thus the first to be reoxidized when introducing oxygen [14]. This can be explain either by the fact that Mo^{V} atoms effectively do not exist during the process before Fe atoms are completely reduced or that the re-oxidation of Mo^{V} → Mo^{VI} takes place (with a redox process through reduction of Fe^{III} → Fe^{II}) with a speed faster than the one of analysis.

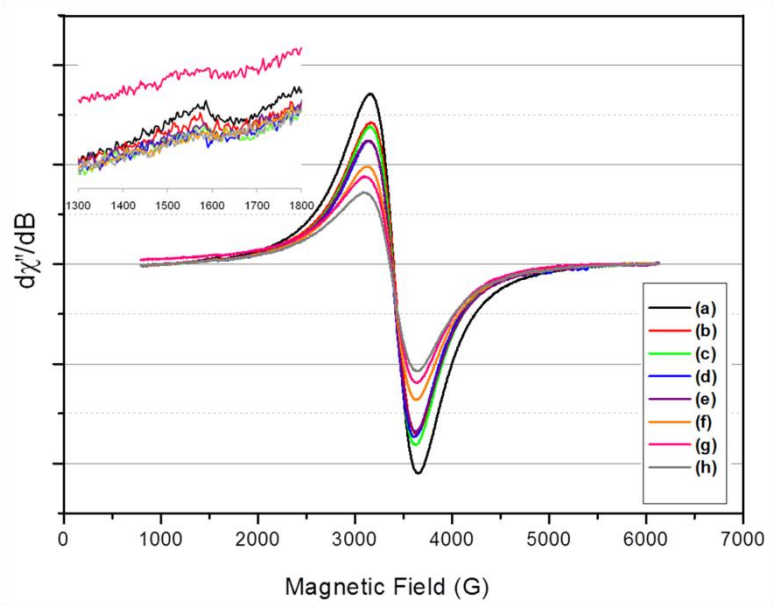

Figure 3-15: Evolution of EPR Fe^{III} signal at g = 2.002 with a magnification of the signal at g = 4.17 recorded for the fresh FeMo3.75 powder at room temperature (a), powder at 255 °C with no gas flow (b), powder treated under 20 mol.% $CH_3OH/Ar/O_2$ flow at 255 °C at t = 0 (c), after 25 min (d), 215 min (e), 240 min (f), 275 min (g), and 320 min (h).

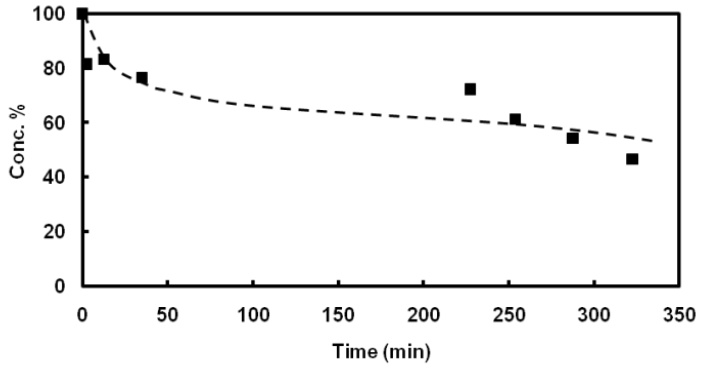

Figure 3-16: Evolution of the quantity of Fe^{III} as determined by EPR spectroscopy deduced from Fig. 3-15.

3.4.4 Temperature-programmed desorption of NH_3

The acidity of iron molybdate catalysts with different Mo/Fe ratios was examined by means of NH_3-TPD experiments. For experimental reasons, we chose to reduce the catalysts with hydrogen instead of methanol. In order to know the differences that the reduction in H_2 or CH_3OH could lead and if to the same results could be expected, the FeMo3.75 catalyst, as a representative of the series, was pre-reduced with H_2 and CH_3OH before conducting TPD-NH_3 experiments. As a result, we obtain essentially the same behavior for the catalysts partially reduced by either H_2 or CH_3OH (Figure 3-17). This conclude that we can indeed run relevant TPD-NH_3 experiments after H_2 pre-reduction, which is much easier while being representative of the effect observed after methanol pre-reduction.

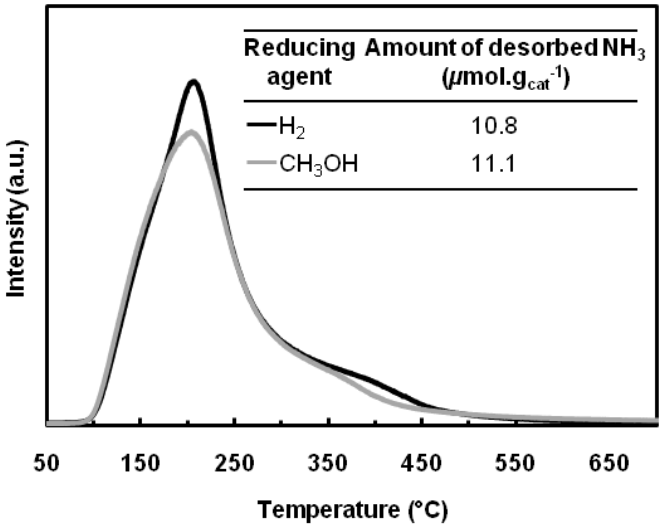

Figure 3-17: Experimental TPD of NH_3 curves for partially reduced FeMo3.75 sample using H_2 (black line) and CH_3OH (grey line) as reducing agents.

In the TPD-NH_3 curves, peaks are generally distributed into two regions – below and above 400 °C, referred to as low-temperature and high-temperature regions, respectively. The peaks in the high temperature region can be attributed to the NH_3 desorption from strong Brønsted and Lewis acid sites, and the assignment of the peaks in the low temperature region is assigned to the desorption of NH_3 from weak acid sites [15]. For the TPD-NH_3 curves shown in Figure 3-18, the major NH_3 desorption peaks in any tested samples appear in the low temperature region below 400 °C, thus suggesting the presence of weak acid sites. In comparison with the freshly calcined sample, the amount of NH_3 desorbed from the surface of FeMo3.75 catalyst partially pre-reduced with H_2 is significantly higher (*i.e.*, 5.55 μmol $NH_3.g_{cat}^{-1}$ *vs.* 10.8 μmol $NH_3.g_{cat}^{-1}$). This implies that more acid sites are formed after partial reduction. Furthermore, the newly formed acids sites upon reduction are stronger, according to a shift of the temperature of the peak from 167 °C to 207 °C. During the course of reaction, the catalyst is being continuously slightly reduced due to the presence of methanol, even if only a partial reduction is observed. The gradual increase in DMM selectivity observed during the first reaction hours (Figure 3-8B) could be ascribed to an increase in the surface acidity, which is relevant for DMM formation. In addition, the amount of desorbed NH_3 increases from 1.45 to 13.4 μmol $NH_3.g_{cat}^{-1}$ with increasing the Mo/Fe ratio from 2.5 to 3.9 (Figure 3-19), which is proportional to the Mo content in the catalyst.

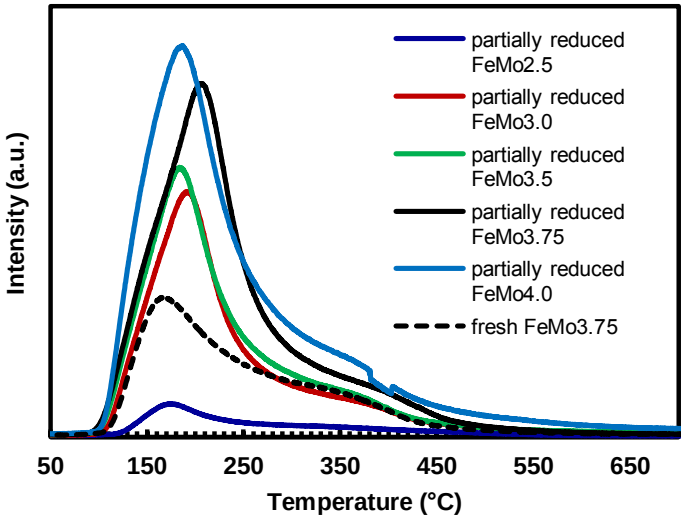

Figure 3-18: Experimental TPD of NH_3 curves for fresh and partially reduced by H_2 FeMo samples.

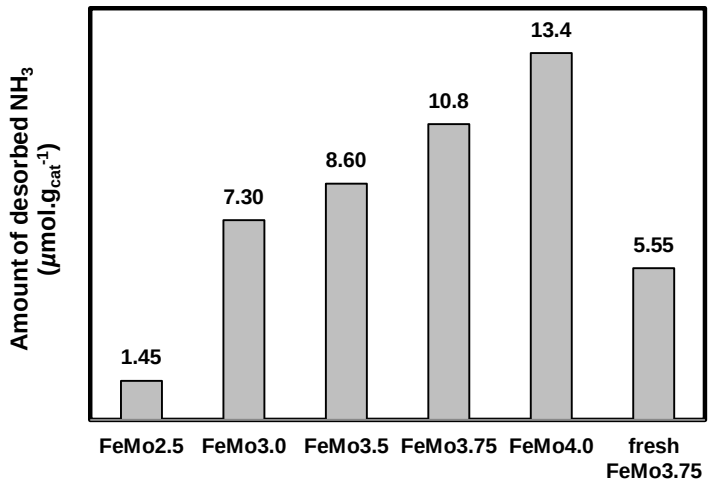

Figure 3-19: Amount of desorbed NH_3 determined from the TPD curves in Figure 3-18.

3.5 Active site of the FeMo mixed oxide catalysts for methanol oxidation to dimethoxymethane

Both increases in conversion and selectivity with time on stream under reaction conditions can be explained taking into account the reducibility and acidity of the iron molybdate mixed oxide catalysts. The catalytic results on single oxides show that either Fe or Mo are able to activate methanol (Figure 3-9A), even if the number of active sites is low. Clearly, there is a synergistic effect when both elements are present together, possibly in strong interaction. With respect to surface analysis results (XPS), molybdenum is being in contact with methanol during reaction meanwhile the partial reduction is taking place intensively on iron. The surface and bulk ratios between molybdenum and iron, determined by XPS and ICP-MS, respectively, are higher than that of stoichiometric iron molybdate (Mo/Fe = 1.5). It is known from the literature that the enrichment of Mo helps preventing the formation of Fe-rich phases, which can favour the oxidation reactions, due to the loss of Mo with water [16-19]. Moreover, in the studied series, the best catalyst contains a relatively high proportion of MoO_3 (36 rel.%, Table 3-1), ensuring the synergistic effect between MoO_3 and $Fe_2(MoO_4)_3$ in agreement with what has been observed for the selective oxidation of methanol to formaldehyde [20-22]. MoO_3 can generate Lewis acidity associated with Mo coordinatively unsaturated sites (CUS) [23]. Pernicone has proposed that the acidity of the Fe-Mo oxide catalyst is connected with Lewis acid sites. On such sites, methanol chemisorption can take place, and they have been described as anionic vacancies produced by dehydroxylation of the catalyst surface [2].

It is well-known that methanol dissociatively chemisorbs over MoO_3 at temperatures as low as 25 °C. Adsorption is thought to occur on coordinatively unsaturated surface Mo species and results in the formation of a surface methoxy and a surface hydroxyl group [24-27]. It has been proposed that the methoxy groups decompose to formaldehyde and that the protons released from the alcohol react with lattice oxygen to form H_2O [24,25]. For the selective oxidation of methanol to formaldehyde, methoxy decomposition is believed to be the rate-limiting step of the reaction, while the incorporation of lattice oxygen into the produced water has been demonstrated with ^{18}O isotopic labelling [27] and, therefore, the reaction obeys to a redox mechanism of the Mars-van Krevelen type [24,28,29]. Coordinatively unsaturated ferrous (CUF) sites can also exist, and have been proposed as active sites over Pt-Fe bicomponent catalysts for catalytic oxidation reactions [30,31].

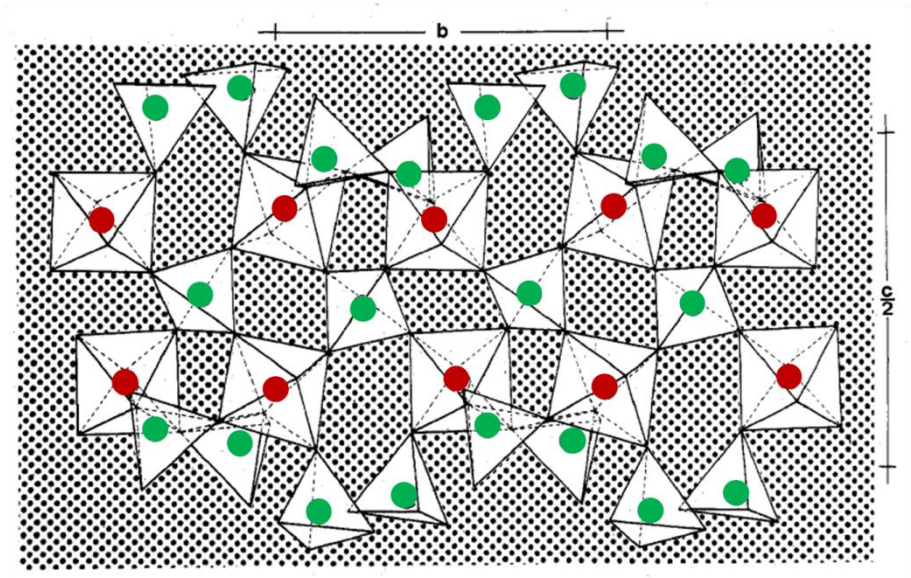

Figure 3-20: Diagrammatic representation of the crystal structure of monoclinic $Fe_2(MoO_4)_3$, indicating the octahedrons around Fe ions (in red) and the tetrahedrons around Mo ions (in green) [11].

According to the literature on the crystalline structure of $Fe_2(MoO_4)_3$, we can assume that, for iron-molybdenum mixed oxides catalysts, MoO_4 tetrahedra are linked with FeO_6 octahedra *via* oxygen atoms (Figure 3-20) [11-13]. The active site, therefore, involves anionic vacancies and O^{2-} species of the solid, as suggested by Pernicone [2], and our observed synergistic effect between Mo and Fe implies that such site intimately incorporates both Mo and Fe cations. Moreover, one can propose that the rate-determining step, related to the rupture of the C-H bond, can then be performed on an anionic vacancy (Lewis acid site) allowing a heterolytic rupture with the help of a O^{2-} species of the solid. This allows the abstraction of a hydride

species from methanol, which then would be located in the vacancy and the formation of a hydroxyl group (Scheme 3-1).

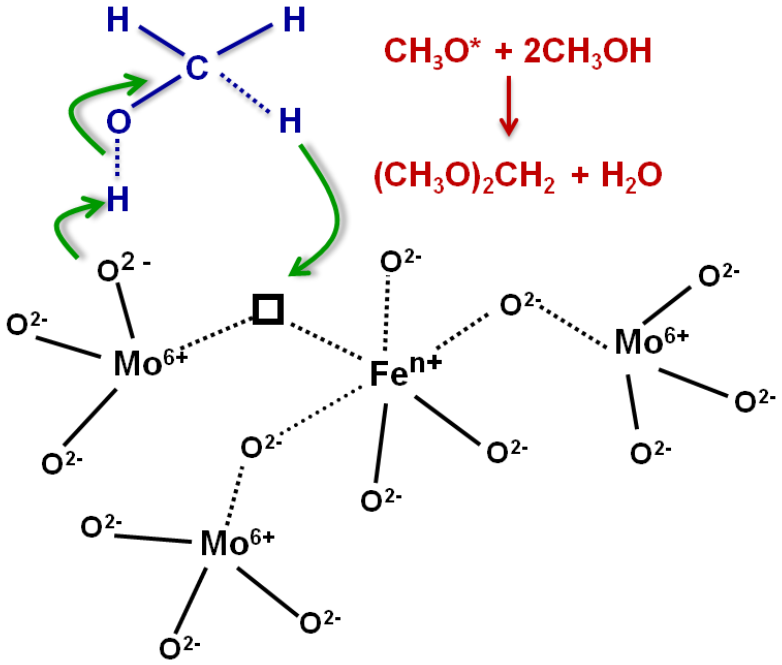

Scheme 3-1: Proposed active site for methanol transformation to DMM − (Fe^{n+} ions: Fe^{3+} or Fe^{2+}, and □: anionic vacancy, number arbitrary).

It is highly probable that the activation of methanol takes place on the proposed active site involving cooperation between Mo and Fe species, yielding adsorbed formaldehyde. NH_3-TPD experiments show that the catalyst reduction leads to an increase in the acidity required to catalyse the sequential condensation/dehydration reaction between formaldehyde and two molecules of methanol to yield DMM. This acidity is provided by anionic vacancies, which are of the Lewis type [2,32], and the number/strength of the acid sites became larger upon the partial reduction of the catalyst with increasing numbers of vacancies. It is notable that the catalyst surface may contain both Lewis and Brønsted acid sites. The latter ones are generated also during the heterolytic splitting and in the presence of water formed during reaction, by Lewis sites hydration. As a matter of fact, this interchange between Lewis and Brønsted acids can also enhance/modify the surface acidity, which is required for acetalization reaction. As a specific feature of the FeMo catalysts, the formation of DMM is facilitated using high concentrations of methanol in the feed. Gaseous oxygen present in the reaction medium is not directly involved in the oxidation reaction, but is responsible for the surface reoxidation of Fe^{II} species in agreement with the Mars-van Krevelen mechanism [24,28,29] and/or react with

speculated hydride species regenerating the active site as described in the following equations [33]:

$$H^- + ½O_2 \rightarrow OH^- \qquad (1)$$

$$2OH^- \rightarrow O^{2-} + \square + H_2O \qquad (2)$$

However, further studies are still needed to propose a complete mechanism. As a matter of fact, all the methanol molecules can be adsorbed on the surface and specific active sites can lead directly to DMM. Hydrogen abstraction from methanol, and thus formation of hydrogen on the solid, can be linked to the reduction of Fe^{III} to Fe^{II}. Nonetheless, the reactivity between hydride species on the solid and oxygen in the gas phase should be very fast, and this phenomenon can explain the slow reduction of the catalyst and the good stability of the catalytic performances.

3.6 Conclusions

Iron molybdate mixed oxides catalysts with different Mo and Fe contents were synthesized using a coprecipitation method from solutions of ammonium molybdate and ferric chloride. The catalysts after calcination at 450 °C in air for 2 h present mixed oxides of crystalline MoO_3 and $Fe_2(MoO_4)_3$, confirmed by XRD analysis. We clearly show herein that the FeMo mixed oxide catalysts are efficient for the gas phase selective conversion of methanol to DMM using a methanol-rich (40 mol.%) reactants mixture. After optimizing reaction conditions and tuning the catalyst composition, the highest DMM yield of 39 % is obtained with a selectivity of 85 % for 46 % conversion at 255 °C over the catalyst with a Mo/Fe ratio of 3.4 (Fe/M_T = 0.228) using the reaction feed containing 13 mol.% of oxygen. This catalyst contained 64 % of $Fe_2(MoO_4)_3$ and 36 % of MoO_3 (seen by XRD), with a relatively high surface area (10 $m^2.g^{-1}$) compared to the other catalysts of the studied series. The good performance in terms of DMM production can be ascribed to the concomitant redox and acid properties present in the catalytic system, which are relevant to undergo consecutive partial oxidation and acetalization reactions. Surface composition and reducibility were investigated by LEIS and XPS. With respect to the LEIS results, the outermost surface layer of the fresh catalyst presents both Mo and Fe species with a Mo/Fe ratio of 3. From the XPS analysis results, we can deduce that the direct synthesis of DMM from methanol using the feed highly concentrated in methanol involves adsorption of methanol on the sites where Mo and Fe atoms are connected. This leads to the partial reduction of some Fe cations from Fe^{III} to Fe^{II}

on the catalyst surface. The same phenomenon is also characterized by the EPR experiments. These catalytic active sites are proposed as anionic vacancies – which can be generated by surface dehydroxylation and are identified as Lewis acid sites surrounded by Mo and Fe atoms. Acidity of the catalyst is determined by NH_3-TPD. The number of acid sites and their strength are increased by pre-reducing the catalyst with H_2. As the catalyst is being continuously reduced under the reducing atmosphere applied during the reaction, due to the presence of methanol, a significant increase in selectivity could be attributed to an increase in acidity, which is required in the acetalization reaction to form DMM, in addition to the redox properties. Owing to the reduction of the catalyst, the number of anionic vacancies become larger. This helps improving the catalytic conversion. Evidence is reported that gaseous oxygen is only responsible for reoxidizing the catalyst surface, especially Fe sites, suggesting that the studied reaction obeys the Mars-van Krevelen mechanism. At last, a clear synergistic influence between Mo and Fe in the catalyst is observed, particularly on methanol conversion. By advisedly optimizing the FeMo catalyst formulation, an optimal DMM yield is achieved, moreover the formulation with Mo/Fe ratio of 3.4 can reach the extrapolated yield value of 50 % yield. Alternatively for methanol oxidation to formaldehyde, this study demonstrates also the importance of the methanol partial pressure but mostly the importance of the average oxidation state on the selectivity. For the formation of DMM, catalyst formulations should be tuned to keep the balancing of oxidation states − (*i.e.*, Fe^{III} and Fe^{II}) − present during the course of reaction.

3.7 References

[1] G.K. Boreskov, G.D. Kolovertnov, L.M. Kefeli, L.M. Plyasova, L.G. Karakchiev, V.N. Mastikhin, B.I. Popov, V.A. Dzisko, D.V. Tarasova, Kinetics and Catalysis (USSR), 7 (1966) 125.

[2] N. Pernicone, J. Less Comm. Metals, 36 (1974) 289.

[3] S. Royer, X. Sécordel, M. Brandhorst, F. Dumeignil, S. Cristol, C. Dujardin, M. Capron, E. Payen, J.-L. Dubois, Chem. Commun. 7 (2008) 865.

[4] J. Gornay, X. Sécordel, M. Capron, G. Tesquet, P. Fongarland, E. Payen, J.-L. Dubois, F. Dumeignil, Oil & Gas Science and Technology 65 (2010) 751.

[5] J. Gornay, X. Sécordel, G. Tesquet, B. de Ménorval, S. Cristol, P. Forgarland, M. Capron, L. Duhamel, E. Payen, J.-L. Dubois, F. Dumeignil, Green Chem. 12 (2010) 1722.

[6] T. Yamashita, P. Hayes, Appl. Surf. Sci. 254 (2008) 2441-2449; M.C. Biesinger, B.P. Payne, A.P. Grosvenor, L.W.M. Lau, A.R. Gerson, R.St.C. Smart, Appl. Surf. Sci. 257 (2011) 2717.

[7] A.P. Grosvenor, B.A. Kobe, M.C. Biesinger, N.S. McIntyre, Surf. Interf. Anal. 36 (2004) 1564.

[8] Y.V. Plyuto, I.V. Babich, I.V. Plyuto, A.D. Van Langeveld, J.A. Moulijn, Appl. Surf. Sci. 119 (1997) 11.

[9] L Briand, O. Tkachenko, M. Guraya, I.E. Wachs, W. Grünert, Surf. Interface Anal. 36 (2004) 238.

[10] X. Huang, J. Liu, J. Chen, Y. Xu, W. Shen, Catal. Letters 108 (2006) 79.

[11] M.H. Rapposch, J. B. Anderson, E. Kostiner, Inorg. Chem. 19 (1980) 3531.

[12] H.Y. Chen, Mat. Res. Bull. 14 (1979) 1583.

[13] G. Fagherazzi, N. Pernicone, J. Catal. 16 (1970) 321.

[14] F. Gesmundo, N. Pernicone, P.F. Rossi, Rend. Accad. Naz. Lincei, VIII, 46 (1969) 436.

[15] F. Lonyl, J. Valyon, Microporous Mesoporous Mater. 47 (2001) 293-301- M. Sawa, M. Niwa, Y. Murakami, Zeolites 10 (1990) 532.

[16] A.P.V. Soares, M. Farinha Portela, A. Kiennemann, L. Hilaire, J.M.M. Millet, Appl. Catal. A: General 206 (2001) 221.

[17] A.P.V. Soares, M. Farinha Portela, A. Kiennemann, L. Hilaire, Chem. Eng. Sci. 58 (2003) 1315.

[18] G. Shi, T. Franzke, M.D. Sánchez, W. Xia, F. Weis, M. Seipenbusch, G. Kasper, M. Muhler, ChemCatChem. 4 (2012) 760.

[19] M.P. House, A.F. Carley, R. Echeverria-Valda and M. Bowker, J. Phys. Chem. C 112 (2008) 4333.

[20] E. Soderhjelm, M. House, N. Cruise, J. Holmberg, M. Bowker, J.-O. Bovin, A. Anderson, Top. Catal. 50 (2008) 145.

[21] I.E. Wachs, J. Catal. 275 (2010) 84.

[22] G. Jin, W. Weng, Z. Lin, N.F. Dummer, S.H. Taylor, C.J. Kiely, J.K. Bartley, G.J. Hutchings, J. Catal. 2012, http://dx.doi.org/10.1016/j.jcat.2012.09.001.

[23] I. Matsuura, S. Mizuno, H. Hashiba. Polyhedron 5 (1986) 111.

[24] W.E. Farneth, F. Ohuchi, R.H. Staley, U. Chowdhry, A.W. Sleight, J. Phys. Chem. 89 (1985) 2493.

[25] W.E. Farneth, R.H. Staley, A.W. Sleight, J. Am. Chem. Soc. 108 (1986) 2327.

[26] J.S. Chung, R. Miranda, C.O. Bennett, J. Catal. 114 (1988) 398.

[27] C.J. Machiels and A.W. Sleight, J. Catal. 76 (1982) 238.

[28] P. Mars and D.W. van Krevelen, Chem. Eng. Sci. 3 (1954) 41.

[29] G. Busca, Catal. Today 27 (1996) 457.

[30] Q. Fu, W.-X. Li, Y. Yao, H. Liu, H.-Y. Su, D. Ma, X.-K. Gu, L. Chen, Z. Wang, H. Zhang, B. Wang, X. Bao. Science 328 (2010) 1141.

[31] H. Xu, Q. Fu, Y. Yao, X. Bao. Energy Environ. Sci. 5 (2012) 6313.

[32] M. Gotić, G. Koščec, S. Musić, J. Mol. Struct. 924-926 (2009) 347.

[33] C. Pirez, M. Capron, H. Jobic, F. Dumeignil, L. Jalowiecki-Duhamel, Angew. Chem . Int. Ed. 50 (2011) 10193.

Chapter 4

Results and discussion: 1,1-diethoxyethane synthesis from ethanol

4.1 Introduction

Herein this chapter, we have transformed the knowledge acquired from the selective partial oxidation reaction of methanol aimed at *1,1*-dimethoxymethane (DMM) formation to the corresponding reaction of ethanol for *1,1*-diethoxyethane (DEE) formation. The idea is based on the similarities between both reaction pathways as mentioned earlier in the literature review (*cf*. Scheme 1-1 and Scheme 1-3 in Chapter 1), from which we can presume that the catalyst functions are comparable. At first, we apply the FeMo mixed oxides in the direct synthesis of DEE from ethanol and it is found that acetaldehyde (ACD) is mainly produced with a significantly higher amount than DEE which is desirable. This indicates that the catalytic functions required to realize the reactions of methanol and ethanol are not fully identical, especially the acidity (numbers of acid sites, their strength and/or density). To enhance the acidity, we first substituted Mo and Fe portions in the FeMo mixed oxides formulation by elements which bring higher acidity, *i.e.*, W and Al, respectively. The performances of FeMo mixed oxides modified with W and Al (FeMoW and FeMoAl) are then compared to those of the unmodified catalysts in the selective oxidation reaction of ethanol. Then, for better understanding on the role of surface acidity on the DEE formation, the acetalization reaction of ethanol and acetaldehyde is decoupled from the consecutive oxidation/condensation reactions and is examined separately. This is performed by co-feeding acetaldehyde and ethanol and carrying out the acetalization reaction over acidic catalysts with different levels of acidity (classified by the quantity of acid sites and their density). Finally, the obtained results are then discussed and corroborated with thermodynamic study developed for the gas phase acetalization of ethanol.

4.2 Catalytic measurements in direct synthesis of DEE from ethanol

4.2.1 FeMo mixed oxide catalysts

As mentioned before, the FeMo mixed oxides catalysts were applied in the direct synthesis of DEE from ethanol. Evolution of the performance indicators in terms of ethanol conversion and products selectivities at different temperatures of the FeMo3.75 catalyst as a representative example of the studied FeMo series is presented in Figure 4-1. As one can see, a range of studied temperatures is slightly lower than that used in the oxidation of methanol presented previously (*cf*. Figure 3-6 in Chapter 3). The choice of working temperature is done by the fact that increasing the reaction temperature leads to a runaway reaction which

producing products from over-oxidation reaction of ethanol (CO_x) due to the high exothermicity of the reaction.

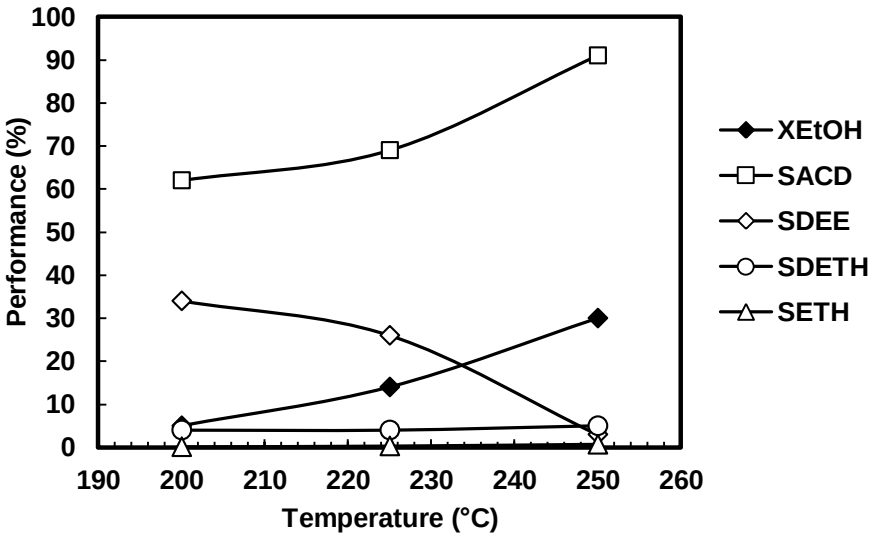

Figure 4-1: Performances as a function of reaction temperature on FeMo3.75 mixed oxide catalyst; reaction conditions: $CH_3CH_2OH/O_2/He$ = 30.8/7/62.2 mol.%, GHSV = 26 $L.h^{-1}.g_{cat}^{-1}$, $m_{catalyst}$ = 150 mg, time on stream = 2 h.

The main detected products are acetaldehyde (ACD), DEE and diethyl ether (DETH with a large excess of ACD (for instance, more than 90 % in selectivity at 250 °C). It is interesting to note that ethylene (ETH) is also present as traces in the mixture. The ethanol conversion does not exceed 30 % in this range of temperature (200-250 °C).

Similar to the prior study in methanol oxidation to acetal DMM, the experiments in the selective ethanol oxidation were conducted on FeMo mixed oxides with different Fe and Mo compositions. The catalysts, including industrial iron molybdate having a Mo/Fe ratio of 2 (IndFeMo2), FeMo3.0, FeMo3.5, and FeMo3.75, were used without any pretreatment. The products selectivities and DEE yield at the same catalyst activities, *i.e.*, 6 % (at 200 °C) and 15 % (at 225 °C) ethanol conversions, are shown in Figure 4-2. From the figure, it is obvious that ACD is a predominant product both at low and high conversions of ethanol. The target product DEE is selectively obtained in a less extent and the general trend in a decrease in the DEE selectivity with the increase of temperature (in other words, of ethanol conversion) is observed. This tendency is different from what we learn in the methanol oxidation reaction in which the DMM selectivity is almost constant up to 60 % of conversion. A maximum DEE selectivity of 40 % is observed on FeMo3.5 catalyst at low conversion. The selectivity of

DETH remains constant (*ca.* 5 %) in any experiments. A small amount (*ca.* 1 %) of ETH and carbon oxides (CO and CO_2) is detected. Unfortunately, there is no significant connection between the catalyst composition, in terms of Mo and Fe contents, and the given ACD/DEE selectivities. Considering the yield of DEE obtained on the tested catalysts in general, the values are greater at higher conversion. However, this increase in DEE yield is likely due to the increase in conversion and no indicative correlation of the obtained yields with the contents of Mo and Fe present in the catalysts is observed.

In order to increase the DEE yield we have tried to play on the pretreatment of the catalyst. The IndFeMo2 catalyst was chosen to test in the selective oxidation of ethanol to DEE and the sample was treated in the flow of O_2 and He (20/80 mol.%) at 340 °C for 15 h prior to the test. The catalyst performances are also presented in Figure 4-2. Apparently the pretreated catalyst shows no improvement in the yield of DEE at low conversion because the selectivities to ACD and DEE are rather not changed from those observed on the non-pretreated catalyst. At higher conversion, DEE yield is significantly lower as a result of a marked increase in ACD selectivity at the expense of DEE selectivity.

As a remark, the highest yield of DEE (*ca.* 4%) obtained on the FeMo mixed oxides series is provided by FeMo3.0, with 15 % ethanol conversion and 29 % DEE selectivity at 225 °C without any pretreatment of the catalyst.

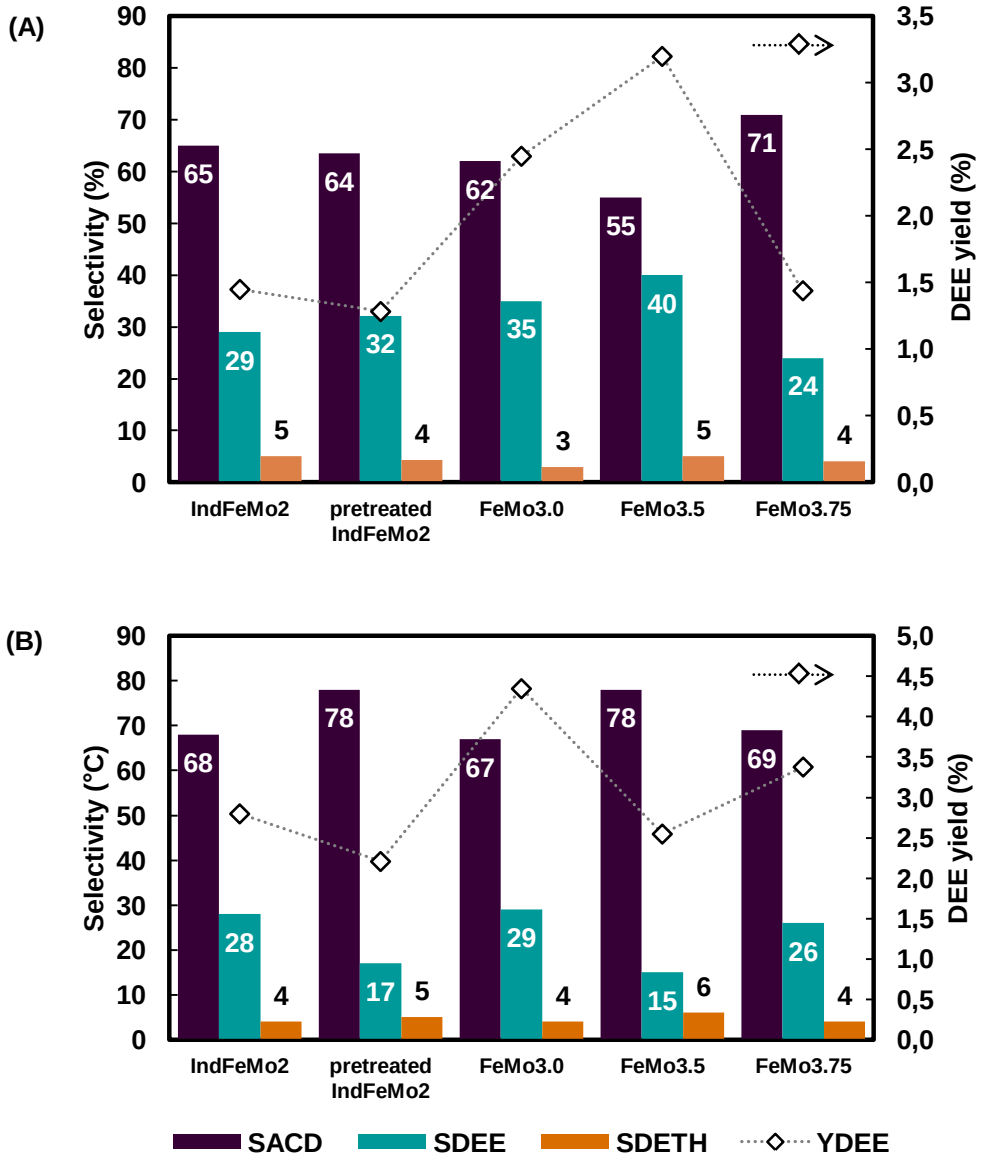

Figure 4-2: Performances at *iso*-conversion of 6 % (A) and 15 % (B) on industrial FeMo mixed oxide catalyst having Mo/Fe of 2 (IndFeMo2) and homemade FeMo3.0, FeMo3.5, and FeMo3.75 catalysts; reaction conditions: $CH_3CH_2OH/O_2/He$ = 30.8/7/62.2 mol.%, GHSV = 26 $L.h^{-1}.g_{cat}^{-1}$, $m_{catalyst}$ = 150 mg, time on stream = 1 h; treatment condition: 20/80 mol.% of O_2/He flow at 340 °C for 15 h.

Quite evidently, we observe that the selectivity of DEE decreases importantly with increasing conversion (concurrently due to the increase in reaction temperature), in contrast to ACD selectivity. This observation can be ascribed to that ACD formation is more favorable when increasing temperature. We also observe the similar trend in methanol oxidation reaction except that the decrease in selectivity is more pronounced at higher temperature (*i.e.*, 280 °C) in the reaction of methanol. Additionally, the numbers of acid sites present in the FeMo mixed oxides system is inadequate to undergo the acetalization reaction or the strength of

these acid sites may be weaker than that of the sites required for DEE formation (see analogous Scheme 1-2 for methanol reaction in Chapter 1 [1]).

4.2.2 FeMo mixed oxide modified with W and Al

To enhance the acid function of FeMo mixed oxide catalyst, we decided to partially substituted a portion of either Mo or Fe atoms by elements which are known to bring more acidity. The first attempt was to replace a part of molybdenum in the FeMo mixed oxides with tungsten. The cations of tungsten (W^{6+}) and molybdenum (Mo^{6+}) cations are both considered Lewis acids because they have vacant orbitals that can accept electron pairs from Lewis bases. The Lewis acid strength of metal ions is said to be proportional to the electronegativity of metals in their oxide form [2]. The electronegativity describes the tendency of an atom to attract electrons or electron density towards itself. In this manner, the acid strength of W^{6+} ions are stronger than that of Mo^{6+} ions due to its higher electronegativity, *i.e.*, χ_W of 2.36 and χ_{Mo} of 2.16 [3].

In our case the selective partial oxidation of ethanol forms a significant amount of water during reaction, which can indeed cause an interchange of Lewis and Brønsted acid sites. It is well known for the Brønsted acids like heteropolyanions (HPAs) that the HPAs containing tungsten are more acid than those containing molybdenum. The terminal O atoms linked to tungsten are less negatively charged comparing to those linked to molybdenum. In this case, the protons located near to them are more mobile and are likely to be donated.

Additionally, we prepared the FeMo mixed oxide catalyst modified with aluminium aimed at tuning the acid property. The preparation was performed by replacing some portion of Fe in the FeMo mixed oxides by aluminium. The concept of modification was based on that alumina (Al_2O_3) is widely used as an acidic support in various heterogeneous catalytic system. The intrinsic acidity of alumina is owed to the Lewis Al^{3+} centers.

4.2.2.1 Catalysts characterization

4.2.2.1.1 FeMoW mixed oxide catalysts

The FeMoW mixed oxides samples after drying were analyzed by DSC measurement in order to study the thermal effect on the catalyst. Figure 4-3 presents a DSC curve of the $FeMoW_{10\%}$ sample before calcination. Similar to the FeMo catalyst series, the curve shows endothermic peaks between 80 °C and 200 °C. These peaks can be ascribed to the elimination of

physisorbed water for temperatures lower than 125 °C, to dehydration for the temperature range between 125 °C and 200 °C, and to the decomposition of NH_4^+ present in both Mo and W precursor ($(NH_4)_6Mo_7O_{24}.4H_2O$ and $(NH_4)_6H_2W_{12}O_{40}.H_2O$, respectively). The crystallization to form mixed oxides phases occurs at higher temperatures in the range of 430 °C and 480 °C as evidenced by two intense exothermic DSC peaks. The XRD patterns of the non-calcined sample, recorded with increasing temperature under an air flow, presented in Figure 4-4, confirms that the crystallization phenomena likely to begin at temperatures between 400 and 450 °C, in agreement with the results of DSC analysis (Figure 4-3). The calcination temperature for all the dried samples in FeMoW series is then chosen at 450 °C where a considerably well-defined crystallization pattern is observed.

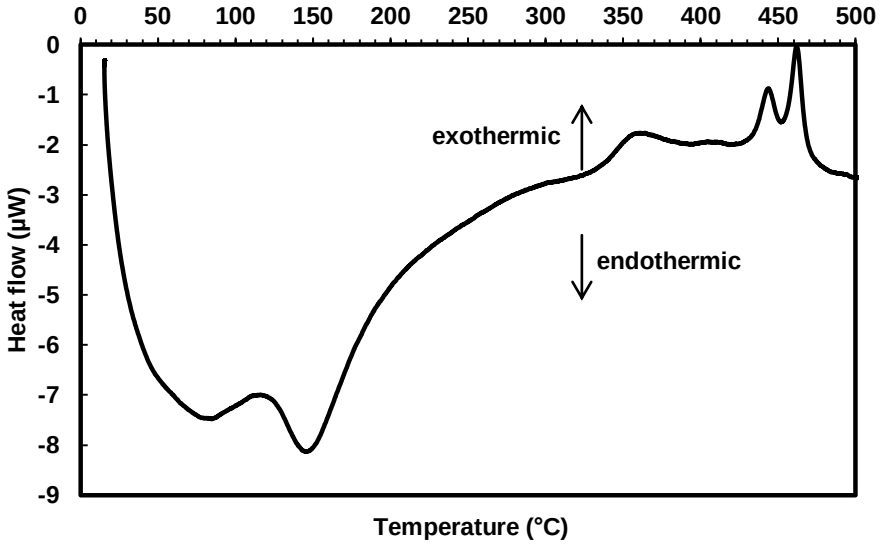

Figure 4-3: DSC curve of the non-calcined $FeMoW_{10\%}$ sample.

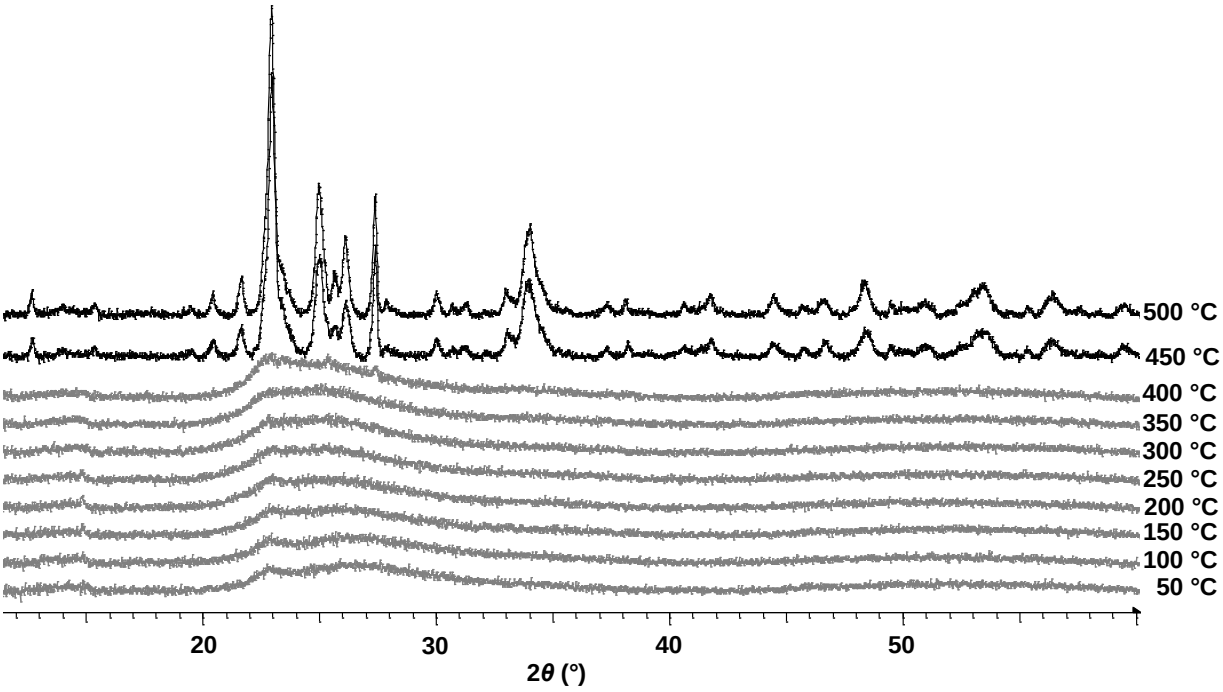

Figure 4-4: XRD diffractograms of the non-calcined $FeMoW_{10\%}$ catalyst recorded every 50° with increasing temperature from 50 °C to 500 °C (increasing temperature rate of 10 °C.min^{-1}).

The Figure 4-5 reveals the XRD patterns of the calcined $FeMoW_{10\%}$ mixed oxide catalyst. The sample exhibits characteristic peaks of ferric molybdate ($Fe_2(MoO_4)_3$, JCPDS#35-0183), molybdite (MoO_3, JCPDS#47-1081), and tungsten molybdenum mixed oxide (θ–$W_{0.4}Mo_{0.6}O_3$, JCPDS#32-1391) phases. Other samples in the series present the same characteristics nevertheless with different contents of each crystalline phase.

The specific surface areas of the calcined FeMoW mixed oxide catalysts determined by nitrogen adsorption are reported in Table 4-1. Addition of more W to the FeMo mixed oxide system leads to a linear decrease in the surface areas from 5.8 $m^2.g^{-1}$ to 2.2 $m^2.g^{-1}$ from 10 % to 20 % W addition.

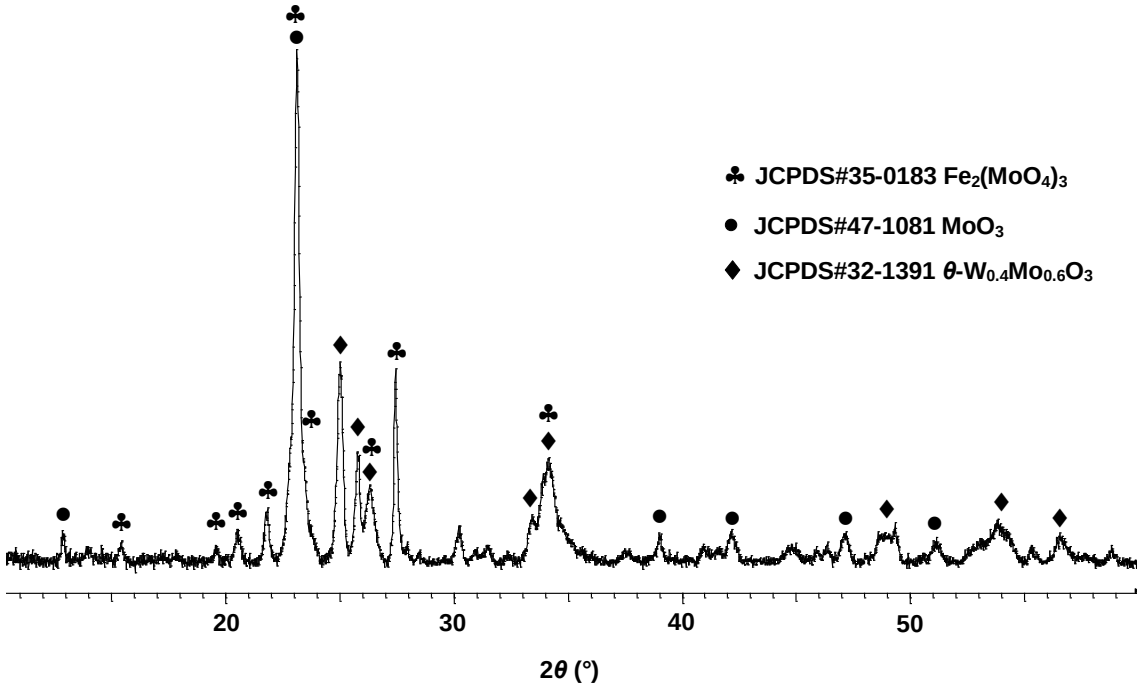

Figure 4-5: XRD pattern of the $FeMoW_{10\%}$ catalyst after calcination at 450 °C in air for 2 h.

Table 4-1: Specific surface area of the calcined FeMoW catalysts.

Catalysts	$FeMoW_{10\%}$	$FeMoW_{15\%}$	$FeMoW_{20\%}$
S_{BET} **($m^2.g^{-1}$)**	5.8	3.6	2.2

4.2.2.1.2 FeMoAl mixed oxides catalysts

The dried $FeMoAl_{10\%}$ sample was analyzed by temperature-programmed XRD in the flow of air to study the thermal effect on the sample before calcination. The diffractograms recorded from 50 °C to 500 °C are presented in Figure 4-6. The crystallization develops at the temperature between 300-350 °C, which is lower than the one of FeMoW mixed oxide samples. The crystallization pattern evolved at 450 °C is more defined than the one evolved at 350 °C, therefore, we chose to calcine both catalysts in the FeMoAl series ($FeMoAl_{10\%}$ and $FeMoAl_{20\%}$) at 450 °C, the same calcination temperature as other FeMo based samples in order to be able to compare all these samples without introducing extra parameters.

The crystalline structure of the calcined $FeMoAl_{10\%}$ catalyst was determined by XRD at ambient temperature in a static air condition.

Figure 4-7 shows the XRD pattern which presents the characteristic peaks of ferric molybdate ($Fe_2(MoO_4)_3$, JCPDS#35-0183), molybdite (MoO_3, JCPDS#35-0609), and aluminum iron mixed oxide ($AlFeO_3$, JCPDS#30-0024) phases. The same feature is also present in the calcined $FeMoAl_{20\%}$ catalyst.

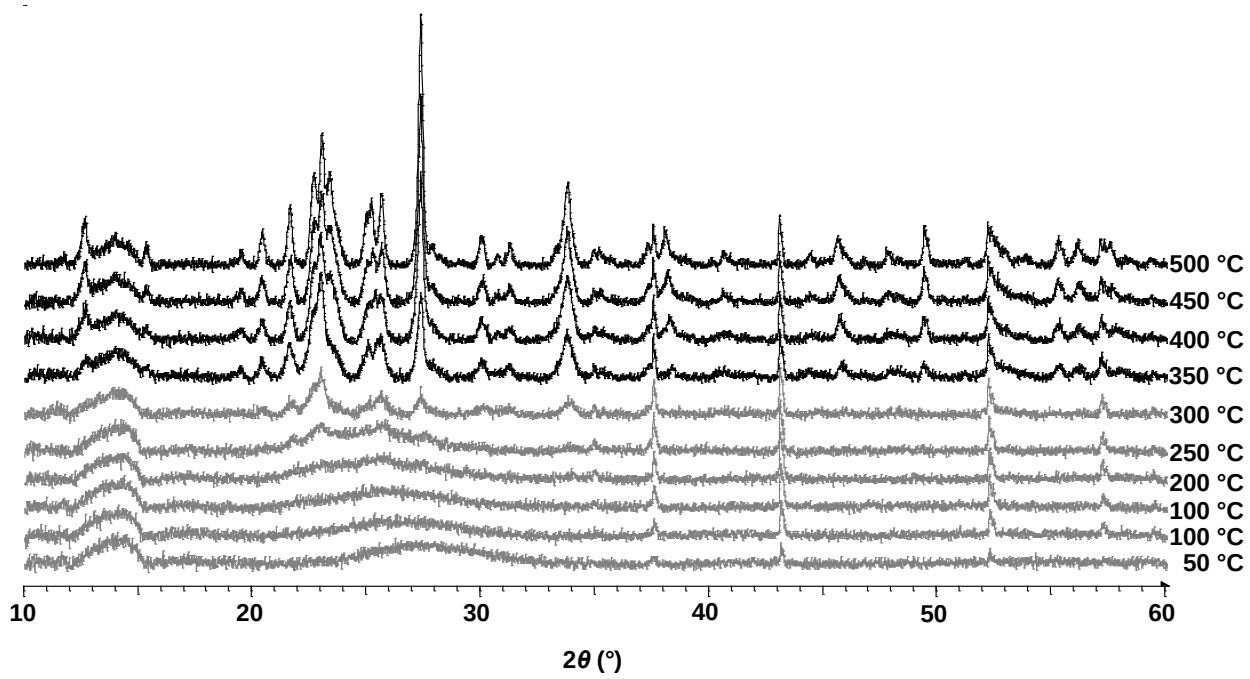

Figure 4-6: XRD patterns of the calcined $FeMoAl_{10\,\%}$ catalyst recorded every 50 °C with increasing temperature from 50 °C to 500 °C (increasing temperature rate of 10 °C.min^{-1}).

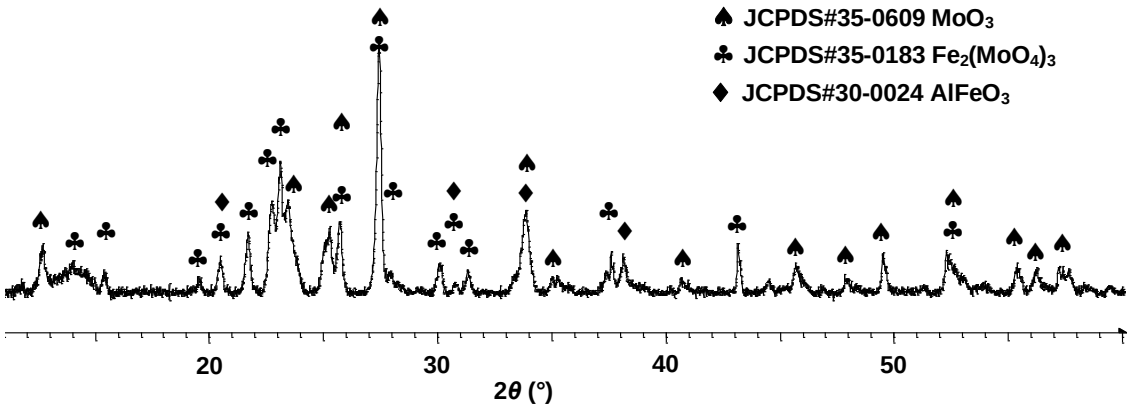

Figure 4-7: XRD pattern of the $FeMoAl_{10\%}$ catalyst after calcination at 450 °C in air for 2 h.

The specific surface areas of the calcined FeMoAl mixed oxide catalysts determined by nitrogen adsorption are reported in Table 4-2. Similar to what is observed for a FeMoW

series, the surface area decreases when adding more Al. $FeMoAl_{10\%}$ catalyst presents 4.3 $m^2.g^{-1}$ surface area which is higher than that of $FeMoAl_{20\%}$ catalyst (3.7 $m^2.g^{-1}$).

Table 4-2: Specific surface area of the calcined FeMoAl mixed oxide catalysts.

Catalysts	$FeMoAl_{10\%}$	$FeMoAl_{20\%}$
S_{BET} ($m^2.g^{-1}$)	4.3	3.7

4.2.2.2 Catalytic performances

4.2.2.2.1 FeMoW mixed oxide catalysts

The catalytic performances at 225 °C and 250 °C in terms of ethanol conversion, products selectivities, and yield in DEE on the FeMoW mixed oxides without any catalyst pretreatment are presented in Figure 4-8A and Figure 4-8B, respectively. From the figures, it is observed that the conversion of ethanol increases when increase the reaction temperature (*ca.* 6 % at 225 °C to *ca.* 15 % at 250 °C), in any tested sample. The most active catalyst in both cases is $FeMoW_{10\%}$ mixed oxide with the lowest amount of W addition. This is probably due to its highest specific surface area compared to other catalysts in the series (5.8 $m^2.g^{-1}$, Table 4-1). The FeMoW mixed oxides are also less active than the FeMo mixed oxide without modification. FeMoW catalysts convert roughly 6 % of ethanol while 15 % of ethanol is converted on FeMo catalyst at the same reaction temperature of 225 °C.

The distribution of products obtained on FeMoW catalysts are acetaldehyde (ACD), DEE, and diethyl ether (DETH). Quite evidently, ACD is a predominant product at both reaction temperatures. Acetal DEE is produced in a less extent than ACD however its selectivity generally increases with the amount of W present in the mixed oxide systems (22 % to 50 % of S_{DEE} at 225 °C and 12 % to 47 % of S_{DEE} at 250 °C). This observation indicates the positive effect of W addition. Unfortunately, a downtrend of DEE selectivity with temperature is still observed. The selectivity to DETH remains constant at *ca.* 12 %. This value is slightly higher than that obtained on FeMo catalysts which implies that stronger acid sites are developed by adding W to the FeMo system. There is a slight improvement on the yield of DEE obtained over the FeMoW catalysts. The highest yield of 6 % is provided by $FeMoW_{20\%}$ with 13 % conversion and 47 % DEE selectivity at 250 °C.

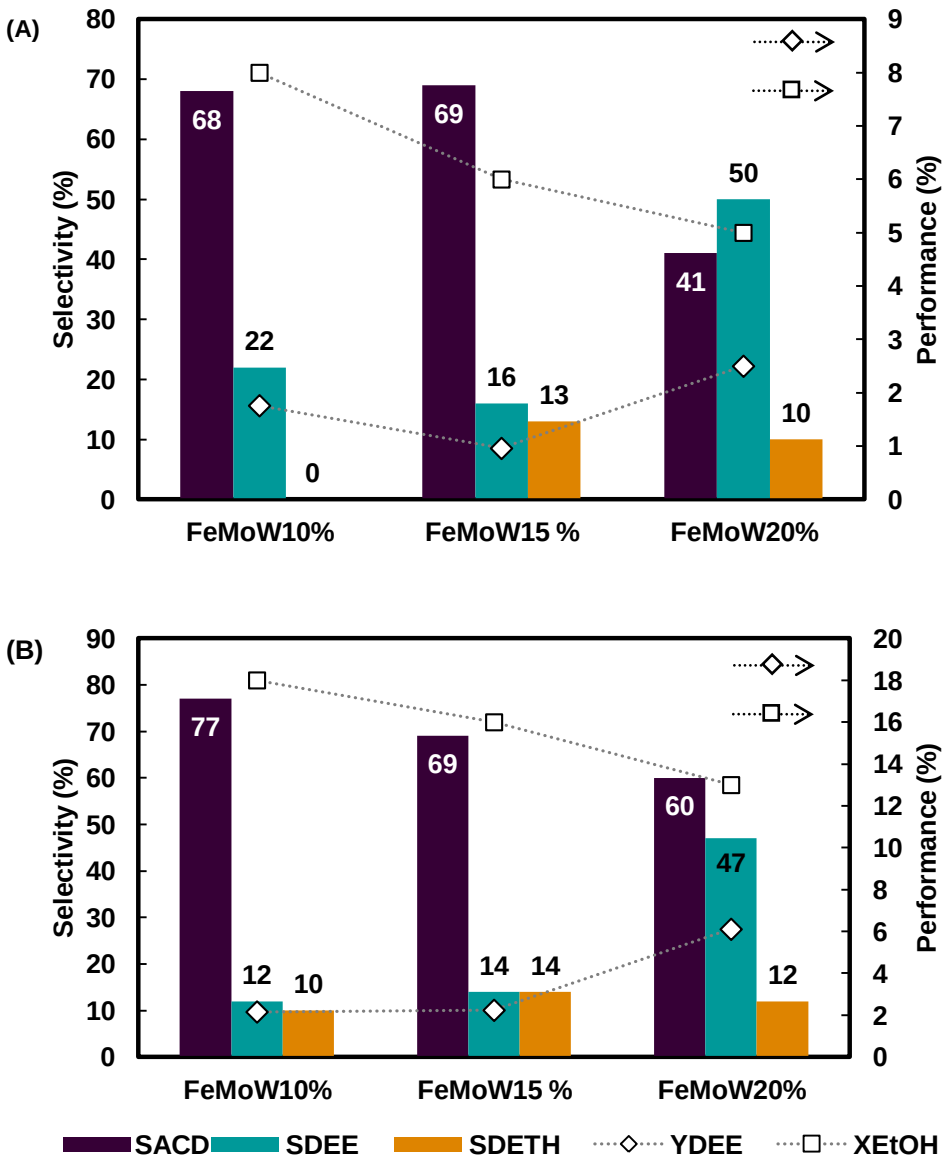

Figure 4-8 : Performances at 225 °C (A) and 250 °C (B) on $FeMoW_{10\%}$, $FeMoW_{15\%}$, and $FeMoW_{20\%}$ mixed oxide catalysts; reaction conditions: $CH_3CH_2OH/O_2/He$ = 30.8/7/62.2 mol.%, GHSV = 26 $L.h^{-1}.g_{cat}^{-1}$, $m_{catalyst}$ = 150 mg, time on stream = 1 h.

4.2.2.2 FeMoAl mixed oxide catalysts

Figure 4-9A and Figure 4-9B present the catalytic performances in terms of ethanol conversion, products selectivities, and yield in DEE on the FeMoAl mixed oxides without any pretreatment of the catalysts at 225 °C and 250 °C, respectively. The FeMoAl catalysts are also less active than the FeMo catalysts with respect to their working reaction temperatures, similar to what we have observed with FeMoW catalysts. Unsurprisingly, the conversion of ethanol increases with temperature and this phenomenon leads to significant dropping of DEE

selectivity. Indeed, ACD is mainly produced with a selectivity as high as those obtained on FeMo catalysts. The catalysts also do not provide more DEE when comparing the amount of the DEE selectivity given by FeMoAl with those given by FeMo catalysts. No change is observed on DETH selectivity where the value is constant at ca. 5 % whatever the amount of Al addition. The selectivity to DETH is close to that given by FeMo catalysts thus one can make an assumption that there is no stronger acid sites (or no more) generated after adding Al to the FeMo system. Nevertheless, the observed decrease in conversion with the content of Al can be pointed out and this is possibly due to the decrease in the specific surface area at higher Al loading (Table 4-2). Regrettably the yield of DEE cannot be improved by modification of FeMo with Al. The highest yield of 4 % is found on $FeMoAl_{10\%}$ catalyst with 17 % conversion and 23 % DEE selectivity at 250 °C.

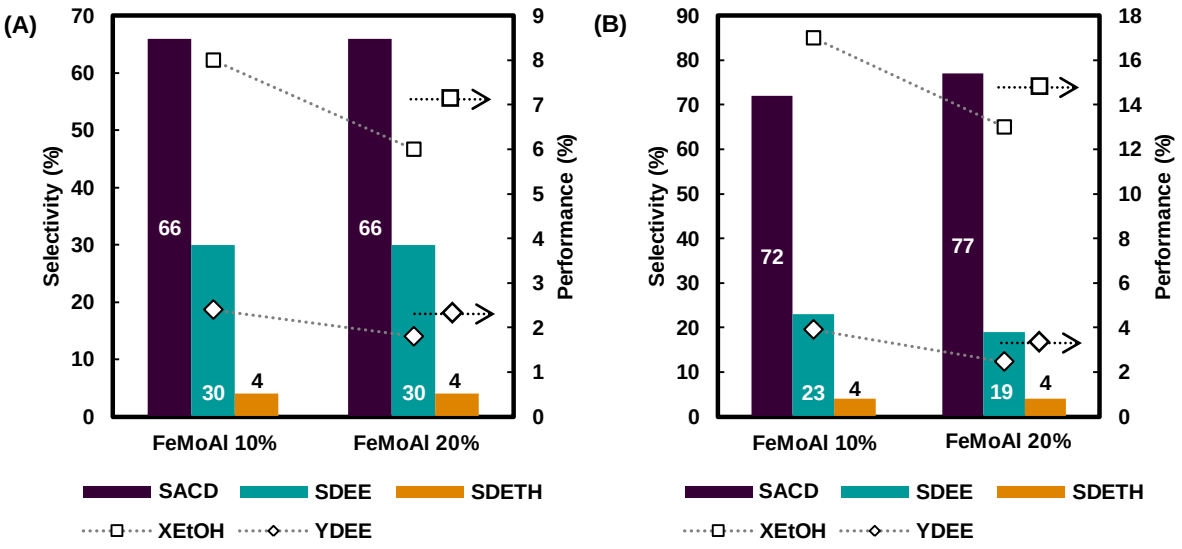

Figure 4-9: Performances at 225 °C (A) and 250 °C (B) on $FeMoAl_{10\%}$ and $FeMoAl_{20\%}$ mixed oxide catalysts; reaction conditions: $CH_3CH_2OH/O_2/He$ = 30.8/7/62.2 mol.%, GHSV = 26 $L.h^{-1}.g_{cat}^{-1}$, $m_{catalyst}$ = 150 mg, time on stream = 1 h.

Regarding the results presented in this part, it seems that one of the obstacles could be the acid strength needed to perform the reaction between one mole of acetaldehyde and two moles of ethanol. In order to examine the acidity scale needed to realize the acetalization reaction, we decided to study the acetalization reaction step separately from the partial oxidation reaction step by co-feeding a stoichiometric ratio of ethanol and acetaldehyde as a reactant mixture and carrying out the reaction on acidic catalysts.

4.3 Catalytic measurements in acetalization of ethanol and acetaldehyde

Four acidic catalysts were selected for testing in the acetalization reaction of acetaldehyde with ethanol to investigate the influence of surface acidity on their reactivity towards DEE formation in gas phase. These catalysts include:

- 20 wt.% ZrO_2 grafted on SBA-15, calcined at 650 °C [4] (hereafter referred to as ZrO_2-SBA15),
- $H_4SiW_{12}O_{40}$ supported on ZrO_2 grafted with SBA-15 [4] (hereafter referred to as STA/ZrO_2-SBA15),
- WO_3/TiO_2 (15/11.4 wt.%), and
- β-zeolite.

All the catalysts were prepared by our team at Unité de Catalyse et de Chimie du Solide (UCCS) in Lille and were characterized by nitrogen adsorption [i] and NH_3-TPD [ii] to measure their specific surface area and acidity, respectively. The characteristics of those aforementioned catalysts are presented in Table 4-3.

[i] A Micromeritics ASAP 2000 was used to measure the specific surface area using N_2 adsorption-desorption experiments on outgassed catalysts. The samples were outgassed at 130°C and 2 µmHg for 3h. The specific surface area, S_{BET}, was calculated using the linear part of the BET plot.

[ii] The acidity of the samples was determined by temperature programmed desorption of ammonia using a Micromeritics AutoChem II 2920 connected to a mass spectrometer (VARIAN). The samples were outgassed at 300 °C under He flow, before being saturated with ammonia using an injection-loop at 100 °C. The desorption of ammonia was performed with a temperature ramp of 10°C.min^{-1} up to 900°C, and followed by a TCD detector and a mass-spectrometer.

Table 4-3: Characteristics of acidic catalysts used in this study.

Catalyst	S_{BET} ($m^2.g^{-1}$)	Amount of NH_3 adsorbed ($mmol.g^{-1}$)	Acid sites density ($\mu mol.m^{-2}$)[a]
20 wt.% ZrO_2 grafted on SBA-15	465	0.18	0.4
Supported $H_4SiW_{12}O_{40}/ZrO_2$ grafted on SBA-15	378	0.44	1.2
WO_3/TiO_2 (15/11.4 wt.%)	55	0.12	2.2
β-Zeolite	540	1.84	3.4

[a] $acid\ sites\ density = \frac{amount\ of\ desorbed\ NH_3\ (\mu mol.g^{-1})}{specific\ surface\ area\ (m^2.g^{-1})}$

The global acetalization reaction of ethanol and acetaldehyde is described via the following equation:

$$2CH_3–CH_2–OH + CH_3–CH{=}O \underset{k_2}{\overset{k_1}{\rightleftharpoons}} CH_3–CH_2–O–\underset{\displaystyle O–CH_2–CH_3}{\underset{|}{CH}}–CH_3 + H_2O \qquad (1)$$

ethanol (EtOH) acetaldehyde (ACD) *1,1*-diethoxyethane (DEE) water (W)

Figure 4-10 presents the conversions of ethanol and acetaldehyde at 80 °C, 100 °C, and 120 °C obtained from ZrO_2-SBA15, STA/ZrO_2-SBA15, WO_3/TiO_2, and *β*-zeolite catalysts. In general, increasing reaction temperature leads to a decrease in both ethanol and acetaldehyde conversions, especially on *β*-zeolite which is completely inactive at 120 °C. DEE is a major product of reaction for all tested catalysts with the selectivity as high as 99 % (on ZrO_2-SBA15 at 80 °C). Other products which can be identified are diethyl ether and a trace of ethyl acetate. Figure 4-11A presents the selectivity to DEE [iii] obtained at different temperatures on the tested catalysts. Similar to the conversion, the selectivity value decreases with increasing temperature, concurrently with an increase in selectivity towards diethyl ether (not shown here).

[iii] For the acetalization reaction of acetaldehyde with ethanol, the selectivity to DEE is calculated as a basis of both reactants by

$$S_{DEE} = \frac{6*n_{DEE}}{2*(n_{EtOH,in}-n_{EtOH,out})+2*(n_{ACD,in}-n_{ACD,out})}$$

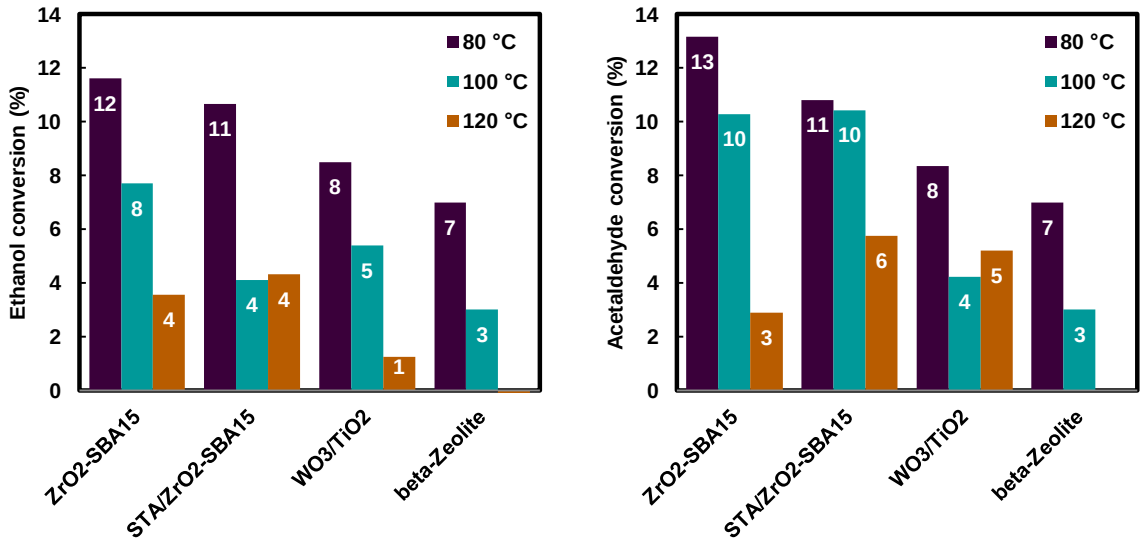

Figure 4-10: Plots of ethanol conversion (left) and acetaldehyde conversion (right) as a function of temperature on ZrO_2-SBA15, STA/ZrO_2-SBA15, WO_3/TiO_2, and *β*–zeolite catalysts; reaction conditions: CH_3CH_2OH/CH_3CHO = 26/13 mol.% dilute in He, GHSV = 26 $L.h^{-1}.g_{cat}^{-1}$, $m_{catalyst}$ = 150 mg, time on stream = 1 h.

It is noticeable that the surface acidity plays a role on the catalytic performances, in terms of DEE selectivity and especially ethanol and acetaldehyde conversions. The activity of *β*-Zeolite having the greatest amount of acid sites determined by NH_3-TPD (Table 4-3) is considerably low compared to other catalysts with lower concentrations of acid sites. The catalyst is also less selective to DEE, particularly at high temperature (100 °C). However, the so-obtained catalytic behavior cannot be explained straightforwardly taking into account the amount of acid sites and even the specific surface area. Combining both aforementioned parameters, the acid sites density is then applied in the correlation between conversions of ethanol and acetaldehyde, as well as the yield in DEE at 80 °C where the catalysts exhibited their best performances (Figure 4-11B). It is evident that the catalyst reactivity decreases linearly with the density of acid sites, or inversely the spacing between them. The conversion of ethanol decreases from 11 % to 7% with the increase in acid sites density from 0.39 to 3.41 $\mu mol.m^{-2}$. The same trend is observed for the conversion of acetaldehyde which decreases from 13 % to 7 %. The diminishing of DEE yield from 11% to 7 % with increasing density of acid sites is also noticeable. Even if the influence of acidity (the density of sites and/or the strength) is not yet understood, thanking to these obtained results, we can make a remark that the dehydration/condensation reaction of ethanol and acetaldehyde in gas phase seems not to be favored at all with the increase in temperature.

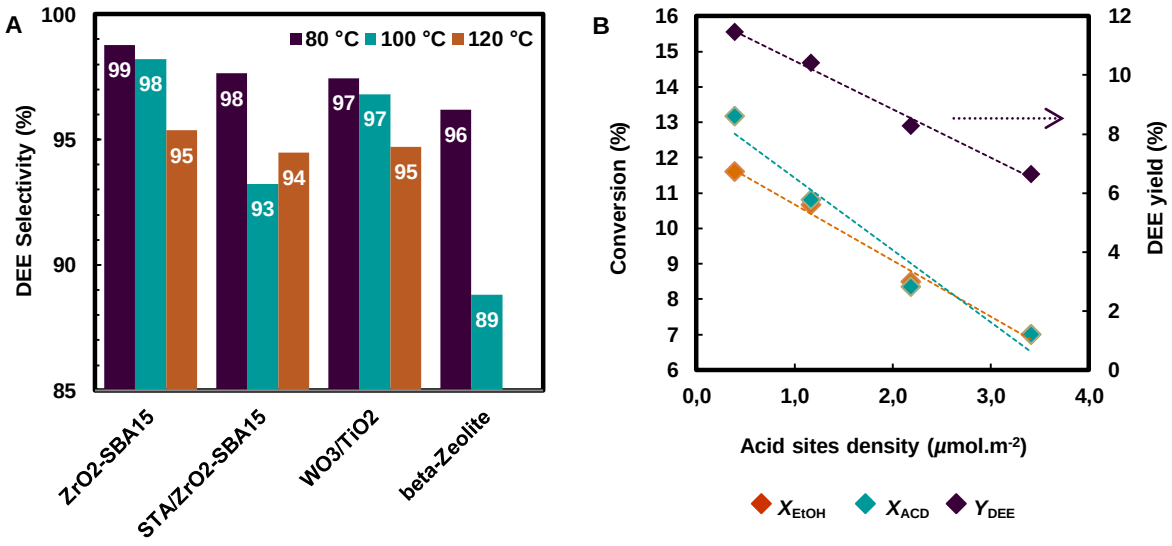

Figure 4-11: (A) DEE yield plot as a function of temperature on ZrO_2-SBA15, STA/ZrO_2-SBA15, WO_3/TiO_2, and *β*–zeolite catalysts, (B) Variation of catalyst activity (ethanol and acetaldehyde conversions) and DEE yield at 80 °C with acid sites density; reaction conditions: CH_3CH_2OH/CH_3CHO = 26/13 mol.% dilute in He, GHSV = 26 $L.h^{-1}.g_{cat}^{-1}$, $m_{catalyst}$ = 150 mg, time on stream = 1 h.

4.4 Thermodynamic considerations

The acid-catalyzed acetalization reactions of aldehydes with alcohols are reversible and the catalyst reactivity and yield of the desired acetal are both limited by unfavorable chemical reaction equilibrium. In our case, we made an attempt to use heterogeneous catalysts in the acetalization of acetaldehyde with ethanol in gas phase condition. However, there is no information in literature on the subject of study due to the fact that in most reports the reactions were practically carried out in liquid phase [5,6]. Thereby, the thermodynamic calculation for the gas-phase acetalization of ethanol and acetaldehyde will be developed herein this subsection.

At equilibrium state, the Gibbs free energy must be stationary, meaning that the change in Gibbs energy for the reaction at constant temperature and pressure ($\Delta_r G_{T,P}$) is equal to the derivative of Gibbs energy with respect to the extent of reaction ($\left(\frac{dG}{d\xi}\right)_{T,P}$). The derivative is equal to zero at the equilibrium thus we obtain

$$\left(\frac{dG}{d\xi}\right)_{T,P} = \Delta_r G_{T,P} = 0 \qquad (2)$$

Referring to the equilibrium equation of the acetalization reaction of acetaldehyde with ethanol described in Eq. 1, the change in Gibbs energy can be defined as

$$\Delta_r G_{T,P} = \Delta_r G^0 + RTln\frac{a_{DEE}a_W}{a_{EtOH}^2 a_{ACD}} \quad (3)$$

hence, $$0 = \Delta_r G^0 + RTln\frac{a_{DEE}a_W}{a_{EtOH}^2 a_{ACD}} \quad (4)$$

or, $$\Delta_r G^0 = -RTln\frac{a_{DEE}a_W}{a_{EtOH}^2 a_{ACD}} \quad (5)$$

For the gas-phase reaction in an ideal system, the activity (a) can be explained in terms of gas concentration which is proportional to the partial pressure. Eq. 5 is then rewritten as

$$\Delta_r G^0 = -RTln\frac{P_{DEE}P_W}{P_{EtOH}^2 P_{ACD}} \quad (6)$$

where R is the gas constant (8.314 J.mol^{-1}.K^{-1}), P is the partial pressure taking into account the mole fraction (γ) of each gas component. Eq. 6 is rearranged to

$$\Delta_r G^0 = -RTln\frac{\gamma_{DEE}\frac{P}{P_0} * \gamma_W \frac{P}{P_0}}{\gamma_{EtOH}^2 \frac{P^2}{P_0^2} * \gamma_{ACD}\frac{P}{P_0}} = -RTln\left(\frac{\gamma_{DEE} * \gamma_W}{\gamma_{EtOH}^2 * \gamma_{ACD}}\right)\left(\frac{P_0}{P}\right) \quad (7)$$

where P_0 is the standard pressure at 1 bar, P is the total pressure of the system, and the ratio of P_0/P is close to 1 when the experiment is carried out at atmospheric pressure.

Given the initial moles of ethanol and acetaldehyde of n_{EtOH}^0 and n_{ACD}^0, respectively, at the beginning of experiment, the mole fraction at equilibrium of the individual, with respect to its stoichiometric ratio, can be described as follows:

ethanol: $$\gamma_{EtOH}^{eq} = \frac{n_{EtOH}^0 - 2\xi^{eq}}{n_{EtOH}^0 - 2\xi^{eq} + n_{ACD}^0 - \xi^{eq} + 2\xi^{eq}} = \frac{n_{EtOH}^0 - 2\xi^{eq}}{n_{EtOH}^0 + n_{ACD}^0 - \xi^{eq}} \quad (8)$$

where $n_{EtOH}^0 - 2\xi^{eq} + n_{ACD}^0 - \xi^{eq} + 2\xi^{eq}$ is the total number of moles at equilibrium and ξ^{eq} is the extent of reaction at equilibrium.

acetaldehyde: $$\gamma_A^{eq} = \frac{n_{ACD}^0 - \xi^{eq}}{n_{EtOH}^0 + n_{ACD}^0 - \xi^{eq}} \quad (9)$$

DEE and water: $$\gamma_{DEE}^{eq} = \gamma_W^{eq} = \frac{\xi^{eq}}{n_{EtOH}^0 + n_{ACD}^0 - \xi^{eq}} \quad (10)$$

Substituting these mole fractions into Eq. 7 thus

$$\Delta_r G^0 = -RTln\left(\frac{\xi^{eq^2}*(n^0_{EtOH}+n^0_{ACD}-\xi^{eq})}{(n^0_{EtOH}-2\xi^{eq})^2(n^0_{ACD}-\xi^{eq})}\right) \quad (11)$$

In our case, we carried out the acetalization reaction using the mixture of ethanol and acetaldehyde with a stoichiometric molar ratio of 2:1. The above equation can be simplified as

$$\Delta_r G^0 = -RTln\left(\frac{\xi^{eq^2}*(3-\xi^{eq})}{(2-2\xi^{eq})^2(1-\xi^{eq})}\right) \quad (12)$$

The term $\frac{\xi^{eq^2}*(3-\xi^{eq})}{(2-2\xi^{eq})^2(1-\xi^{eq})}$ is the thermodynamic equilibrium constant (K^{eq}) of the studied reaction. The extent of reaction at equilibrium (ξ^{eq}) can then be estimated from the standard Gibbs Free energy which is related to the standard enthalpy and entropy changes by

$$\Delta_r G^0 = \Delta_r H^0 - T\Delta_r S^0 \quad (13)$$

Table 4-4: Standard thermodynamic properties at 25 °C and 1 bar of gas-phase reactants and products involving in the acetalization of acetaldehyde with ethanol [iv].

Chemical component	**Molecular formula**	H_f^0 **(Ha)**	S^0 **(Cal.mol^{-1}.K^{-1})**
Ethanol	CH_3CH_2OH	-154.550076	64.46
Acetaldehyde	CH_3CHO	-153.381616	62.666
1,1-Diethoxyethane	$(CH_3CH_2O)_2CHCH_3$	-386.26576	100.114
Water	H_2O	-76.238357	45.079

1 Ha = 627.509 kcal.mol^{-1}.K^{-1}, 1 cal = 4.1814 J

Table 4-4 presents the standard enthalpy and entropy of reactants and products involving in the studied reaction (Eq. 1). The standard enthalpy $\Delta_r H^0$ and entropy $\Delta_r S^0$ changes of

[iv] Due to the lack of information in literature, the thermodynamic properties were theoretically calculated specifically for this study. The calculations have been performed with the G03 software by Professor S. Cristol (Unité de Catalyse et de Chimie du Solide (UCCS), Université de Lille 1). The use of the Möller-Plesset second order perturbation method associated with the split-valence 6-311G(d,p) basis set (MP2/6-311G**) ensure the determination of good equilibrium geometries as well as precise evaluation of the electronic energy. The evaluation of the thermodynamic properties has been performed with the inclusion of all the translational, rotational and vibrational degrees of freedom.

reaction are estimated to -58.68 kJ.mol^{-1} and -194.11 J.mol^{-1}.K^{-1}, respectively. The calculated $\Delta_r G^0$ values at different reaction temperatures are presented in Table 4-5, as well as the so-obtained equilibrium constants (K^{eq}) determined from Eq. 12 and products distribution calculated from the reaction extent at equilibrium (ξ^{eq}).

Table 4-5: Estimated values of $\Delta_r G^0$, equilibrium constants, and equilibrium compositions at different temperatures between 25 °C (298.15 K) and 150 °C (423.15 K).

Temperature (K)	$\Delta_r G^0$ (kJ.mol^{-1})	Equilibrium constant (K^{eq})	Equilibrium extent (ξ^{eq})	Equilibrium compositions			
				Ethanol $\left(\frac{2-2\xi eq}{3-\xi eq}\right)$	Acetaldehyde $\left(\frac{1-\xi eq}{3-\xi eq}\right)$	DEE $\left(\frac{\xi eq}{3-\xi eq}\right)$	Water $\left(\frac{\xi eq}{3-\xi eq}\right)$
298.15	-0.8039	1.40389	0.5126	0.3922	0.1961	0.2058	0.2058
323.15	4.0489	0.22465	0.3228	0.5059	0.2529	0.1206	0.1206
353.15	9.8721	0.03509	0.1688	0.5872	0.2936	0.0596	0.0596
373.15	13.7543	0.01202	0.1084	0.6167	0.3083	0.0375	0.0375
393.15	17.6364	0.00459	0.0710	0.6344	0.3172	0.0242	0.0242
413.15	21.5186	0.00192	0.0472	0.6454	0.3227	0.0160	0.0160
423.15	23.4597	0.00128	0.0394	0.6489	0.3244	0.0133	0.0133

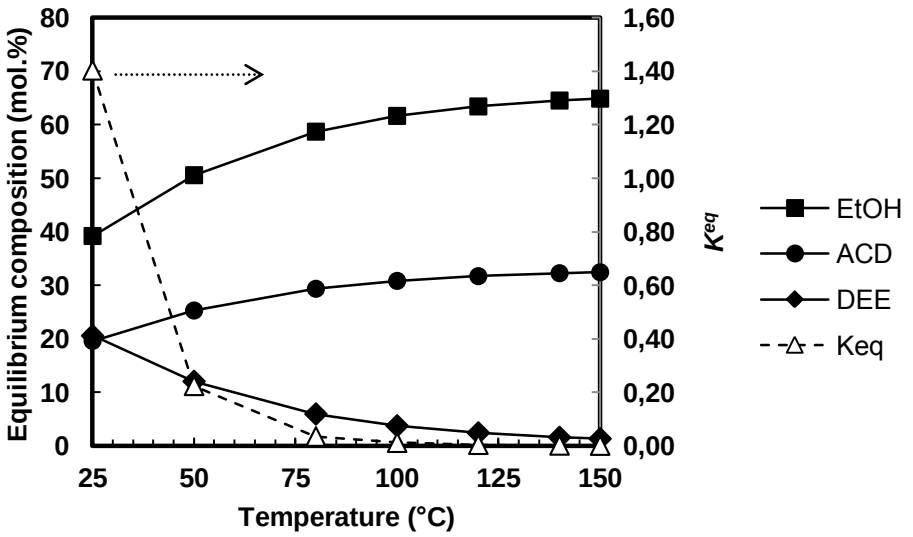

Figure 4-12: Variation of equilibrium compositions of ethanol, acetaldehyde, and DEE at temperatures between 25 °C and 150 °C, covering the range of working temperatures in this study.

The variation of equilibrium constants and chemical compositions, depicted in mol.%, at equilibrium is illustrated in Figure 4-12. Clearly the reaction of ethanol with acetaldehyde towards DEE is less favorable when increasing temperature as evidenced by a gradual decrease in K^{eq}. At high temperatures the reaction occurs with more difficulty as the

equilibrium tends to shift back towards the reactants (ACD and EtOH), as shown in the figure. The compositions at equilibrium of EtOH and ACD increase with temperature. Therefore, lower conversion is observed at higher temperature. This observation is in agreement with the results we obtain in the study

This is confirmed by a continuous decrease in the DEE composition at equilibrium. The decrease in DEE composition at equilibrium is in agreement with the diminishing trend of selectivity with temperature observed in our study (Figure 4-13). Likewise, the increase in both EtOH and ACD compositions with temperature implies how we can observe the decrease in their conversions.

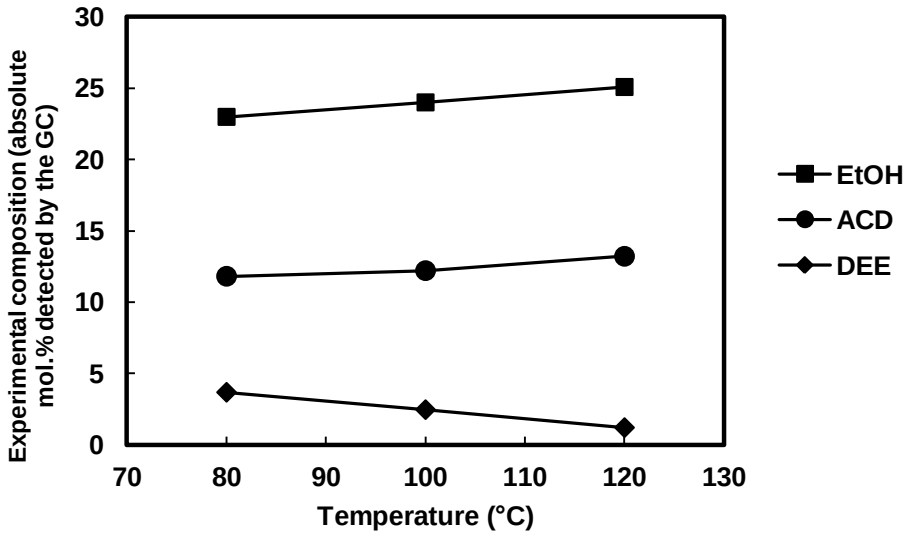

Figure 4-13: Experimental compositions at different temperatures on ZrO_2-SBA15 as a representative example of the studied catalysts tested in the acetalization reaction of acetaldehyde with ethanol; reaction conditions: CH_3CH_2OH/CH_3CHO = 26/13 mol.% dilute in He, GHSV = 26 $L.h^{-1}.g_{cat}^{-1}$, $m_{catalyst}$ = 150 mg, time on stream = 1 h.

4.5 Conclusions

A series of FeMo mixed oxide catalysts including those which were prepared in-house, *i.e.*, FeMo3.0, feMo3.5, FeMo3.75, as well as an industrial catalyst (IndFeMo2) were applied for the direct synthesis of DEE from ethanol. The experiments were carried out with the reactant mixture comprised of a high ethanol concentration, *i.e.*, 30.8 mol.%, and 7 mol.% of O_2, diluted in He. The working temperatures were chosen in the range of 200°C and 250 °C, which is slightly less than those applied in methanol reaction due to the higher exothermicity.

The FeMo catalysts were first tested in their freshly calcined condition, without any pretreatment. The conversion of ethanol increases with temperature however the value does not exceed 30 % due to the studied temperature range. Globally, instead of producing DEE, an excess of ACD is formed selectively while the formation of DEE is significantly less. The maximum yield of DEE of *ca.* 4 % is obtained at 225 °C with 15 % conversion of ethanol and 29 % DEE selectivity on the FeMo mixed oxides with Mo/Fe ratio of 3. Nevertheless no indicative correlation between Fe and Mo contents in the catalysts with their performances could be developed.

The FeMo based catalyst was also pretreated before using in the experiment. IndFeMo2 catalyst was selected as a representative of the samples in the studied series and it was placed in the flow of O_2 and He (20/80 mol.%) at 340 °C for 15 h, prior to the tests. The pretreated catalyst does not provide any better yield of DEE at low conversion because of no change in conversion and DEE selectivity. The yield of DEE drops significantly at higher conversion as a result of a marked decrease in DEE selectivity.

We can ascribe the predominant formation of ACD on the FeMo mixed oxide catalysts, instead of the expected DEE formation, to that (i) the numbers of acid sites present in the FeMo system is inadequate to undergo the acetalization reaction or (ii) the strength of these acid sites is inadequate than that of the sites required for DEE formation. To enhance the acidity, a portion of Mo and Fe in the FeMo formulation was then replaced by elements which are known to provide more acidity. A series of FeMoW mixed oxides catalysts were prepared by coprecipitation method from solutions of ammonium molybdate, ammonium metatungstate monohydrate, and ferric chloride. In this case, 10, 15, and 20 wt.% of Mo portion in the FeMo formulation was substituted by W. The catalysts after calcination at 450 °C in air for 2 h present mixed oxides of crystalline MoO_3 and $Fe_2(MoO_4)_3$, and θ–$W_{0.4}Mo_{0.6}O_3$ confirmed by XRD analyses.

The catalysts were tested in the selective oxidation of ethanol to DEE at 225 °C and 250 °C without any pretreatment. Similar trends of increasing ethanol conversion and of deceasing DEE selectivity with temperature are noticed on FeMoW catalysts. We observe that the most active catalyst in this series is the one with the lowest amount of W loading ($FeMoW_{10\%}$) and this is probably due to its highest specific surface area than others. However, the activity of FeMoW catalysts is less than that of FeMo ones without modification. For instance, $FeMoW_{10\%}$ gives only 6 % conversion of ethanol at 225 °C whereas FeMo-based catalysts

can convert 15 % of ethanol. Addition of W to the FeMo system is beneficial by means of increasing the DEE selectivity. Nonetheless, a downtrend of selectivity to DEE with temperature is still observed. A slight increase in DEE yield, compared to FeMo mixed oxides, is obtained on this series of FeMoW catalysts but at higher temperature. The maximum yield of 6 % is brought by $FeMoW_{20\%}$, showing 13 % conversion and 47 % DEE selectivity at 250 °C.

A series of FeMoAl mixed oxide catalysts were prepared by coprecipitation method from ammonium molybdate, ferric chloride, and aluminum nitrate nonahydrate solutions. 10 and 20 wt.% of Fe portion in the FeMo formulation was substituted by Al. The catalysts after calcination at 450 °C in air for 2 h present mixed oxides of crystalline MoO_3 and $Fe_2(MoO_4)_3$, and $AlFeO_3$ confirmed by XRD analyses. The catalysts were tested in the selective oxidation of ethanol to DEE at 225 °C and 250 °C without any pretreatment. The catalysts are less active than FeMo catalysts with respect to the conversion given at the same working temperature. The specific surface area plays a role in the conversion and the FeMoAl10% catalyst having higher specific surface area presents higher conversion of ethanol. Obviously the conversion of ethanol increases with temperature but the selectivity to DEE diminishes. Unfortunately, the yield of DEE does not improve when the FeMo formulation is modified with Al. The maximum yield is only 4 % on $FeMoAl_{10\%}$ catalyst showing 17 % conversion and 23 % DEE selectivity at 250 °C.

Focusing more on the role or the influence of surface acidity in the DEE formation, various acidic catalysts were tested in the acetalization of ethanol and acetaldehyde in gas phase. These catalysts include ZrO_2 grafted on SBA-15, $H_4SiW_{12}O_{40}$ supported on ZrO_2 grafted with SBA-15, WO_3/TiO_2, and *β*-zeolite, with different number of acid sites and acid sites density. We observe that the catalyst activity, *i.e.*, ethanol and acetaldehyde conversions, gradually decreases with increasing temperature from 80 °C to 120 °C. The performances (EtOH/ACD conversions and DEE yield) of these acidic catalysts are well-correlated to the acid sites density, taking into account both amount of acid sites and the specific surface area of the solids. When increasing the acid sites density (in other words, their proximity to each other), the catalyst activity and DEE yield decrease. The unfavorable reaction of acetaldehyde and ethanol in gas phase with the increase in temperature is supported by thermodynamic calculation at 80-120 °C. Effectively, the equilibrium constant decreases with temperature and this implies more difficulty to proceed the reaction towards DEE formation.

4.6 References

[1] J.-M. Tatibouët, Appl. Catal. A: Gen. 148 (1997) 213.; J.M. Tatibouet, J. E. Germain, J. Catal. 72 (1981) 375; J.-M. Tatibouët, H. Lauron-Pernot, J. Mol. Catal. A: Chem. 171 (2001) 205.

[2] http://chemistry.tutorvista.com/inorganic-chemistry/lewis-acid.html#, verified on February 5, 2013.

[3] http://www.lookchem.com/Periodic-Table, verified on February 5, 2013.

[4] B. Katryniok , S. Paul , M. Capron , C. Lancelot , V. Bellière-Baca , P. Rey and F. Dumeignil. Green Chem. 12 (2010) 1922.

[5] V.M.T.M. Silva, A.E. Rodrigues, Chem. Eng. Sci. 56 (2001) 1255.

[6] M. Gomez, A.L. Arru, AbelloMa.C., J. Chem. Technol. Biot. 79 (2004) 391.

General discussions of the results, conclusions and perspectives

This thesis is performed under the 7th framework European Program EuroBioref (European Multilevel Integrated Biorefinery Design for Sustainable Biomass Processing). The aim of this study is to synthesize acetals – *1,1*-dimethoxymethane (DMM) and *1,1*-diethoxyethane (DEE) – in a single step process from their corresponding alcohols, *i.e.*, methanol and ethanol, respectively, and to achieve a maximum yield of acetals over a catalytic system with bifunctional, *i.e.*, redox and acidic, characters.

In the previous chapters, we have commented in details the results of the catalytic tests for the iron molybdate (FeMo) mixed oxide catalytic system in a single step synthesis of acetals. Those obtained results and observations will be summarized and a global discussion and conclusions, as well as several perspectives, will be given hereafter.

In chapter 3, describing the synthesis of DMM from methanol, FeMo mixed oxide catalysts with different loadings of Mo and Fe are synthesized by a simple coprecipitation method. It is clearly shown that the FeMo mixed oxide catalytic system is highly productive in DMM formation, due to the presence of relevant and adequately balanced redox potential and acidity. When placing the catalysts under a reaction mixture highly concentrated in methanol, the DMM selectivity is boosted. Besides, the selectivity is almost constant up to 60 % of conversion of methanol. These specific and unique features lead us to extensively characterize this family of particular catalysts. LEIS analysis reveals the presence of both Mo and Fe species on the outermost atomic layer of the catalysts. The good catalytic performances are attributed to a synergistic effect between Mo and Fe species, especially seen on methanol conversion. The observed synergy leads us to propose that the first step of methanol adsorption occurs on an active site intimately incorporating Mo and Fe cations. This site involves an anionic vacancy generated by dehydroxylation of the catalytic surface and an oxygen species (O^{2-}) of the solid. XPS and *in situ* EPR measurements show that the Fe cations are responsible for the redox property. The acidic properties of FeMo mixed oxides are attributed to anionic vacancies acting as Lewis acid sites. XPS analysis also shows that oxygen from the gas phase is useful to reoxidize the catalyst surface allowing the active sites regeneration, in agreement with the well-known Mars-van Krevelen mechanism.

The highest DMM yield of 39 % is obtained on the FeMo catalyst with a Mo/Fe ratio of 3.4 (Fe/M_T = 0.23, where M_T = Fe + Mo), showing 46 % conversion and 85 % selectivity at 255 °C. This catalyst contains 64 % of $Fe_2(MoO_4)_3$ and 36 % of MoO_3 (seen by XRD), with a relatively high surface area (10 $m^2.g^{-1}$) compared to other catalysts in the studied series.

This part of the study permit us envisaging that it is possible to transform the existing industrial formaldehyde plants working practically with the FeMo-based catalyst into a DMM plant, else, to adapt the existing facilities to produce DMM instead of formaldehyde production. This can be simply carried out by changing the reactant feed composition (shifting from low to high concentration of methanol) and the range of working temperature as illustrated below in Figure 1.

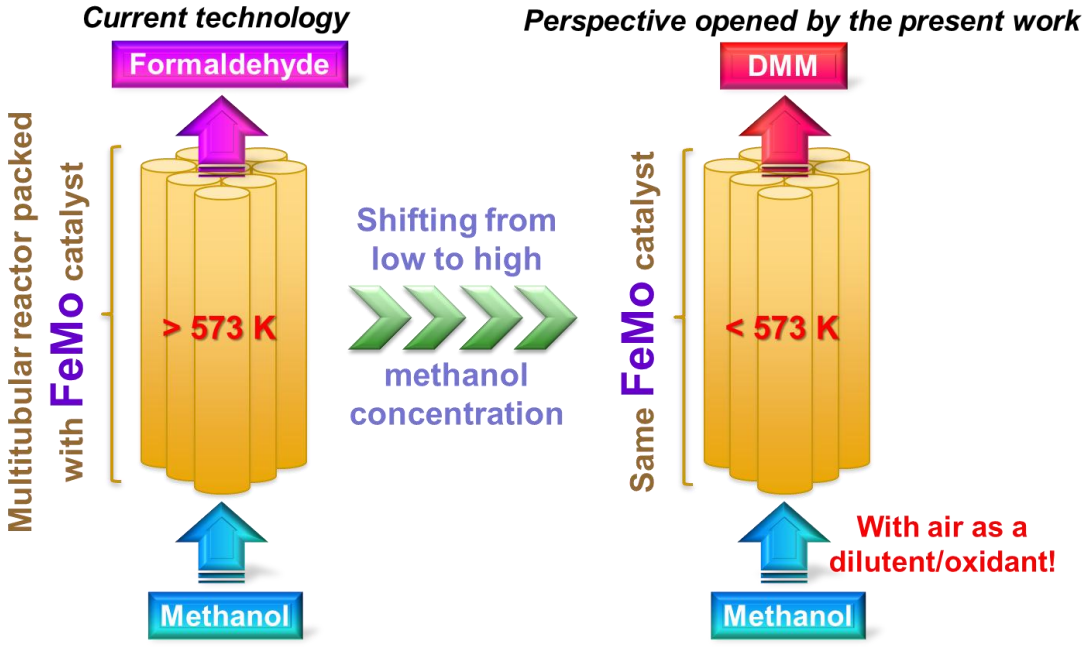

Figure 1: Interchangeable strategies between formaldehyde and DMM production over a FeMo mixed oxide catalyst.

In chapter 4, we focus on the direct synthesis of DEE from ethanol. An assumption was made that FeMo mixed oxide catalysts could be applied to the reaction of ethanol owing to that the reaction pathway of methanol oxidation is analogous to that of ethanol oxidation. With respect to this, we could presume that the redox and acid properties of the FeMo catalyst are sufficient in producing DEE from ethanol. The FeMo mixed oxide catalysts with different Mo and Fe contents were then tested using the reactant mixture comprised of a high ethanol concentration, in regards to what we have applied in the reaction of methanol. However, the working temperatures are slightly less than those used in methanol reaction due to the higher exothermicity. Instead of yielding mainly DEE, the FeMo-based catalysts give a predominant amount of acetaldehyde (ACD), in any tested catalyst compositions. The FeMo catalyst was also treated in an air flow at 340 °C for 15 h before carrying out the test. There is still no improvement in DEE production. ACD is a major product in any case and its selectivity

increases with temperature, while the DEE selectivity is suppressed by temperature rising. These results can be ascribed to i) a deficiency in the number of acid sites present in the FeMo system to undergo the acetalization reaction and/or to ii) the strength of these acid sites that could be less adequate than that of the sites required for DEE formation. To enhance the acidity, a portion of Mo and Fe cations in the FeMo formulation was then replaced by W and Al, respectively. Addition of W to the FeMo system is advantageous by means of increasing the DEE selectivity. Nonetheless, a downtrend of selectivity to DEE with temperature is still observed. A slight increase in DEE yield is obtained on the FeMoW catalyst having low amount of W loading while no improvement in the DEE yield is obtained on the FeMo formulation containing Al.

To understand more on the role or the influence of surface acidity in the DEE formation, the acetalization of ethanol and acetaldehyde in gas phase was studied independently from the partial oxidation of ethanol (*cf.* Scheme 1-3, Chapter 1). ZrO_2 grafted on SBA-15, $H_4SiW_{12}O_{40}$ supported on ZrO_2 grafted with SBA-15, WO_3/TiO_2, and β-zeolite, with different number of acid sites and acid sites density were tested. It is observed that the catalyst activity, *i.e.*, ethanol and acetaldehyde conversions, gradually decreases with increasing temperature. The performances (ethanol/ACD conversions and DEE yield) of these acidic catalysts are well-correlated to the acid sites density or their proximity. Both the catalyst activity and DEE yield decrease when the sites are too close to each other, suggesting that a steric hindrance exists which certainly has an adverse effect on the reactivity. The acetalization reaction of acetaldehyde and ethanol in gas phase is not favored with the increase in temperature and this is then supported by thermodynamic calculations at 80-120 °C. The equilibrium constant decreases strongly with temperature and this implies more difficulty to proceed the reaction towards DEE formation.

As evidenced in the part of our study dedicated to the direct ethanol acetalization to produce DEE, it is quite clear that this reaction is not straightforwardly transposable as it could be for methanol acetalization. It is shown that, when working with a mixture of ethanol and acetaldehyde catalysed by acidic catalysts, the DEE yield is still low even if a high DEE selectivity of more than 90 % is obtained. One way to increase the yield of DEE might be to first perform the reaction with a mixture composed by ethanol and acetaldehyde (the latter could be obtained *via* the partial oxidation of ethanol on the FeMo catalyst) while keeping the reaction at low conversion (at low reaction temperature). The products (mainly DEE) could then be separated from the reaction medium and the reactants mixture after separation

recycled to the same reactor to increase the conversion. Another possibility is to carry out the direct conversion of ethanol to DEE at low reaction temperature and attempt to improve the conversion of ethanol by adding more active metals (*e.g.*, Ni) while maintaining high DEE selectivity. In addition, we can focus on working at high reaction temperature and enhance the surface acidity by means of number of acid sites and/or their strength to improve the DEE selectivity. With a high conversion of ethanol that we obtain in this temperature range, the larger yield in DEE can be achieved.

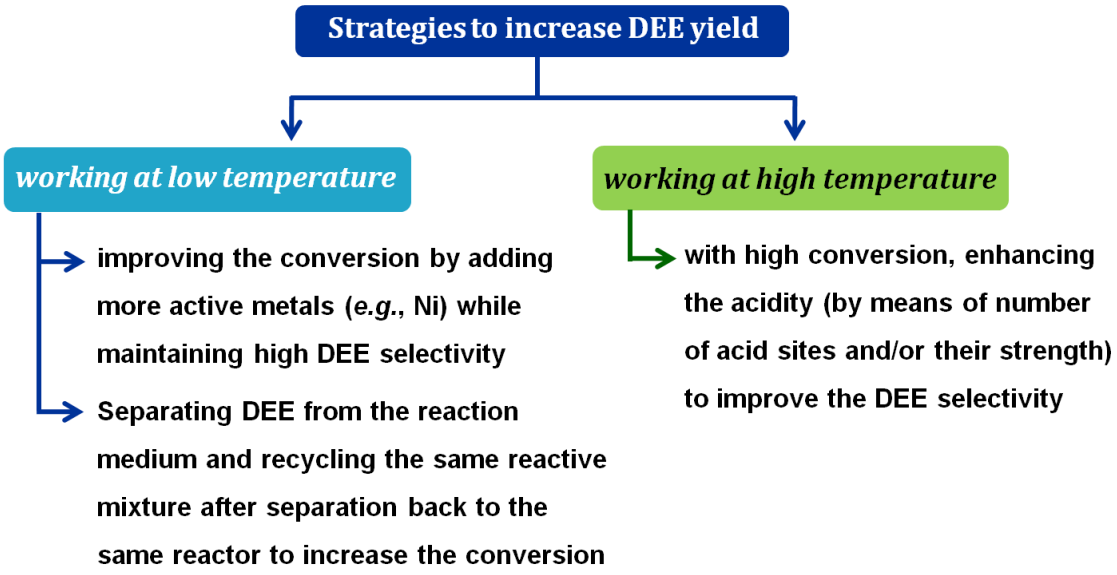

Figure 2: Strategies to increase the yield in DEE based on the research findings.

It appears that, the FeMo mixed oxide catalyst is not efficient in the direct synthesis of DEE from ethanol, possibly due to the stearic effect, or the strength of acid sites. In order to perform a full screening of catalysts, a high throughput apparatus labelled REALCAT has been settled at UCCS (**REALCAT** : Plateforme intégREe AppLiquée au criblage haut débit de CATalyseurs pour les bioraffineries). A wide range of catalyst formulations and compositions can be tested directly in this apparatus. This will give in the near future, the opportunity to discover and to develop new catalytic systems which can be selective and indeed productive in the direct synthesis of DEE from ethanol.